6302

NRL Report 6293
AFML-TR-64-408

UNCLASSIFIED

Electron Microscope Fracture Examination to Characterize and Identify Modes of Fracture

C. D. BEACHEM

Physical Metallurgy Branch
Metallurgy Division

September 28, 1965

U.S. NAVAL RESEARCH LABORATORY
Washington, D.C.

CONTENTS

ELECTRON MICROSCOPE FRACTURE EXAMINATION TO CHARACTERIZE AND IDENTIFY MODES OF FRACTURE

1. INTRODUCTION

The examination and study, in the electron microscope, of replicas of fracture surfaces has proved very useful in studies of fracture mechanisms. Fine-scale fracture surface features that are characteristic of specific causes of fracture in specific materials have been recognized in the past as a sufficient basis for the performance of certain failure analyses and of invaluable aid in performing others. However, research into fracture mechanisms and the systematic collection of electron fractographs from well documented fractures are primary necessities for the performance of failure analyses through the use of electron fractography.

The specific aims in this program were: (1) to continue the NRL collection of electron fractographs which characterize fracture surfaces created in the laboratory under known conditions, (2) to investigate fracture mechanisms basic to certain types of fracture, (3) to use electron fractography in the performance of critical failure analyses, (4) to provide guidance to Douglas Aircraft Company during the compilation of the Failure Analysis Handbook, and (5) to train personnel in the techniques of replication and interpretation of electron fractographs.

Specimens with documented histories were obtained from various sources within the Metallurgy and Mechanics Divisions of NRL after they had been fractured in the routine execution of various fracture toughness evaluation programs. None of the specimens were broken specifically for the present contract. Since each NRL Group that supplied specimens for this program was collecting only the data they felt were significant, some of the results reported herein are not complete in all respects. For example, some of the fatigue surfaces examined were fatigue-cracked in order to provide a sharp notch for crack toughness evaluations, and no records of the fatigue stresses were kept.

The cellulose acetate replication process was used almost exclusively in the preparation of replicas. The standard practice was to use 5 mil tape, shadow with palladium at 45° (in the direction of macroscopic crack propagation) and rotate the plastic replica while carbon was evaporated at about 45° angle. The carbon replicas were then freed from the cellulose acetate by washing the replicas in three baths of acetone. In a few instances direct carbon replicas were used. Technique details in these instances are described along with the discussion of the fracture surfaces.

Shadowing direction is indicated in each fractograph by an arrow above the micron marker.

In sampling the fracture surfaces, replicas were made of five or six locations on large specimens. Only the square, or plane strain, fracture surfaces were examined in most instances. Each carbon-backed replica was then cut into grid-size pieces and each piece was studied in the microscope. In each case an overly sufficient number of fractographs were made to make certain of a good characterization. Only those pictures necessary for describing the characteristic features are included in this report.

2. CHARACTERIZATION OF ALUMINUM ALLOY FRACTURE SURFACES

a. 2020 T651

Figures 1-12 are taken from two 2020 T651 aluminum plate specimens fatigue-cracked and broken in an Izod machine which had been modified to hold full-thickness

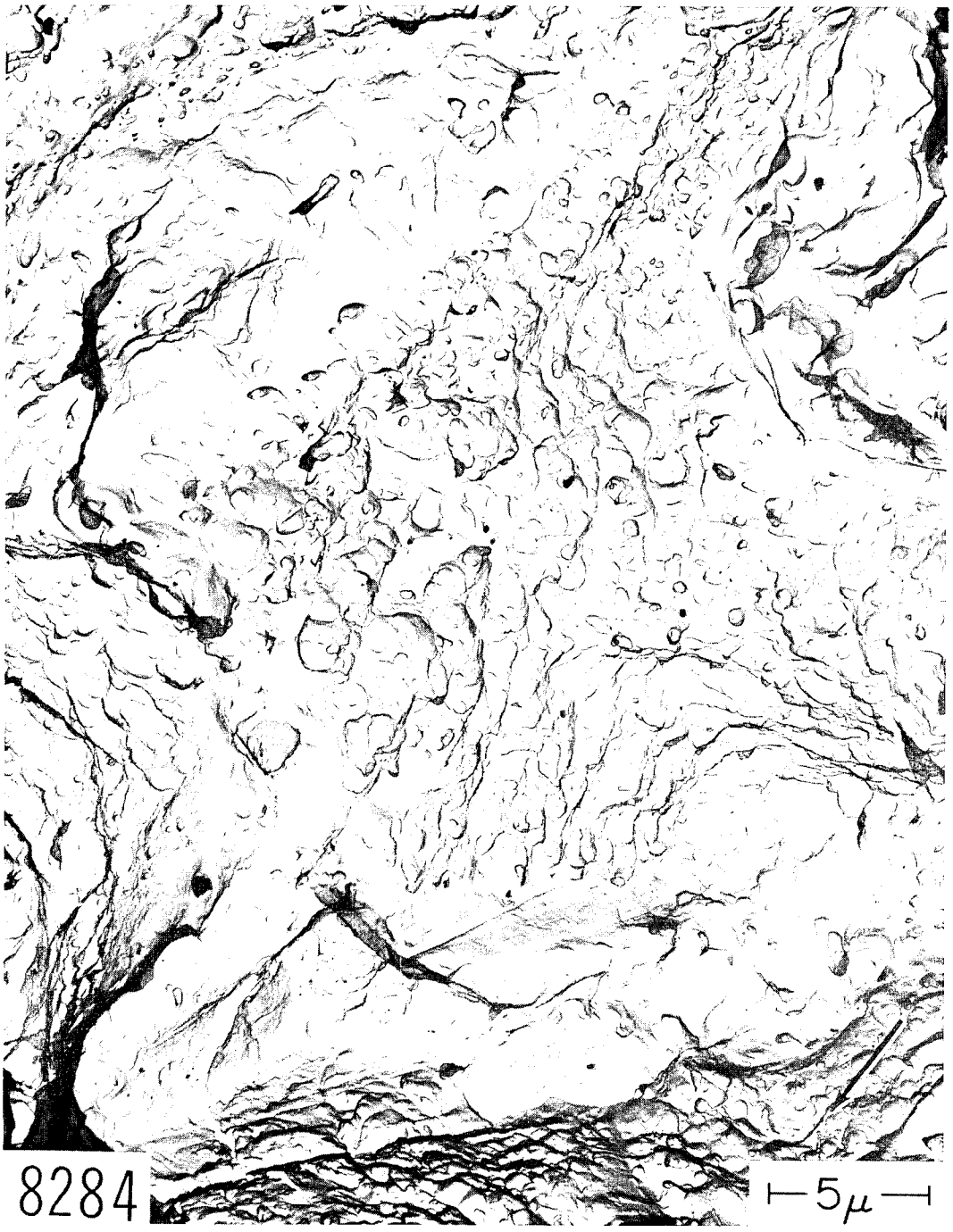

Fig. 1 - Room temperature impact square fracture plane-strain dimpled rupture in 2020 T651 aluminum alloy. Scraping artifacts are evident at the bottom of the fractograph. Cellulose acetate-carbon replication technique. Palladium shadowed. 6000X

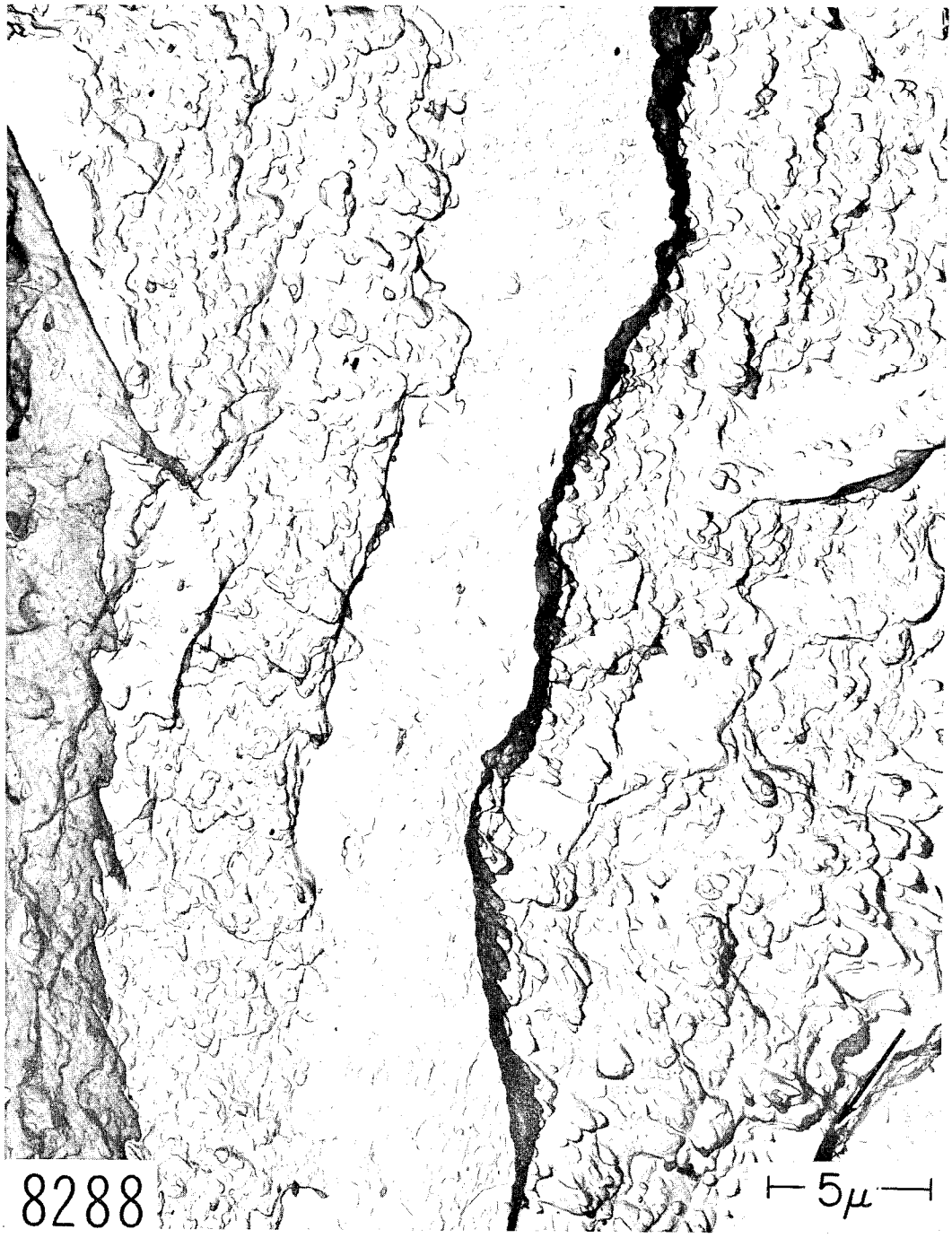

Fig. 2 - Room temperature impact square fracture plane-strain dimpled rupture in 2020 T651 aluminum alloy. Cellulose acetate-carbon replication technique. Palladium shadowed. 6000X.

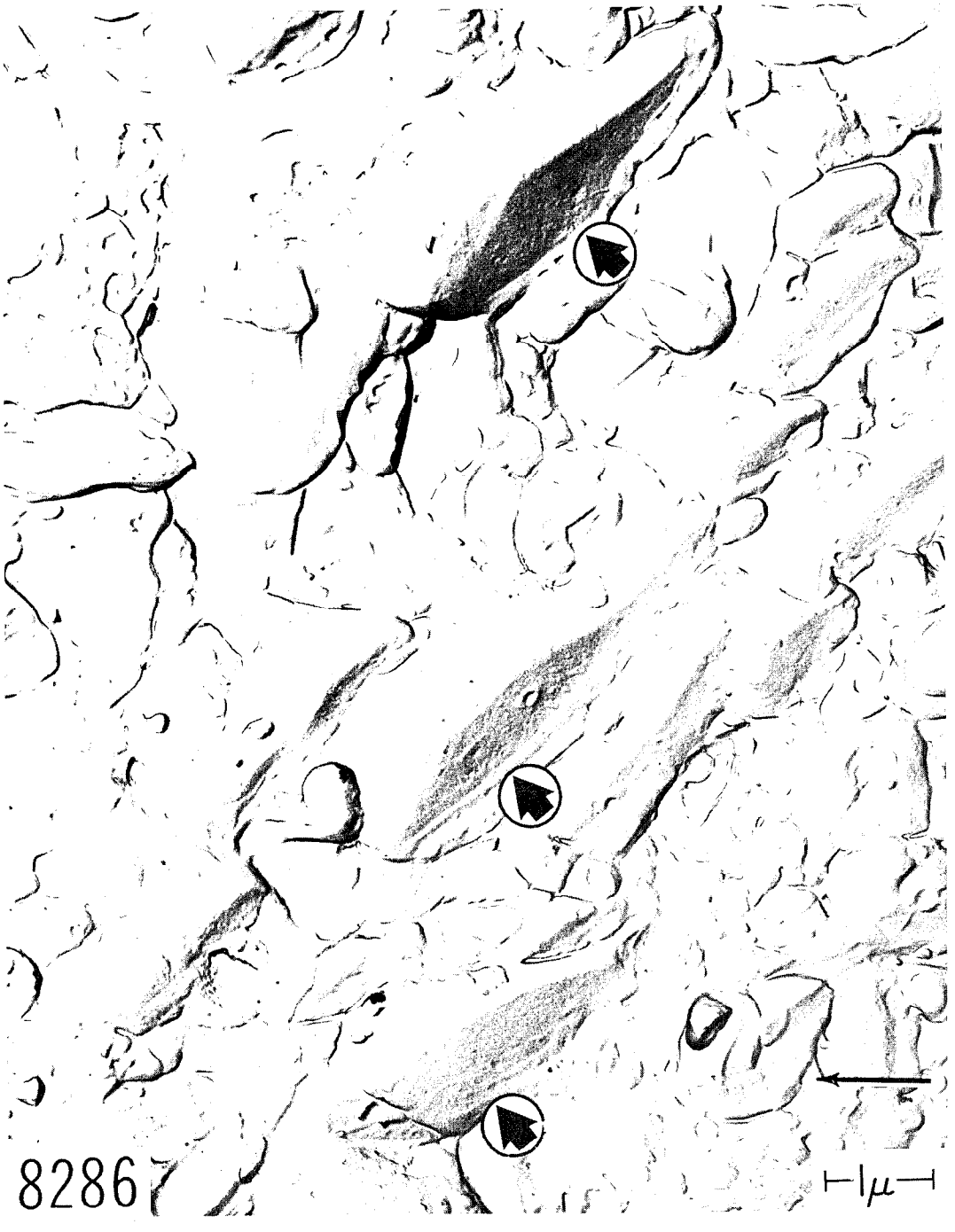

Fig. 3 - Room temperature impact square fracture plane-strain dimpled rupture in 2020 T651 aluminum alloy. Arrows indicate flat plate-like particles often associated with dimples in this material. Cellulose acetate-carbon replication technique. Palladium shadowed. 21,000X.

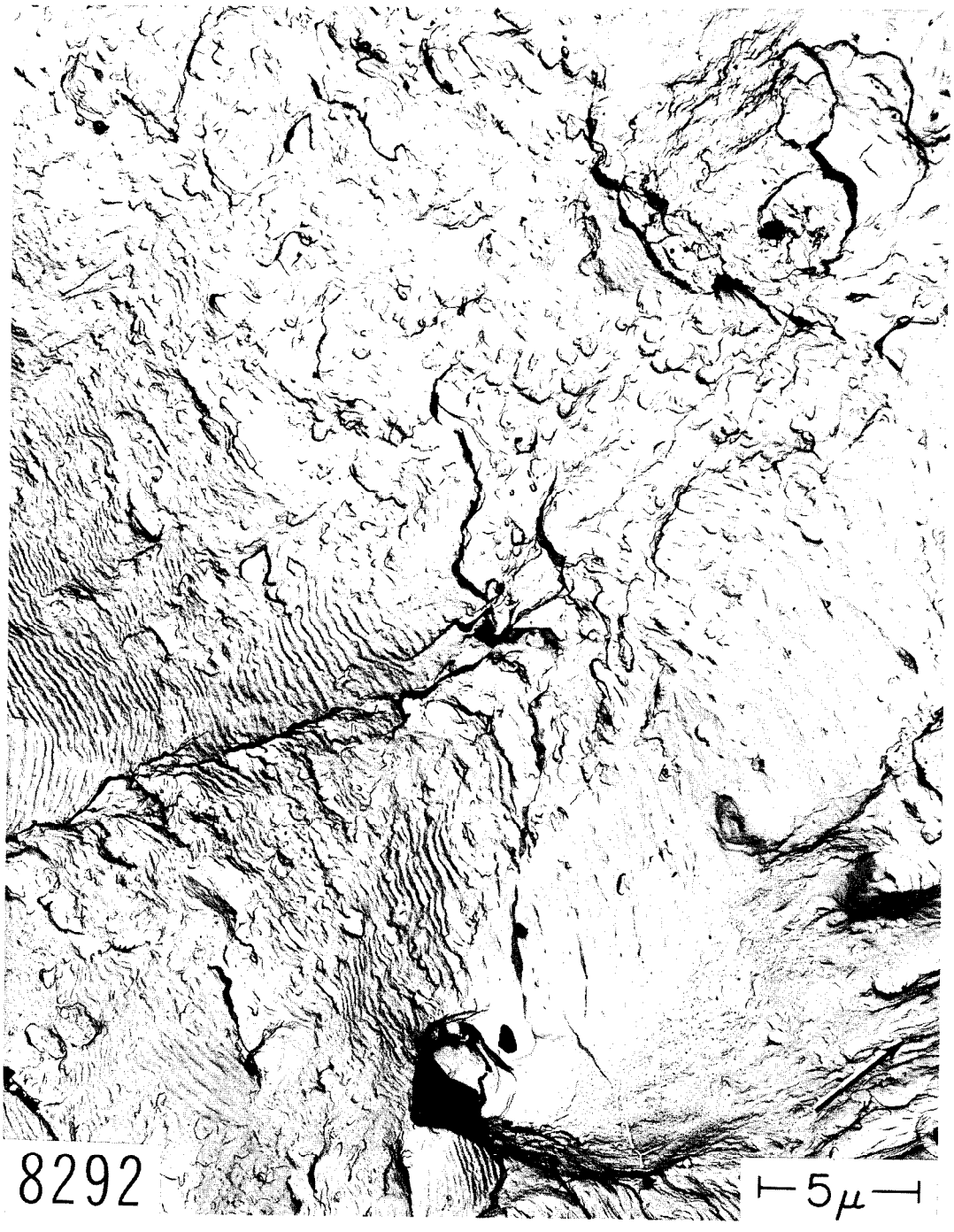

Fig. 4 - Tension-tension plane-strain fatigue markings in an RW fatigue crack in 2020 T651 aluminum alloy. Striations are often mixed with tear dimples. Cellulose acetate-carbon replication technique. Palladium shadowed. 6000X.

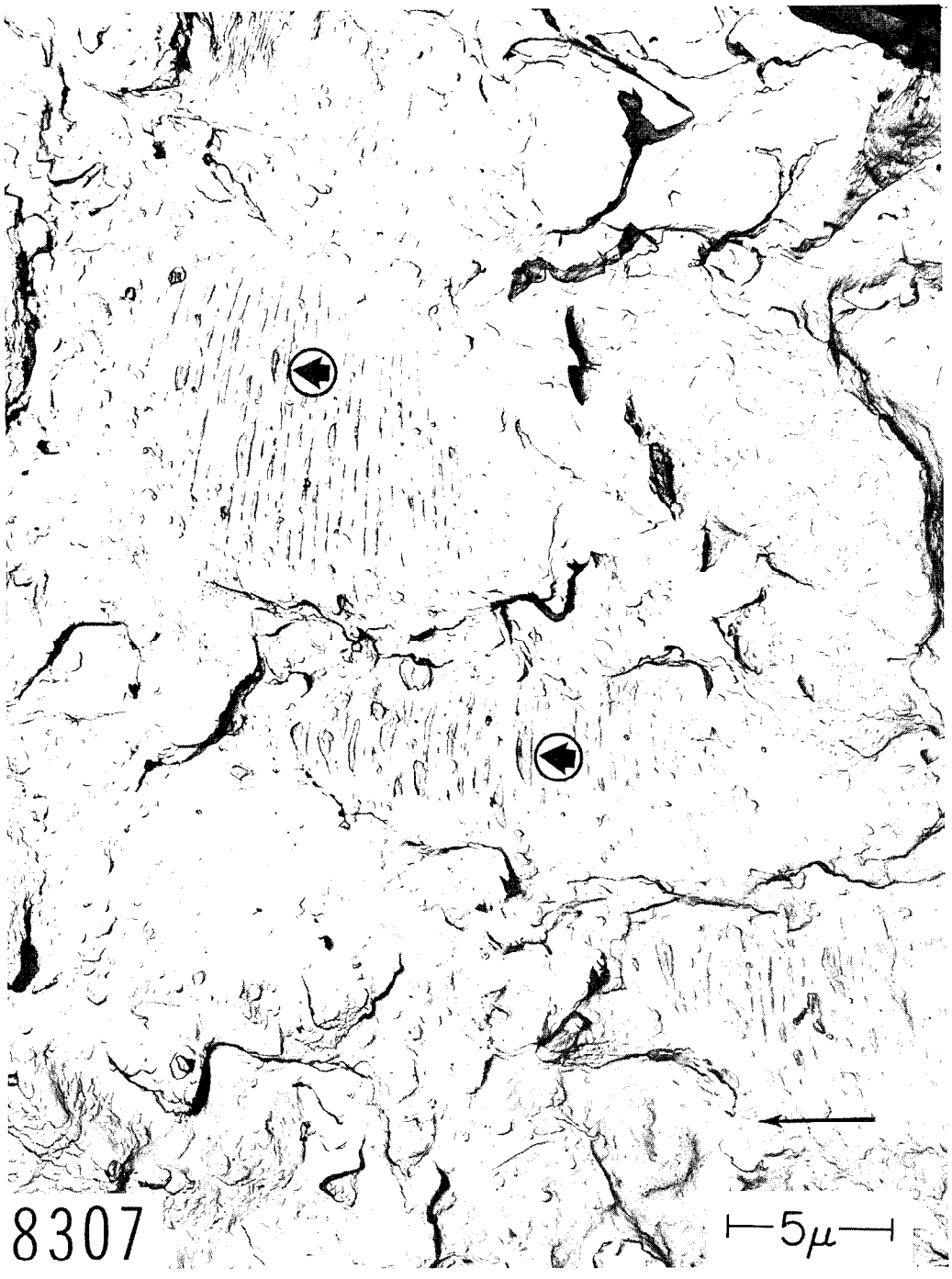

Fig. 5 - Tension-tension plane-strain fatigue markings in an RW fatigue crack in 2020 T651 aluminum alloy. Arrows indicate tongue-shaped cracks along parts of some of the striations. Cellulose acetate-carbon replication technique. Palladium shadowed. 6000X.

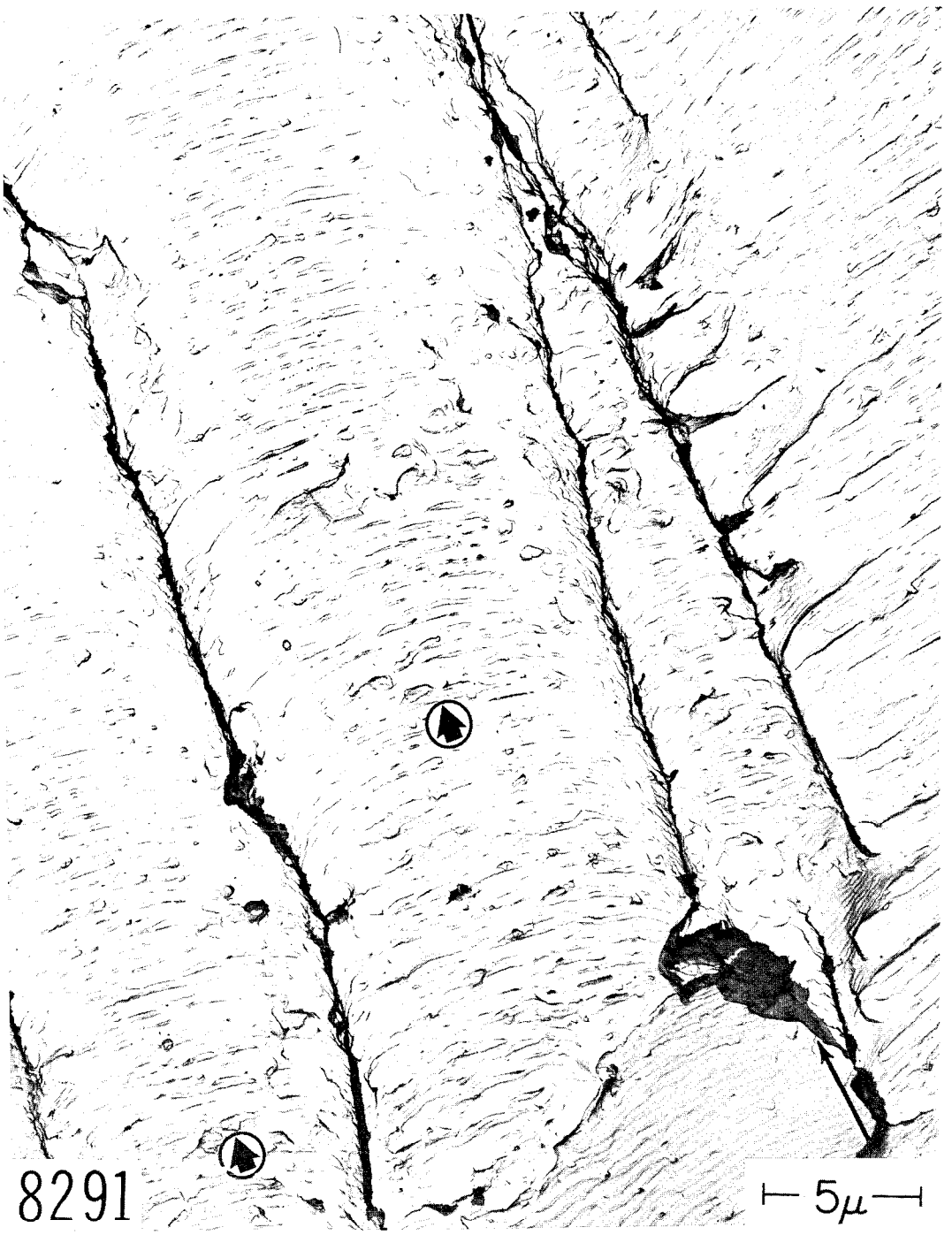

Fig. 6 - Tension-tension plane-strain fatigue markings in an RW fatigue crack in 2020 T651 aluminum alloy. Arrows indicate tongue-shaped cracks along parts of some of the striations. Cellulose acetate-carbon replication technique. Palladium shadowed. 6000X.

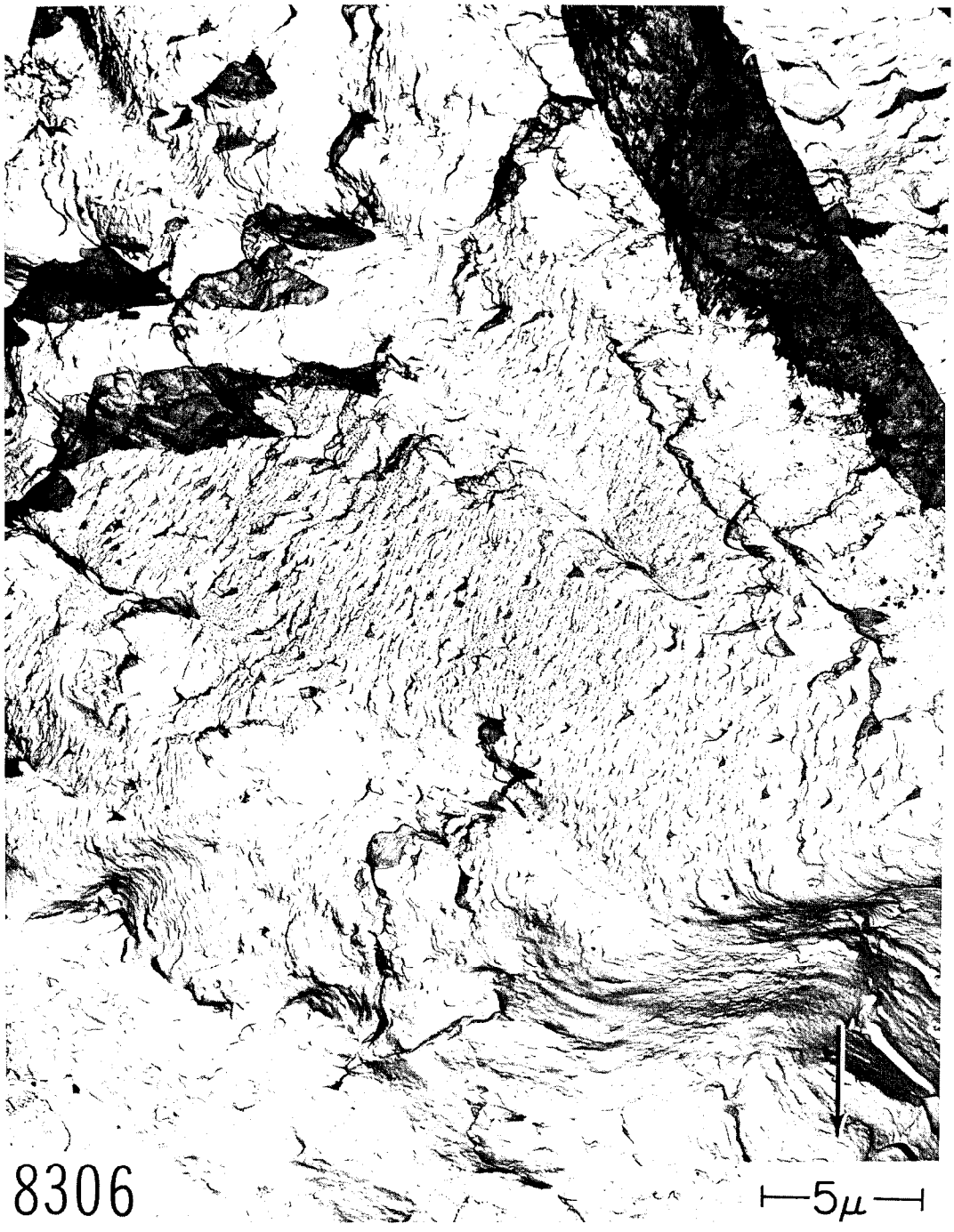

Fig. 7 - Tension-tension plane-strain fatigue markings in the WR fracture direction in 2020 T651 aluminum alloy. Cellulose acetate-carbon replication technique. Palladium shadowed. 6000X.

Fig. 8 - Tension-tension plane-strain fatigue markings in the WR fracture direction in 2020 T651 aluminum alloy. Cellulose acetate-carbon replication technique. Palladium shadowed. 6000X.

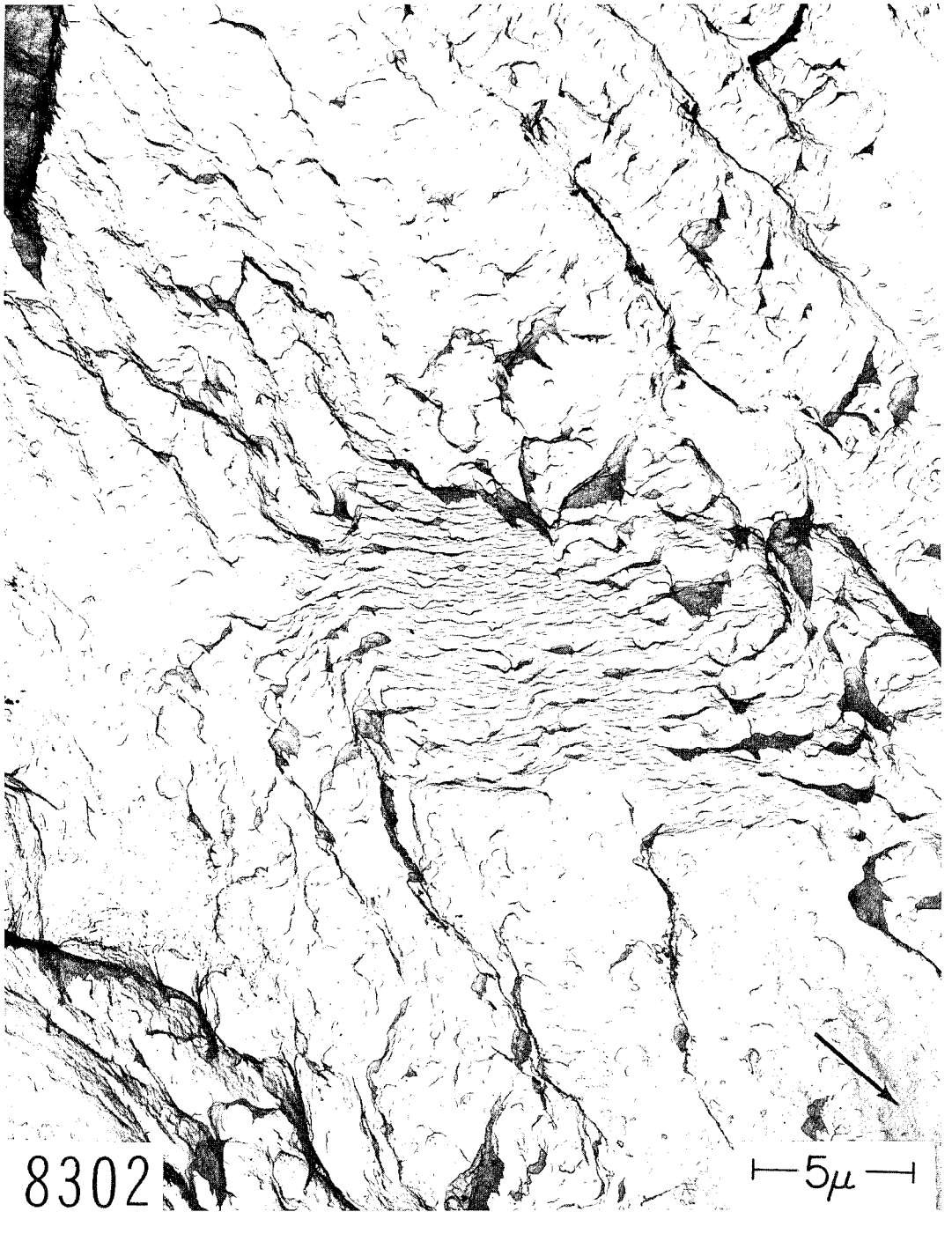

Fig. 9 - Tension-tension plane-strain fatigue markings in the WR fracture direction in 2020 T651 aluminum alloy. Cellulose acetate-carbon replication technique. Palladium shadowed. 6000X.

Fig. 10 - Tension-tension plane-strain fatigue markings in the WR fracture direction in 2020 T651 aluminum alloy. Cellulose acetate-carbon replication technique. Palladium shadowed. 6000X.

Fig. 11 - Tension-tension plane-strain fatigue markings in the WR fracture direction in 2020 T651 aluminum alloy. Cellulose acetate-carbon replication technique. Palladium shadowed. 6000X.

Fig. 12 - Tension-tension plane-strain fatigue markings in the WR fracture direction in 2020 T651 aluminum alloy. Short deep cracks are indicated by arrows. Cellulose acetate-carbon replication technique. Palladium shadowed. 6000X.

plate specimens. The specimens were 3/4 in. thick, 2 in. wide, and 5 in. long. The fatigue cracks were propagated under tension-tension loading (2000 pounds to 5000 pounds) at 3600 cycles per minute. The specimens were broken after precracking by impact loading. One specimen was tested in the TW direction.* The impact energies for both specimens were about 15 foot pounds. Plane strain fracture surfaces are shown in Figs. 1-3. Though these were taken from the RW specimen, they are characteristic of the fracture surface features of the plane strain surfaces in both specimens. Figure 1 shows typical dimples and some scraping artifacts (2). Figure 2 shows what is probably the effect of a banded structure. Figure 3 shows some of the flat regions (arrows) that were often associated with dimples. The fatigue markings for the RW direction are shown in Figs. 4-6. Figures 4 and 5 show that the fatigue markings often were mixed with tear dimples. Figures 5 and 6 show that striations often had tongue-shaped cracks (arrows) along parts of their lengths. Figures 7-12 show the fatigue markings found on the WR fracture surface. In Figs. 7 and 8, the fatigue markings are largely of the usual type (expected in aluminum alloys). However, Figs. 9-12 show, in increasing order, some markings that are not nicely shaped, smoothly curved groups of striations, but consist of short deep cracks as evidenced by thin films of carbon standing in relief on the replica surface (arrows in Fig. 12). Figure 12 also shows a patch of dimples in the upper portion.

b. 2024 T851 and T4

Specimens from three orientations (RW, WR, TR) were cut from a 5-in. thick plate of 2024 T851. The specimens were prepared and tested in the Mechanics Division and were of the short Single Edge Notched (SEN) type - 1/4 in. × 1-1/2 in. × 3.3 in. The fracture toughness values were 46.2 KSI $\sqrt{\text{in.}}$ for the RW direction, 37.5 KSI $\sqrt{\text{in.}}$ for the WR direction, and 23.2 KSI $\sqrt{\text{in.}}$ for the TR direction. The fatigue precracks were made in bending on a lathe and no records of the stresses were made. Figures 13-24 show the influence of orientation on the appearance of the fatigue markings. Figures 13-16 show the RW markings to be, in general, evenly spaced, gently curved striations arranged in groups that are separated by steps (black near-vertical lines in Fig. 15).

Figures 17-20 show typical fatigue surface features in the WR direction. The first three fractographs show short, deep cracks (arrows in Fig. 17) while the fourth (Fig. 20) shows a rather smooth surface. Figure 18 shows a "river pattern" of steps with the same sense of convergence that is found in cleavage (i.e., the fracture propagates down-river). It is also apparent in Fig. 18 that individual segments of the local fatigue crack propagated on different planes. The near horizontal dark bands across the top (between the large arrows) are examples of fatigue on a set of planes whose orientation as a group is different from that of the region as a whole. This strongly suggests a crystallographic influence on the fatigue mechanisms, with the fatigue crack segments possibly seeking to propagate along certain crystallographic planes. A number of these segments (small arrows) are seen to be replicated partially as secondary cracks and partially as portions of the major fracture surface.

Figures 21-24 show typical markings on the fracture surface created by propagating a fatigue crack in the TR direction. Figures 21 and 22 show large numbers of short secondary cracks that are approximately parallel to one another (their lengths extend in a direction from upper left to lower right). Figures 23 and 24 show markings that are much less systematic in their shapes, sizes, and orientations.

A 2024 T4 specimen of the Lehigh bend fatigue type (3), in which a surface crack was caused to propagate by high strain, balanced-cycle, tension-compression loading, yielded the fatigue markings shown in Figs. 25 and 26. This fatigue crack was propagated in the RW direction with the resulting fracture surface features having the same general characteristics as those shown for the same orientation in the previous specimens (Figs. 13-16).

*The ASTM designations of fracture directions are used in this report (1).

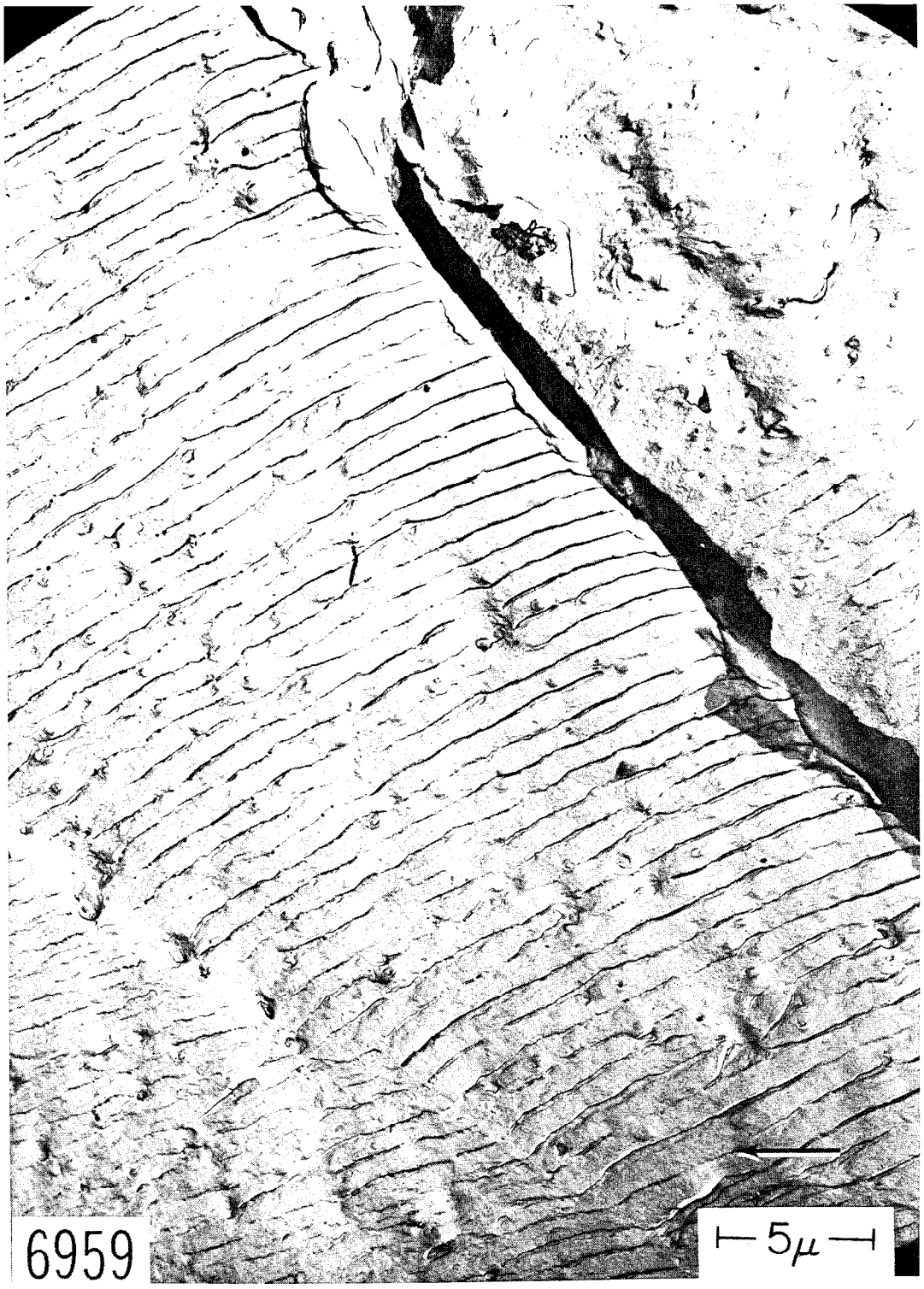

Fig. 13 - Tension-tension plane-strain RW fatigue markings in 2024 T851 aluminum alloy plate. Cellulose acetate-carbon replication technique. Palladium shadowed. 6000X.

Fig. 14 - Tension-tension plane-strain RW fatigue markings in 2024 T851 aluminum alloy plate. Cellulose acetate-carbon replication technique. Palladium shadowed. 6000X.

Fig. 15 - Tension-tension plane-strain RW fatigue markings in 2024 T851 aluminum alloy plate. Cellulose acetate-carbon replication technique. Palladium shadowed. 6000X.

Fig. 16 - Tension-tension plane-strain RW fatigue markings in 2024 T851 aluminum alloy plate. Cellulose acetate-carbon replication technique. Palladium shadowed. 6000X.

Fig. 17 - Tension-tension plane-strain WR fatigue markings in 2024 T851 aluminum alloy plate. Cellulose acetate-carbon replication technique. Palladium shadowed. 6000X.

Fig. 18 - Tension-tension plane-strain WR fatigue markings in 2024 T851 aluminum alloy plate. Cellulose acetate-carbon replication technique. Palladium shadowed. 6000X.

Fig. 19 - Tension-tension plane-strain WR fatigue markings in 2024 T851 aluminum alloy plate. Cellulose acetate-carbon replication technique. Palladium shadowed. 6000X.

Fig. 20 - Tension-tension plane-strain WR fatigue markings in 2024 T851 aluminum alloy plate. Cellulose acetate-carbon replication technique. Palladium shadowed. 6000X.

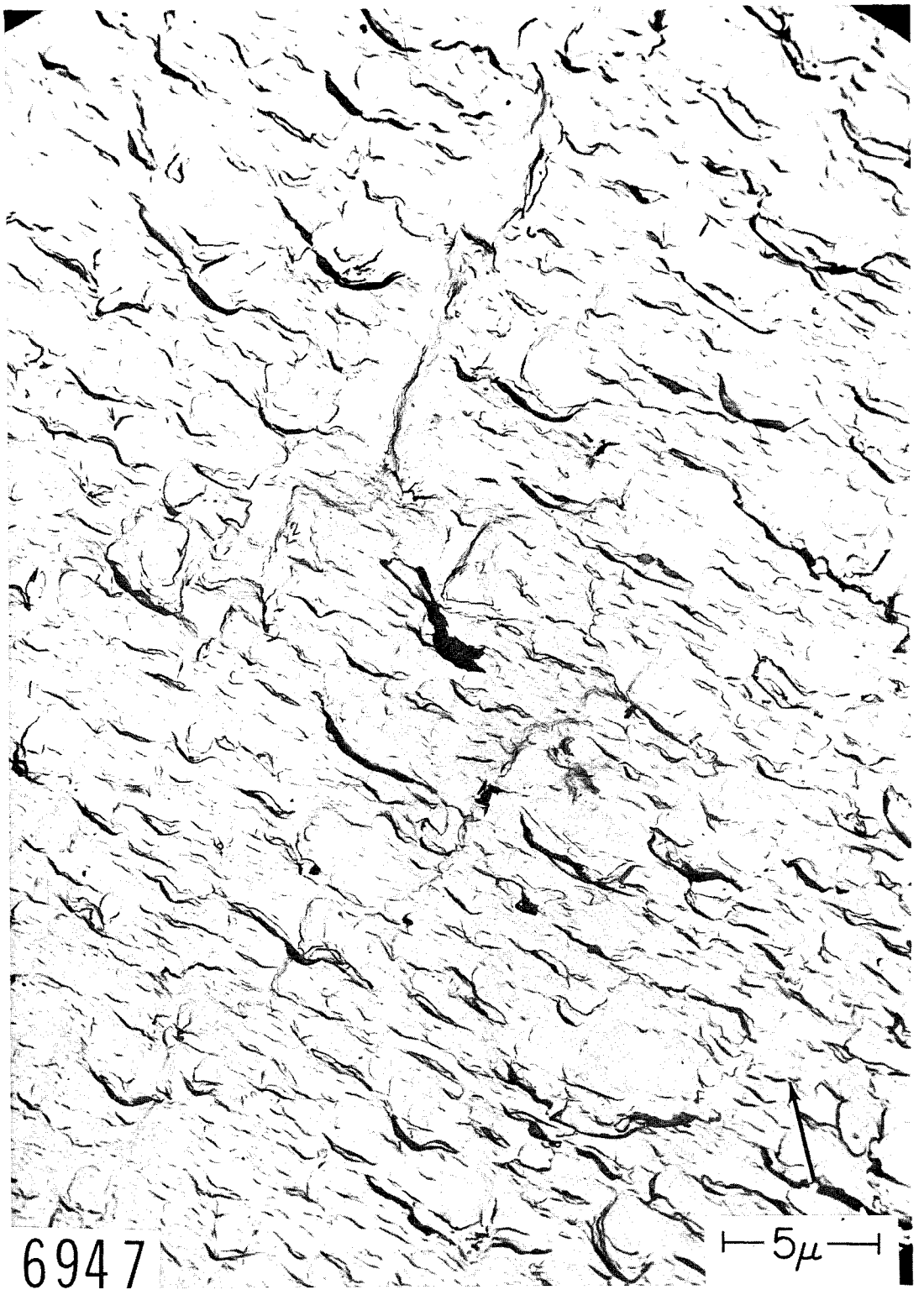

Fig. 21 - Tension-tension plane-strain TR fatigue markings in 2024 T851 aluminum alloy. Cellulose acetate-carbon replication technique. Palladium shadowed. 6000X.

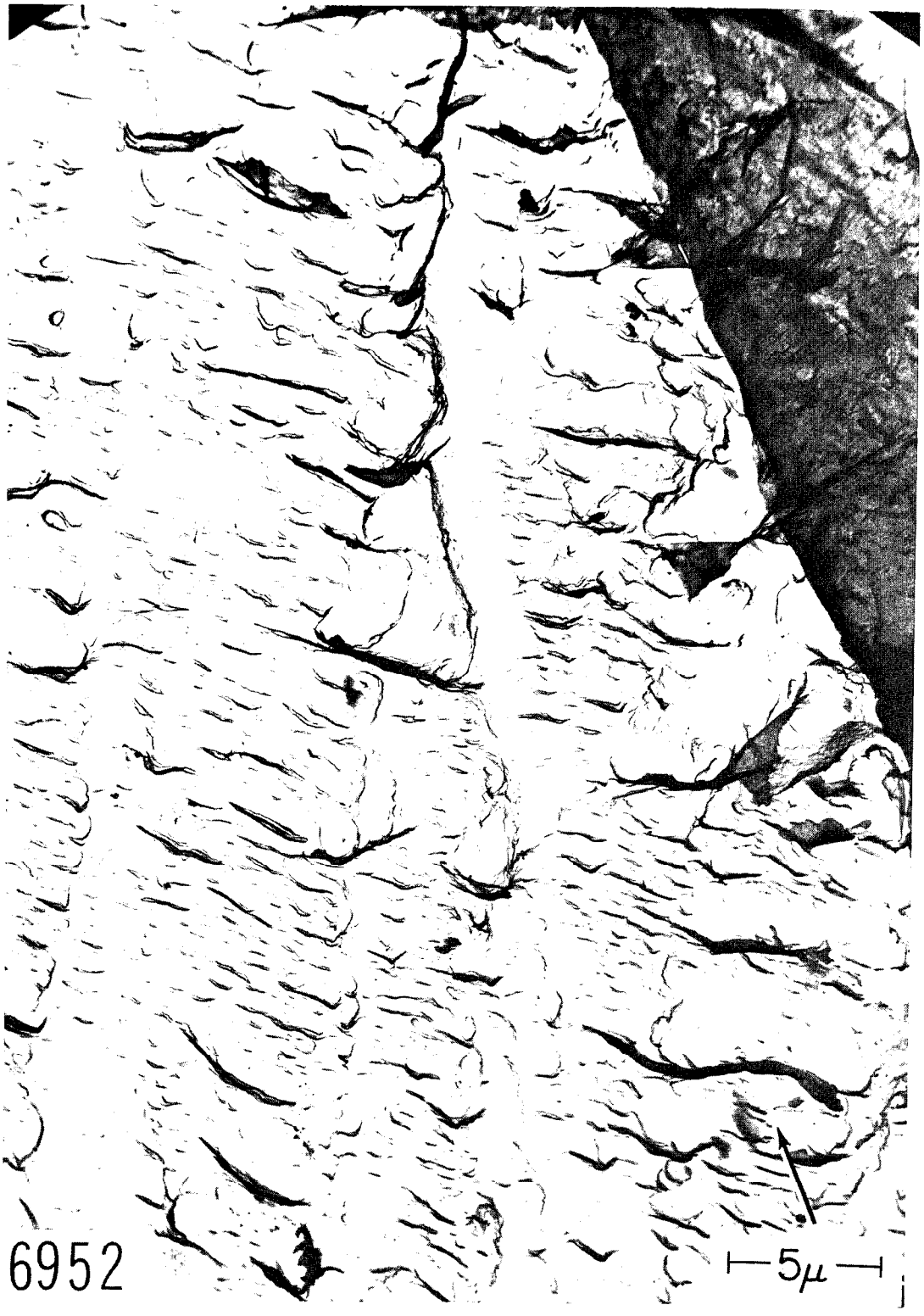

Fig. 22 - Tension-tension plane-strain TR fatigue markings in 2024 T851 aluminum alloy. Cellulose acetate-carbon replication technique. Palladium shadowed. 6000X.

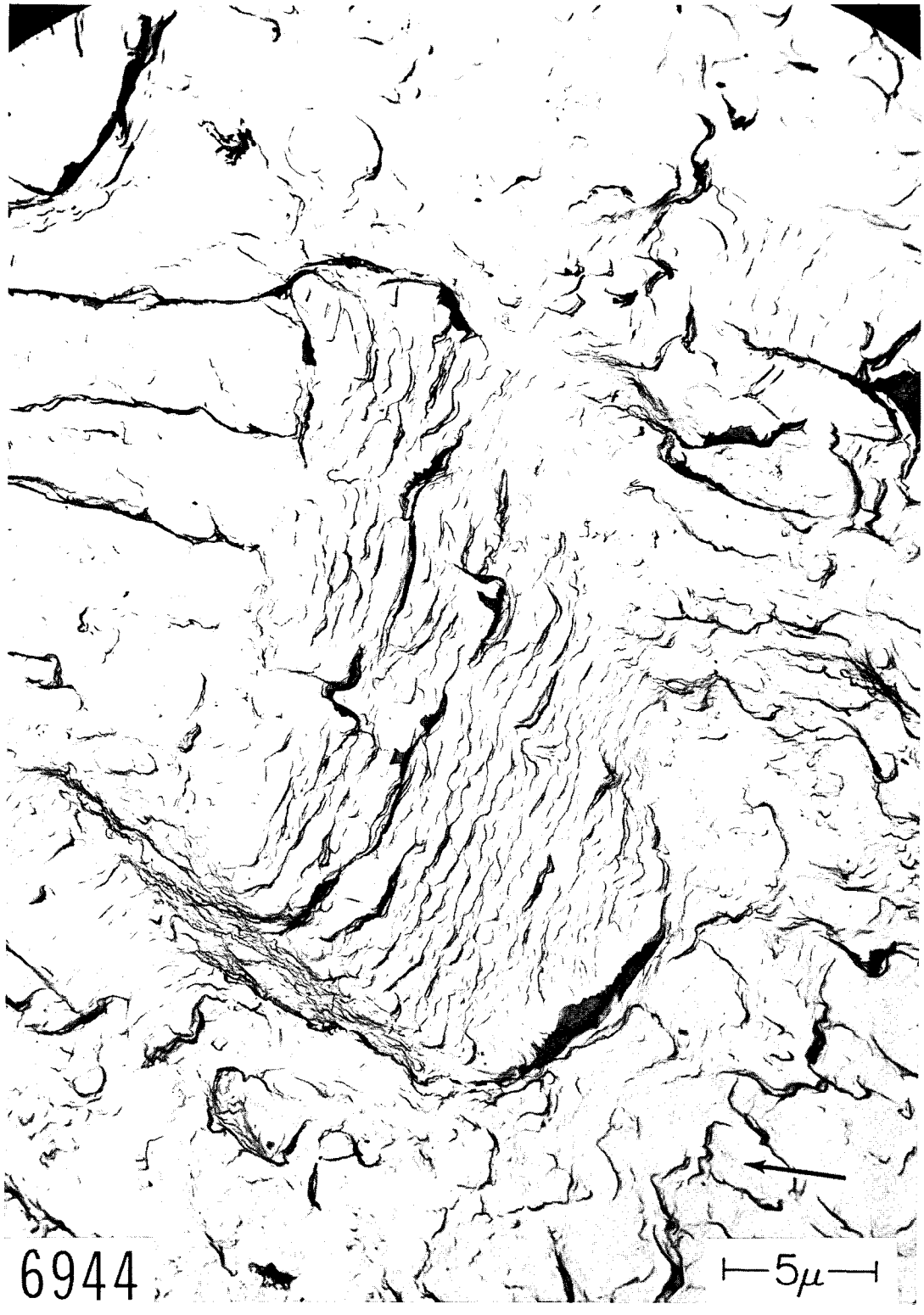

Fig. 23 - Tension-tension plane-strain TR fatigue markings in 2024 T851 aluminum alloy. Cellulose acetate-carbon replication technique. Palladium shadowed. 6000X.

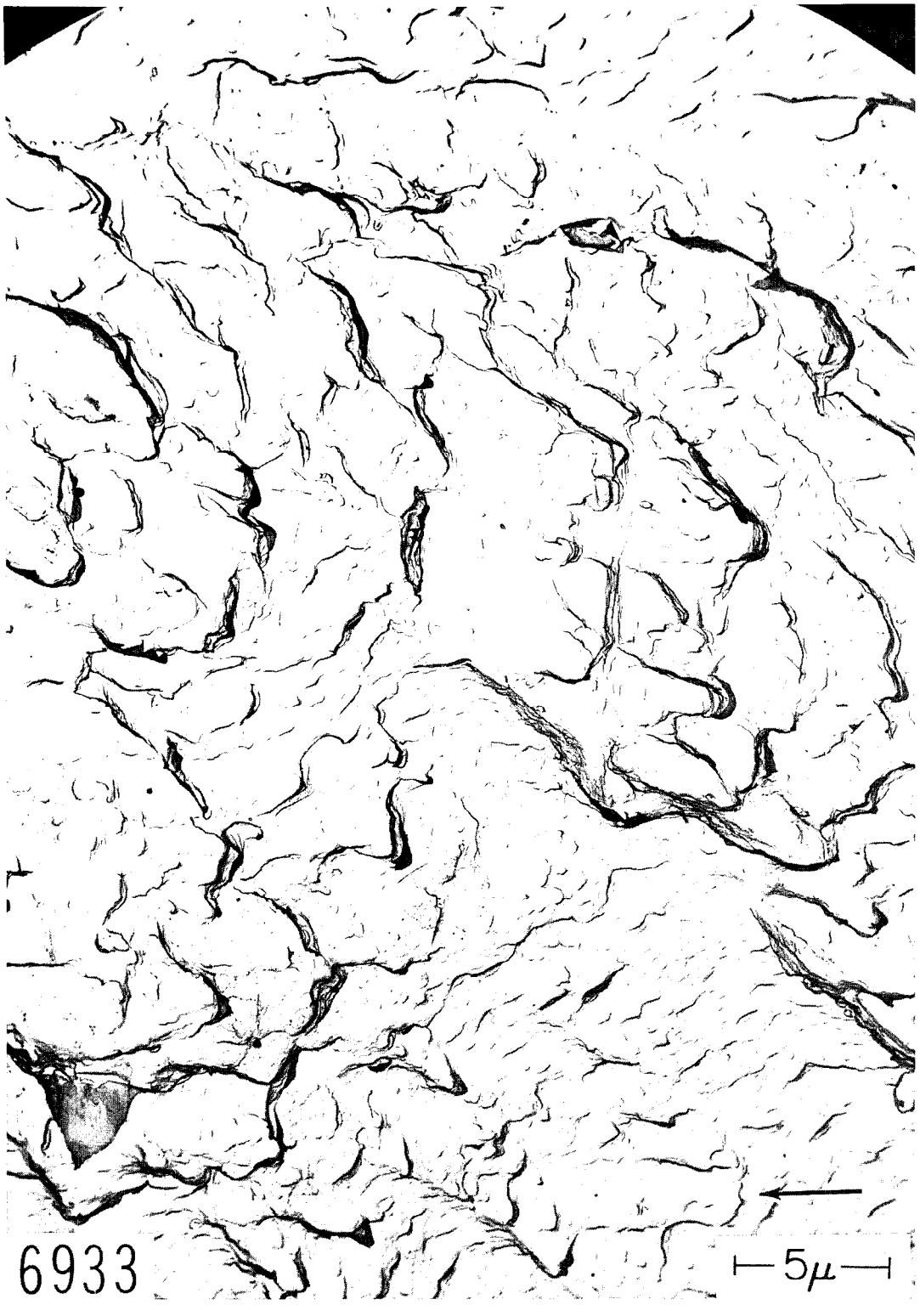

Fig. 24 - Tension-tension plane-strain TR fatigue markings in 2024 T851 aluminum alloy. Cellulose acetate-carbon replication technique. Palladium shadowed. 6000X.

Fig. 25 - Tension-compression high-strain RW fatigue markings in 2024 T4 aluminum alloy. Cellulose acetate-carbon replication technique. Palladium shadowed. 6000X.

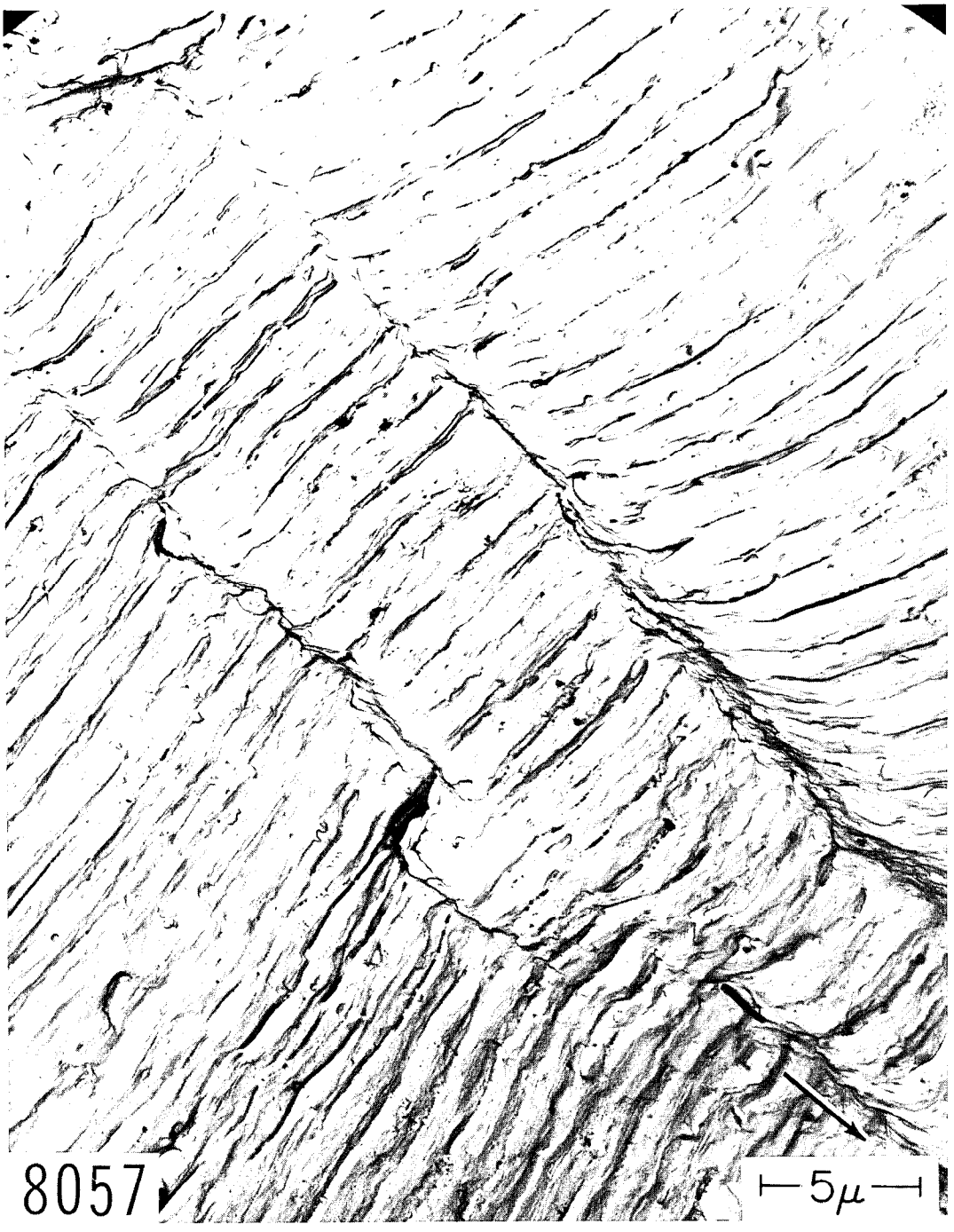

Fig. 26 - Tension-compression high-strain RW fatigue markings in 2024 T4 aluminum alloy. Cellulose acetate-carbon replication technique. Palladium shadowed. 6000X.

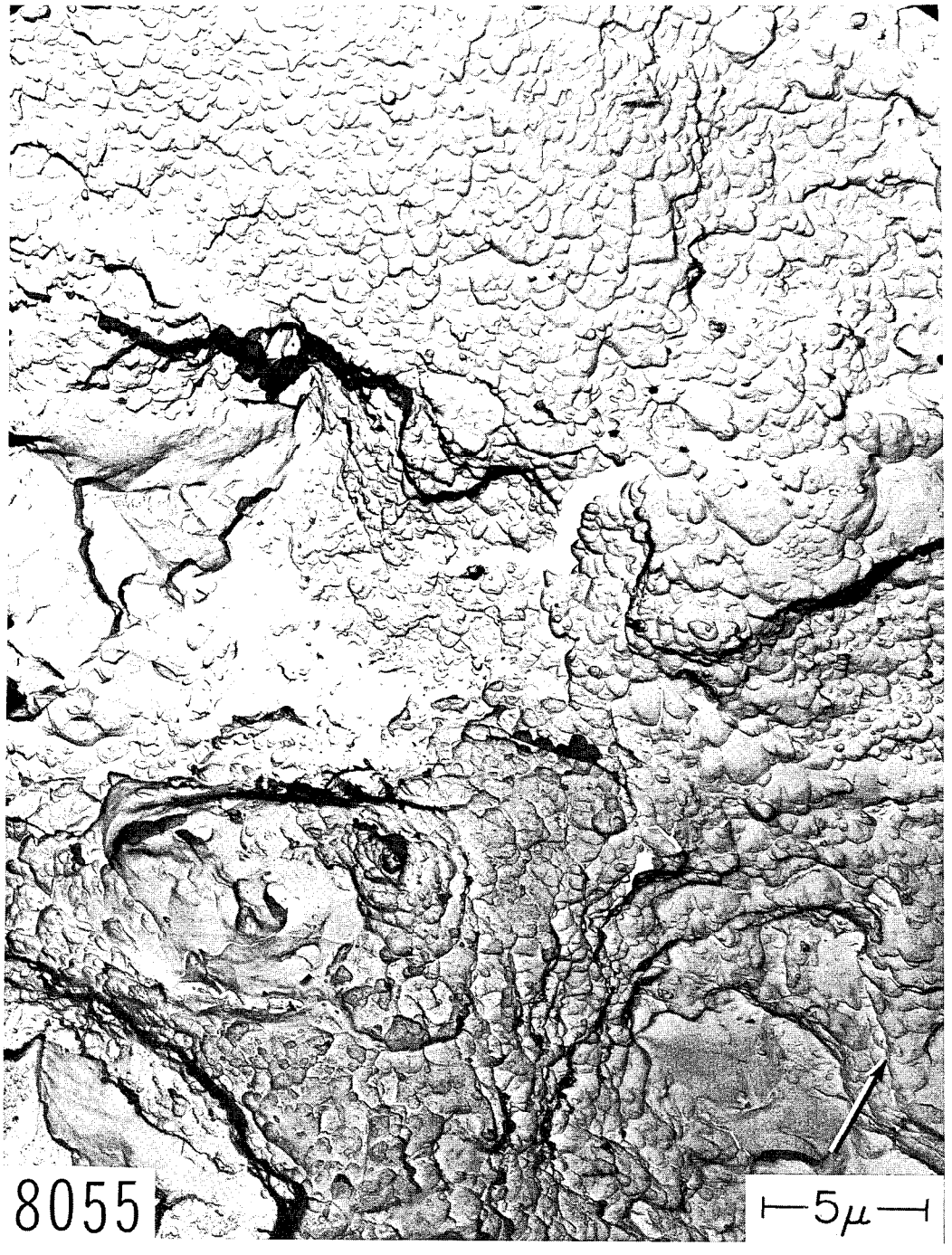

Fig. 27 - Plane-strain room temperature fracture in 2024 T4 aluminum alloy. Cellulose acetate-carbon replication technique. Palladium shadowed. 6000X.

Figures 27 and 28 show the flat fracture surface created after the fatigue test. Figures 27 and 28 show that fracture occurred almost entirely by void coalescence mechanisms.

c. 6061 T651

A Lehigh fatigue specimen, in which a surface crack is propagated by fully reversed conditions, was prepared in such a manner that the crack propagated in the WT

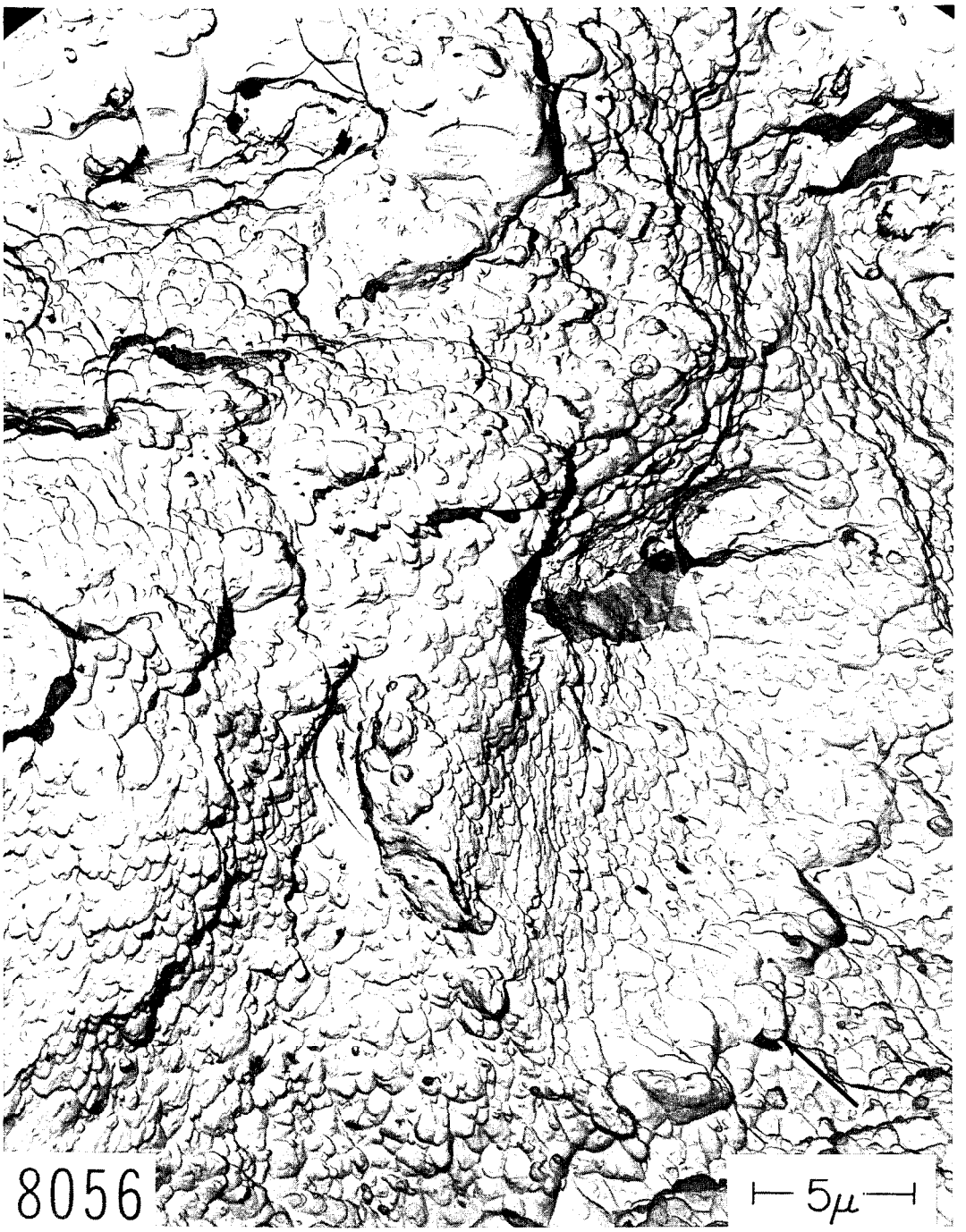

Fig. 28 - Plane-strain room temperature fracture in 2024 T4 aluminum alloy. Cellulose acetate-carbon replication technique. Palladium shadowed. 6000X.

direction. The fatigue surface features are shown in Figs. 29-31. The groups of striations in these fractographs are characteristic of those found in most aluminum alloys. Large and small dimples characterize the flat monotonic fracture surface shown in Figs. 32 and 33.

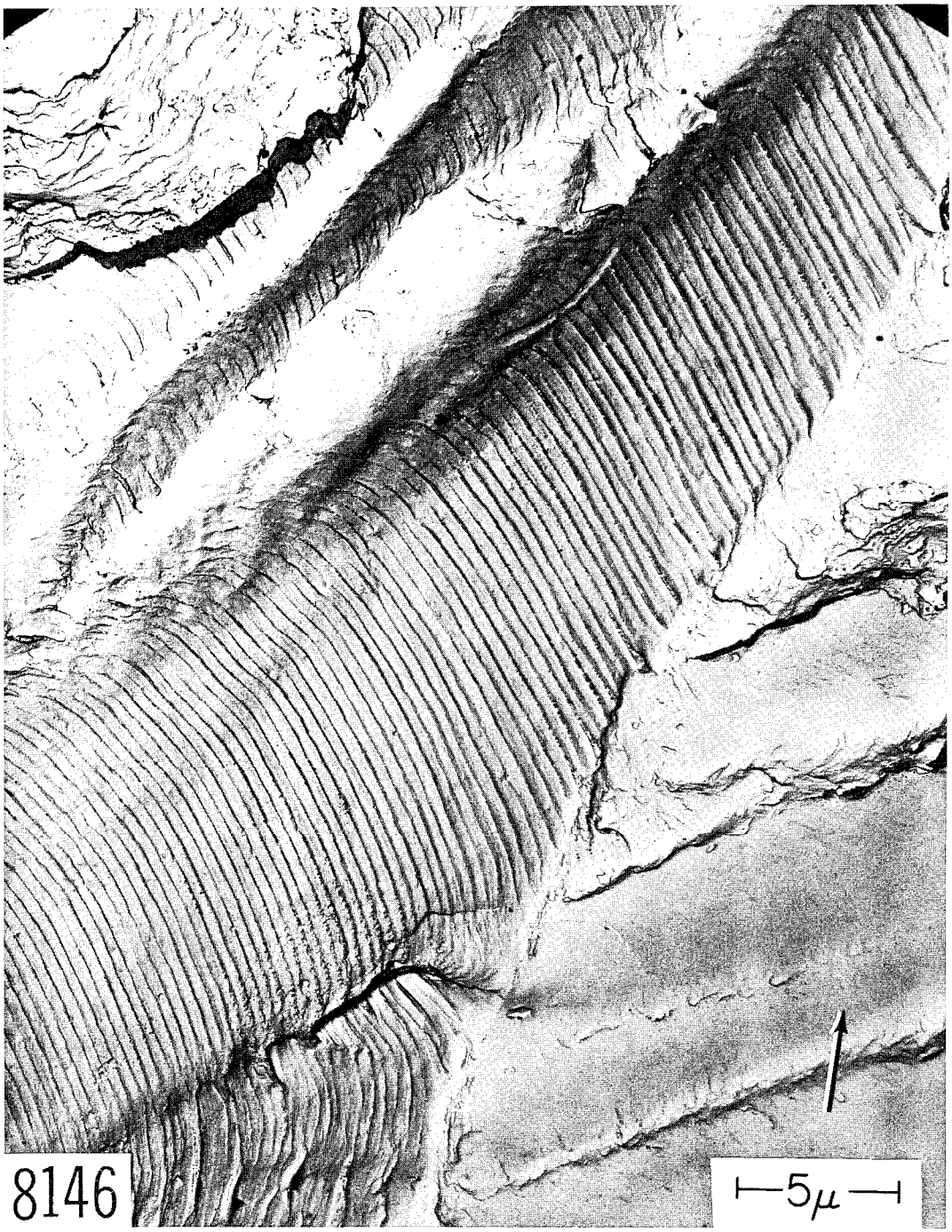

Fig. 29 - Plane-strain tension-compression high-strain room temperature fatigue markings in a crack propagated in the WR direction in a plate of 6061 T651 aluminum alloy. Cellulose acetate-carbon replication technique. Palladium shadowed. 6000X.

Fig. 30 - Plane-strain tension-compression high-strain room temperature fatigue markings in a crack propagated in the WR direction in a plate of 6061 T651 aluminum alloy. Cellulose acetate-carbon replication technique. Palladium shadowed. 6000X.

Fig. 31 - Plane-strain tension-compression high-strain room temperature fatigue markings in a crack propagated in the WR direction in a plate of 6061 T541 aluminum alloy. Cellulose acetate-carbon replication technique. Palladium shadowed. 6000X.

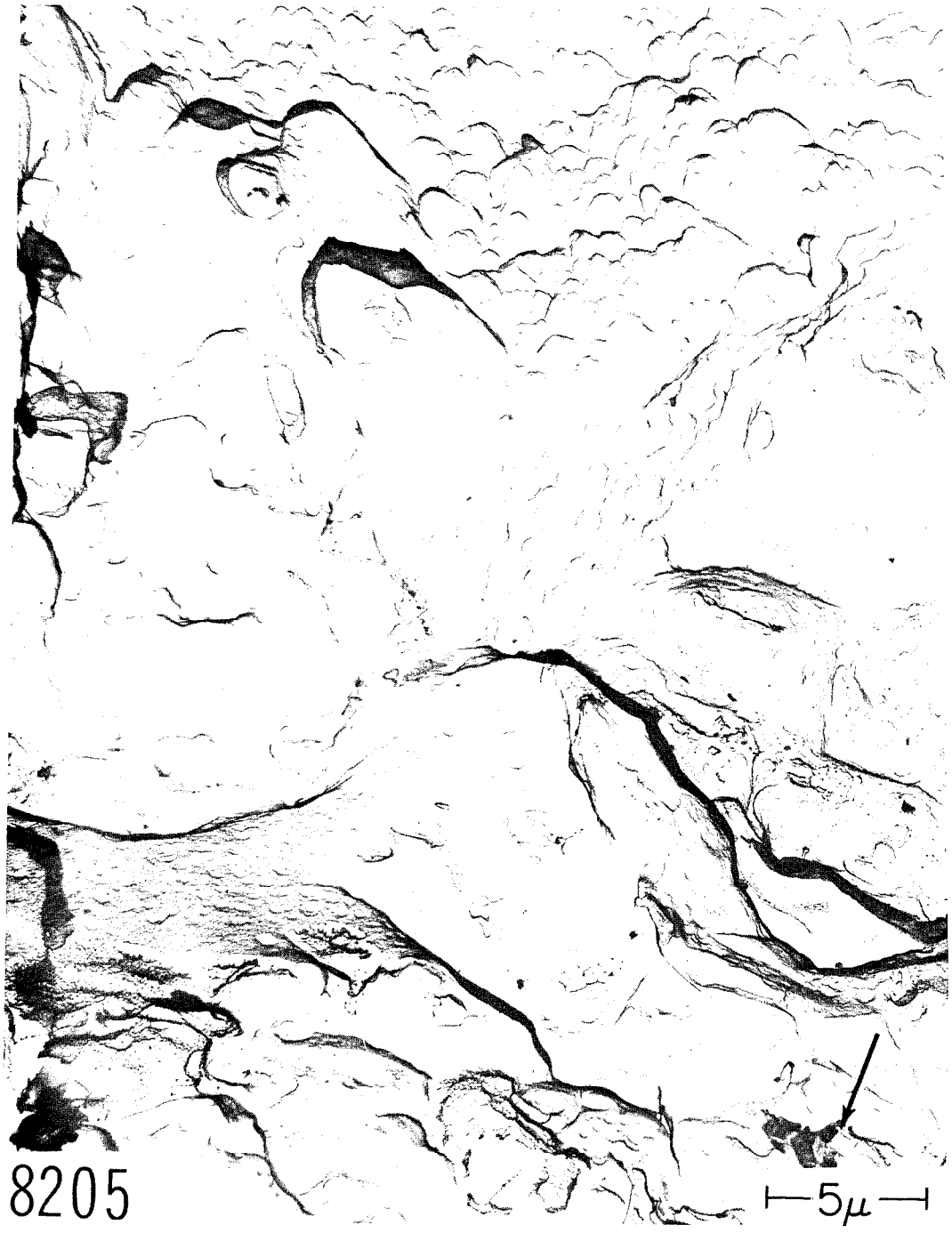

Fig. 32 - Room temperature plane-strain monotonic fracture in 6061 T651 aluminum alloy. Cellulose acetate-carbon replication technique. 6000X.

Fig. 33 - Room temperature plane-strain monotonic fracture in 6061 T651 aluminum alloy. Cellulose acetate-carbon replication technique. 6000X.

d. 7178 T6

A short single-edge notch specimen of 7178 T6 aluminum alloy was fatigue pre-cracked and broken with an indicated toughness K_{Ic} of 21.3 KSI $\sqrt{\text{in.}}$ The fatigue markings are shown in Figs. 34 and 35. Dimples in the plane strain (monotonic) fracture surface are shown in Figs. 36-38.

Fig. 34 - Room temperature tension-tension fatigue markings in 7178 T6 aluminum alloy. Cellulose acetate-carbon replication technique. Palladium shadowed. 21,000X.

Fig. 35 - Room temperature tension-tension fatigue markings in 7178 T6 aluminum alloy. Cellulose acetate-carbon replication technique. Palladium shadowed. 21,000X.

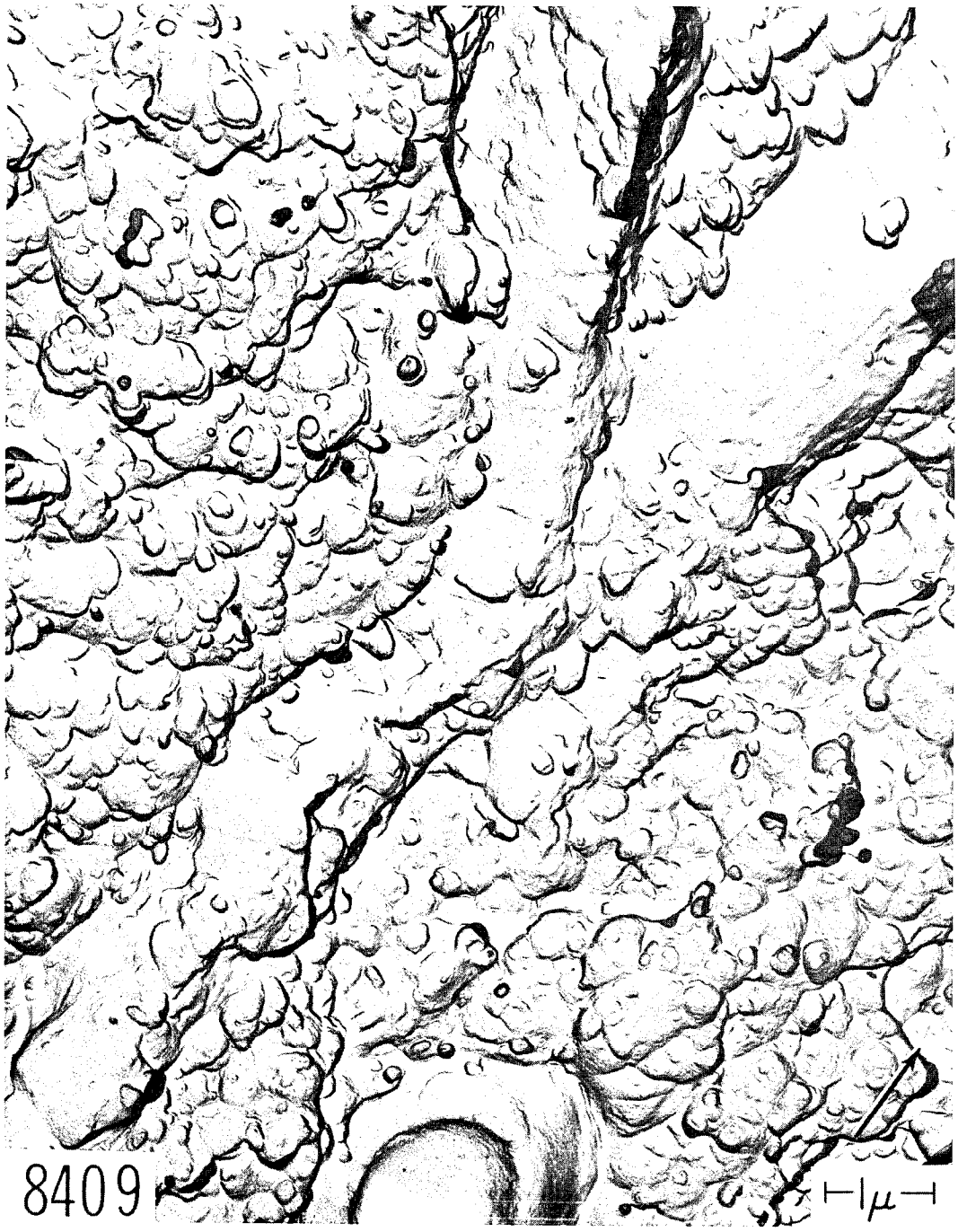

Fig. 36 - Room temperature monotonic plane-strain fracture surface in 7178 T6 aluminum alloy. Cellulose acetate-carbon replication technique. 21,000X.

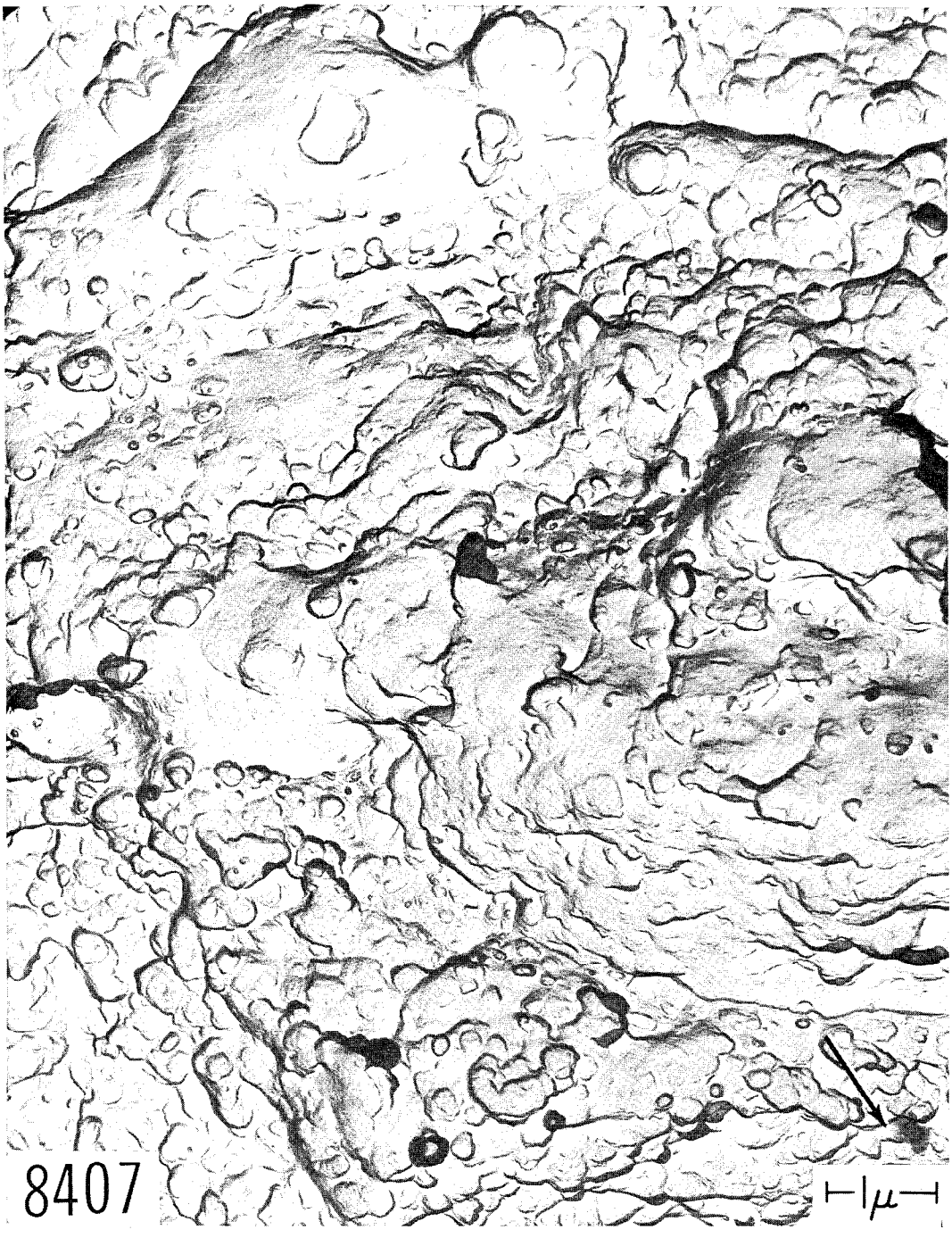

Fig. 37 - Room temperature monotonic plane-strain fracture surface in 7178 T6 aluminum alloy. Cellulose acetate-carbon replication technique. 21,000X.

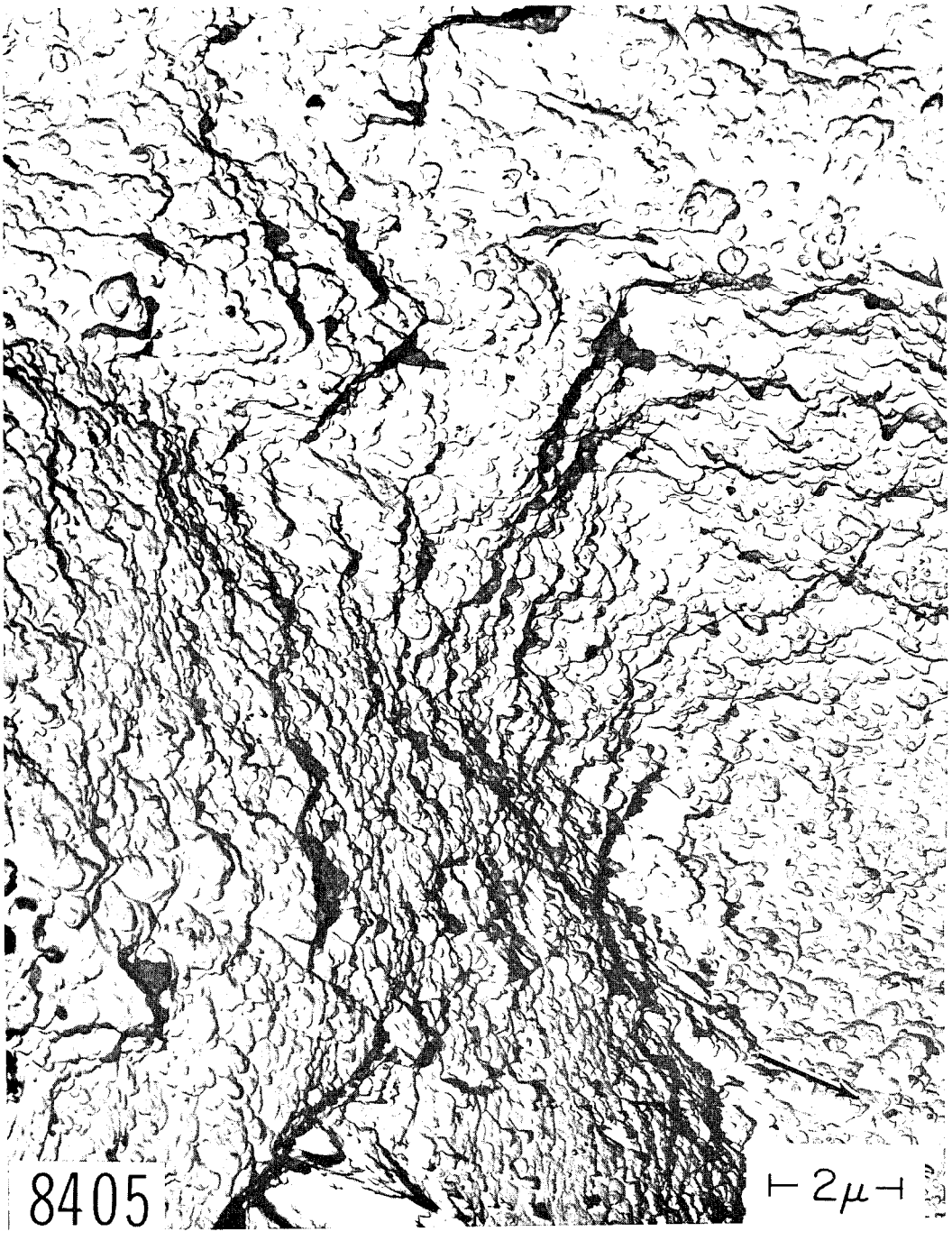

Fig. 38 - Room temperature monotonic plane-strain fracture surface in 7178 T6 aluminum alloy. Cellulose acetate-carbon replication technique. 12,000X.

e. 7075 T6

Figures 39-41 show fatigue markings and Figs. 42 and 43 show dimples that characterize the fatigue and monotonic flat fracture surfaces of a 7075 T6 plate Lehigh fatigue specimen. These striations were formed under conditions of tension-compression with loads sufficient to cause high strains in both tension and compression.

Fig. 39 - Room temperature tension-compression high-strain fatigue markings in 7075 T6 aluminum alloy plate. Cellulose acetate-carbon replication technique. Palladium shadowed. 6000X.

Fig. 40 - Room temperature tension-compression high-strain fatigue markings in 7075 T6 aluminum alloy plate. Cellulose acetate-carbon replication technique. Palladium shadowed. 6000X.

Fig. 41 - Room temperature tension-compression high-strain fatigue markings in 7075 T6 aluminum alloy plate. Cellulose acetate-carbon replication technique. Palladium shadowed. 6000X.

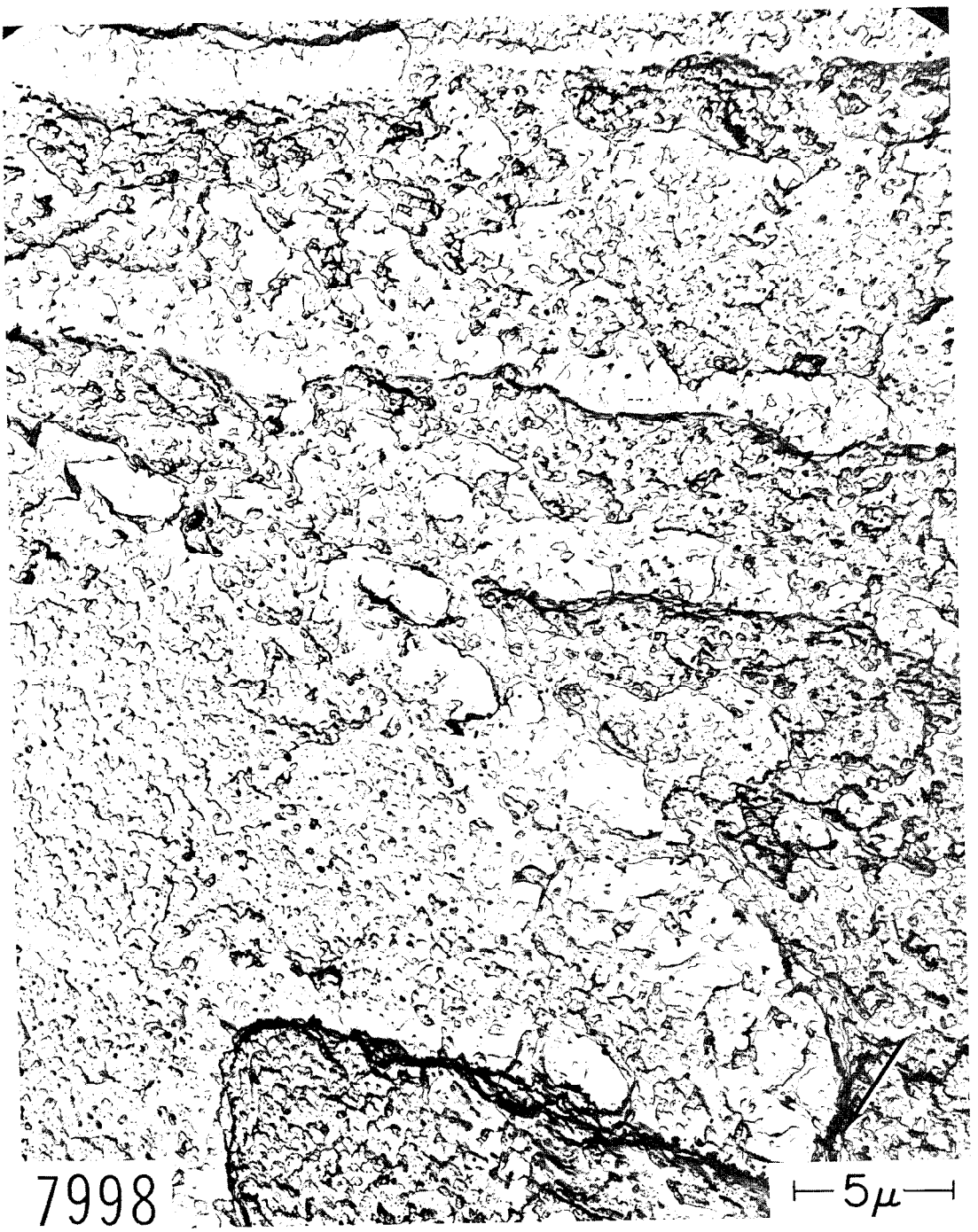

Fig. 42 - Room temperature monotonic plane-strain fracture surface of 7075 T6 aluminum alloy plate. Cellulose acetate-carbon replication technique. Palladium shadowed. 6000X.

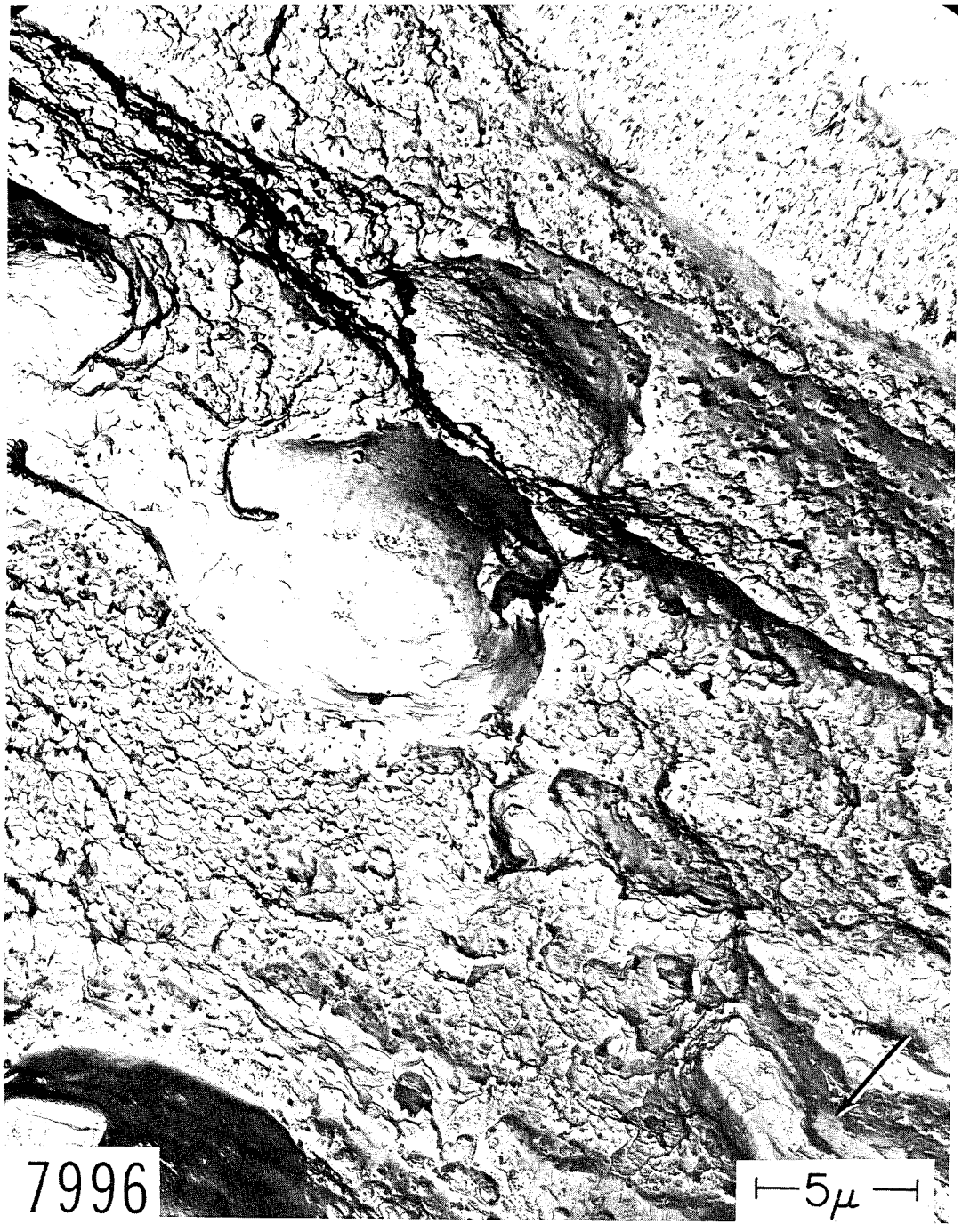

Fig. 43 - Room temperature monotonic plane-strain fracture surface of 7075 T6 aluminum alloy plate. Cellulose acetate-carbon replication technique. Palladium shadowed. 6000X.

Four categories of fine-scale fracture surfaces have been identified in the monotonic fracture surfaces of a notched-round tensile bar cut from a 1 in. thick 7075 T6 plate. Replicas were prepared from both fracture surfaces by shadowing with palladium and backing with carbon and then freeing the replica by electropolishing.*

*Specimen was made the anode in a beaker of 7.8% perchloric acid, 12% distilled water, 70% ethyl alcohol, and 10% Butylcellosolve. Replicas were freed in 5 to 10 minutes.

Precision matching studies showed that fracture occurred by void coalescence (Figs. 44-47), stretching (4) around broken intermetallic particles (Figs. 44-47), separation along boundaries between intermetallic particles and cleavage of intermetallic particles (Figs. 48-51), and a low deformation rupture process which is presently unidentified

Fig. 44 - Tear dimples in plane-strain monotonic fracture surface of a 7075 T6 specimen which was broken at room temperature. Surface is matched with that shown in Fig. 45. Palladium shadowed direct carbon replica. 11,000X.

Fig. 45 - Tear dimples in plane-strain monotonic fracture surface of a 7075 T6 specimen which was broken at room temperature. Surface is matched with that shown in Fig. 44. Palladium shadowed direct carbon replica. 11,000X.

(Figs. 50 and 51). Both the region bounded by arrows in Fig. 50 and its mating region on the opposite surface have been studied stereoscopically and have been seen to be concave fracture surfaces – but only slightly so. The fine detail in these regions is in general too small to be analyzed for elevation above or depression below the surrounding fracture

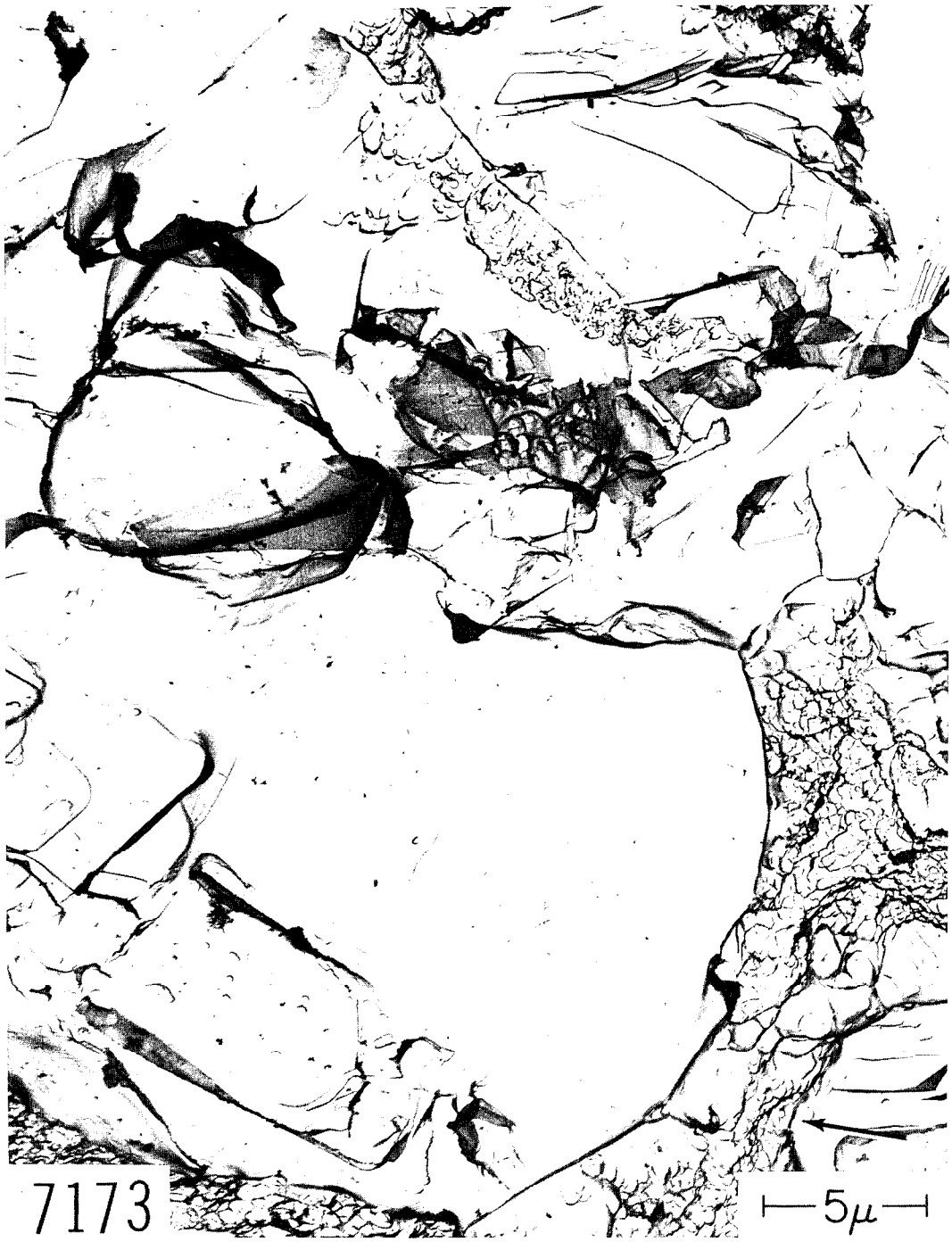

Fig. 46 - Smooth stretched surfaces formed by extreme plastic deformation of matrix at particle-matrix interfaces in room temperature monotonic plane-strain fracture of 7075 T6 specimen. Matched with Fig. 47. Palladium-shadowed direct carbon replication technique. 6000X.

surface. Some of the larger features, such as the circled ones, have been found to mate, with a raised feature on one surface fitting into a depressed feature on the other surface. More work is necessary before the underlying mechanisms can be understood. The one significant observation that can be reported so far is that considerably less local

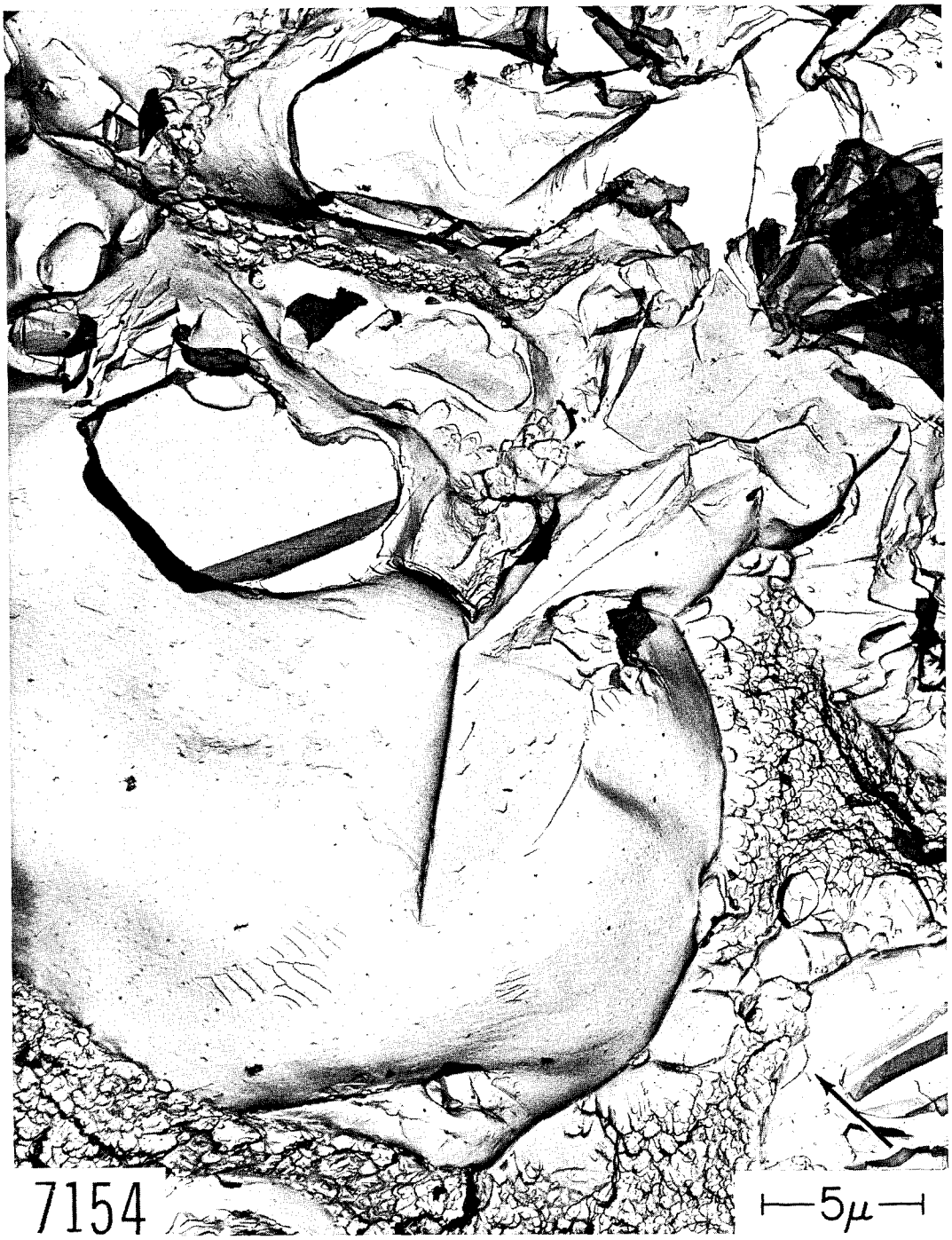

Fig. 47 - Smooth stretched surfaces formed by extreme plastic deformation of matrix at particle-matrix interfaces in room temperature monotonic plane-strain fracture of 7075 T6 specimen. Matched with Fig. 46. Palladium-shadowed direct carbon replication technique. 6000X.

deformation is involved than in the mechanisms of stretching or microvoid coalescence. Thinner replicas of higher fidelity than those used in this study will be required to study the sub-micron features of – and the fracture mechanisms which create – these little understood surfaces.

Fig. 48 - Separation at intermetallic particle interface and cleavage of intermetallic particles in room temperature monotonic plane-strain fracture of 7075 T6 aluminum alloy. Matched with Fig. 49. Palladium-shadowed direct carbon replication technique. 10,500X.

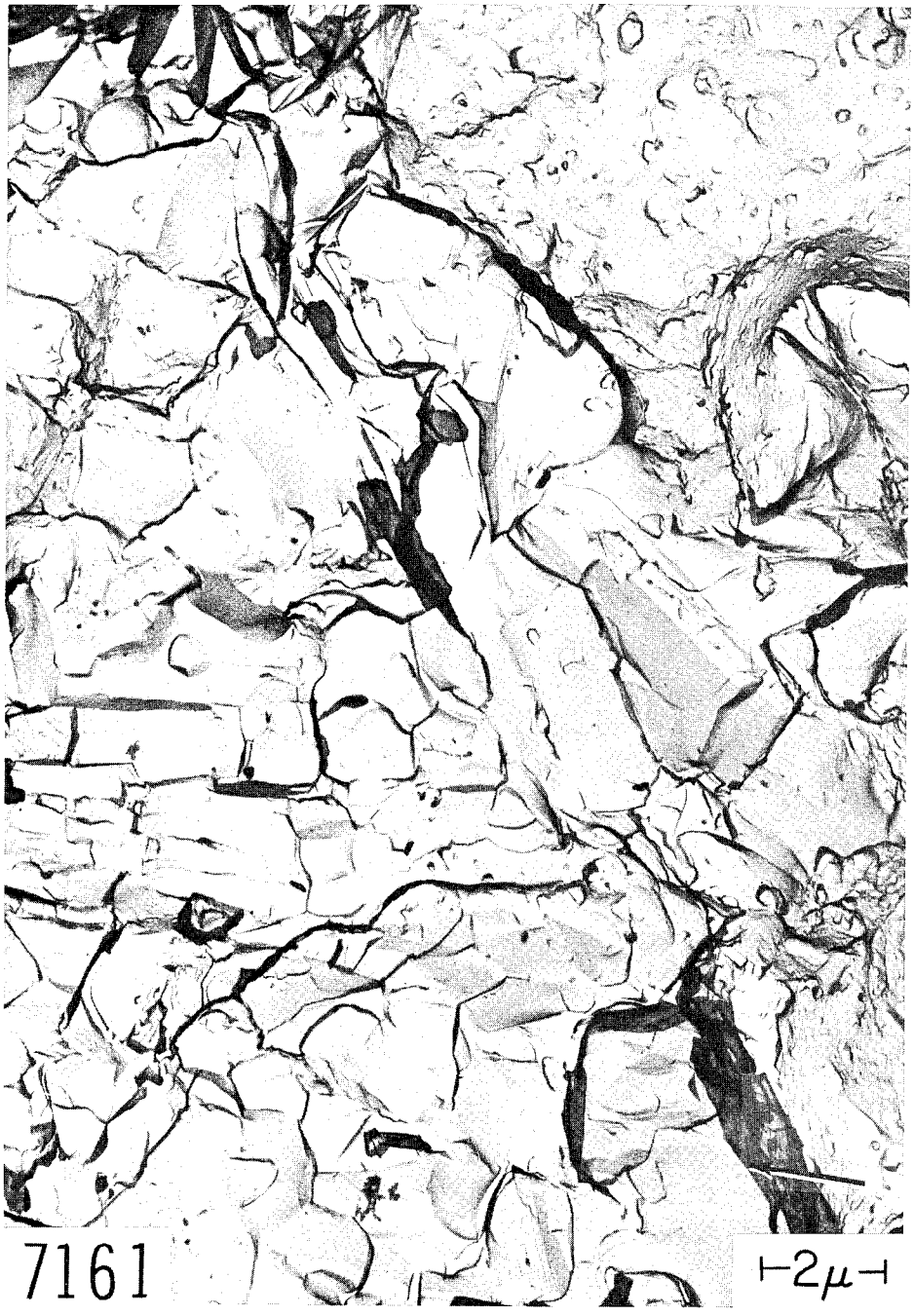

Fig. 49 - Separation at intermetallic particle interface and cleavage of intermetallic particles in room temperature monotonic plane-strain fracture of 7075 T6 aluminum alloy. Matched with Fig. 48. Palladium-shadowed direct carbon replication technique. 10,500X.

Fig. 50 - Example (bounded by arrows) of a fracture surface feature in 7075 T6 aluminum alloy that is formed by unknown, but low deformation processes. Region on the left was formed by deformation at particle-matrix interface. Matched with Fig. 51. Palladium-shadowed direct carbon replication technique. 10,500X.

Fig. 51 - Example of a fracture surface feature in 7075 T6 aluminum alloy that is formed by unknown, but low deformation, processes. Region on the left was formed by deformation at particle-matrix interface. Matched with Fig. 50. Palladium-shadowed direct carbon replication technique. 10,500X.

3. CHARACTERIZATION OF TITANIUM FRACTURE SURFACES

All of the monotonic overload fracture surfaces in the titanium alloys examined so far, regardless of the temperature at which they were formed, have been formed by plastic flow mechanisms. The fracture surfaces are composed of variously sized and shaped dimples and stretched regions.

a. Low-Interstitial Unalloyed Titanium

Figures 52 and 53 show typical features from a pure titanium fracture surface. The specimen was a Lehigh type fatigue specimen, shown in Fig. 54. Typical fatigue markings are shown in Figs. 55 and 56. Individual striations are generally straight.

Fig. 52 - Monotonic fracture surface of a low interstitial titanium specimen broken at room temperature. Cellulose acetate-carbon replication technique. Palladium shadowed. 6000X.

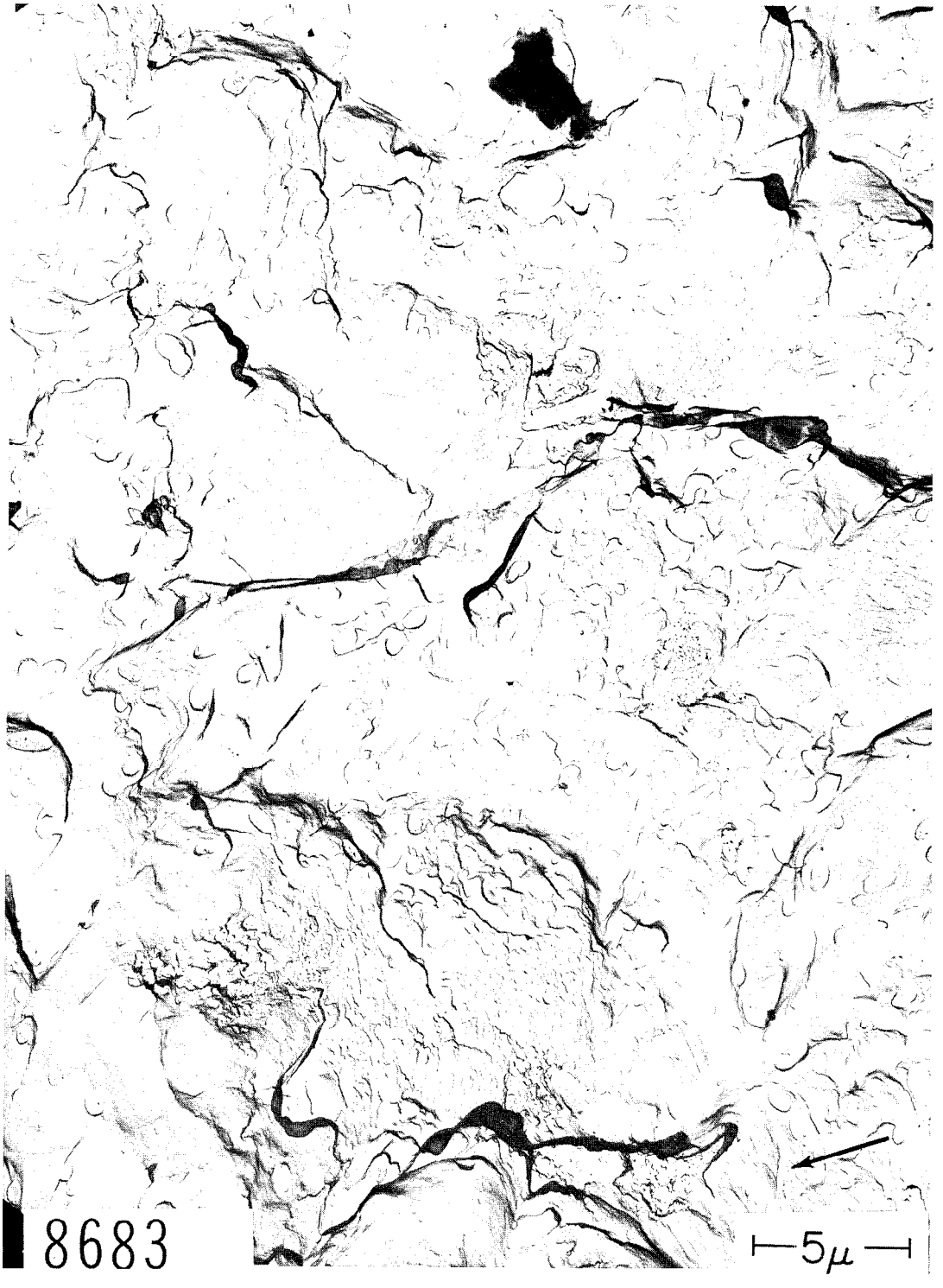

Fig. 53 - Monotonic fracture surface of a low interstitial titanium specimen broken at room temperature. Cellulose acetate-carbon replication technique. Palladium shadowed. 6000X.

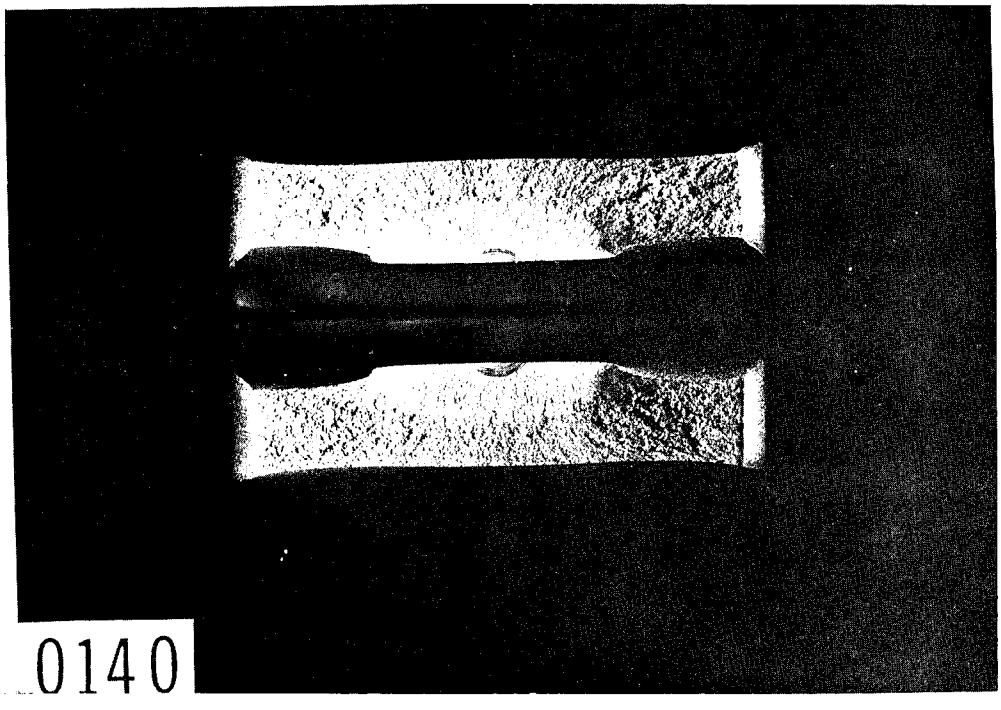

Fig. 54 - Lehigh fatigue specimen of low interstitial unalloyed titanium. 1X.

Fig. 55 - Fatigue markings in low interstitial unalloyed titanium. Cellulose acetate-carbon replication technique. Palladium shadowed. 6000X.

Fig. 56 - Fatigue markings in low interstitial unalloyed titanium. Cellulose acetate-carbon replication technique. Palladium shadowed. 6000X.

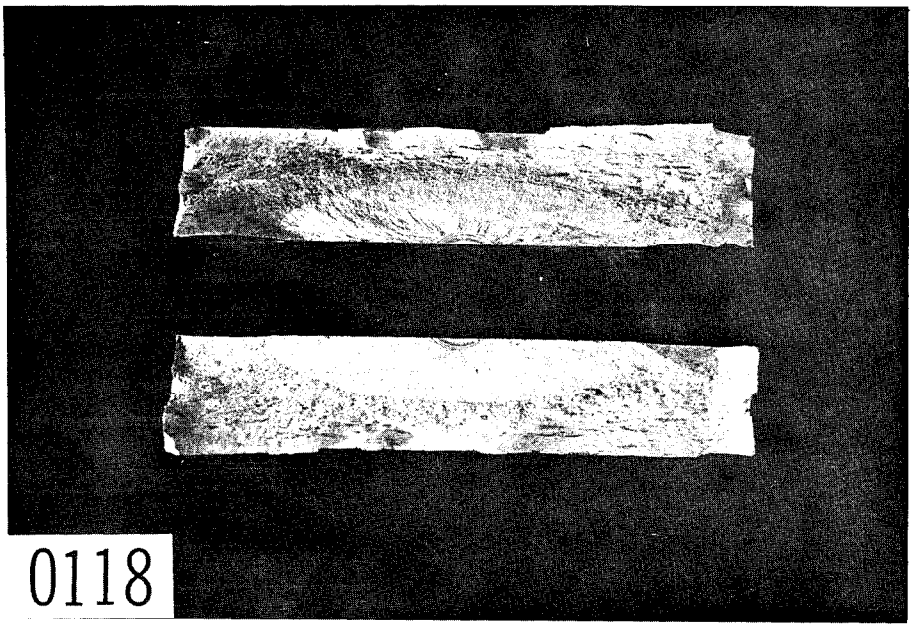

Fig. 57 - Macroscopic view of a Lehigh fatigue specimen of Ti-6Al-4V showing fatigue and monotonic fracture surfaces. 1X.

b. Ti-6Al-4V

Figure 57 shows the macroscopic appearance of the Lehigh specimen of Ti-6Al-4V broken partially by fatigue and then broken monotonically in a tensile machine. The dimpled appearance of the overload fracture surface is seen in Fig. 58. Fatigue markings are shown in Figs. 59-61.

Figure 62 shows a 1-1/2 in. wide center-cracked sheet crack-toughness specimen of this material in the solution treated condition with an RW crack propagation direction, and Fig. 63 shows a similar specimen with a WR crack propagation direction. Characteristic fatigue markings are shown in Fig. 64 for the RW direction and Fig. 65 for the WR direction. Both specimens were tension-tension fatigued for 25,000 cycles with the load ranging from 1200 pounds to 3000 pounds. Striations are well marked in these particular fractographs, but areas without striations are common. Marked differences in elevation between patches of striations are visible when stereoscopic pairs are examined.

c. Ti-8Al-1Mo-1V

Figure 66 shows a short single-edge-notched type specimen of a Ti-8Al-1Mo-1V, 0.052 in. thick and 0.981 in. wide. A K_{Ic} of 45.2 KSI $\sqrt{in.}$ was calculated for this specimen. A portion of the plane strain fracture surface is seen in Fig. 67. Figures 68 and 69 show characteristic fatigue markings. Loads during the fatigue cracking were not recorded.

d. Ti-4Al-3Mo-1V

Two center-cracked sheet specimens, one with a WR crack direction and one with an RW direction are shown in Figs. 70 and 71 respectively. The WR fatigue markings are shown in Fig. 72 and the RW markings are shown in Figs. 73 and 74. The three fractographs show characteristic fracture appearances for the WR and RW modes of specimens aged 12 hours at 1150°F (R_c 33), and the RW mode of a specimen aged 12 hours at 925°F

Fig. 58 - Dimpled rupture appearance of monotonic plane-strain fracture in specimen shown in Fig. 57. Cellulose acetate-carbon replication technique. Palladium shadowed. 6000X.

Fig. 59 - Fatigue markings in Ti-6Al-4V. Cellulose acetate-carbon replication technique. Palladium shadowed. 6000X.

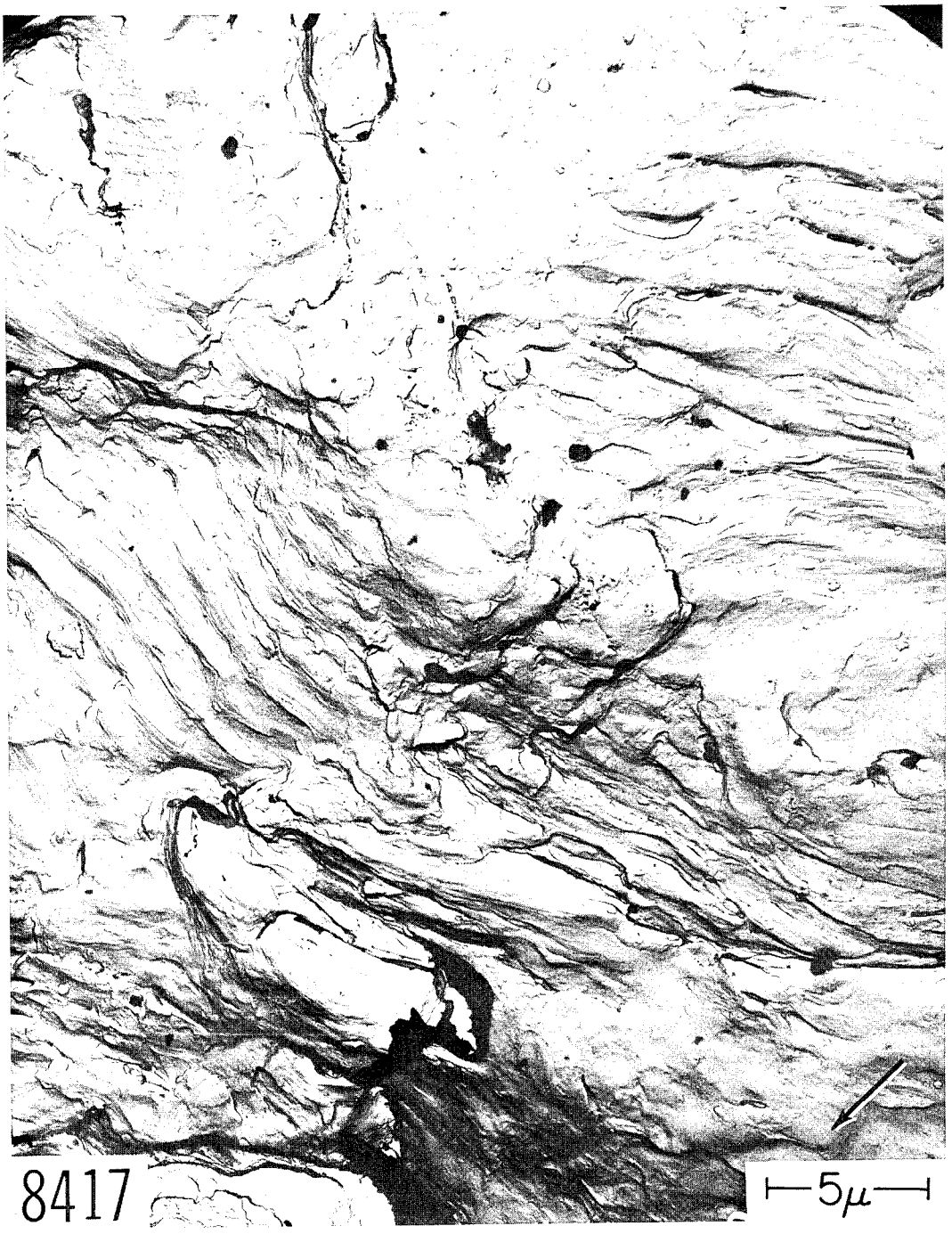

Fig. 60 - Fatigue markings in Ti-6Al-4V. Cellulose acetate-carbon replication technique. Palladium shadowed. 6000X.

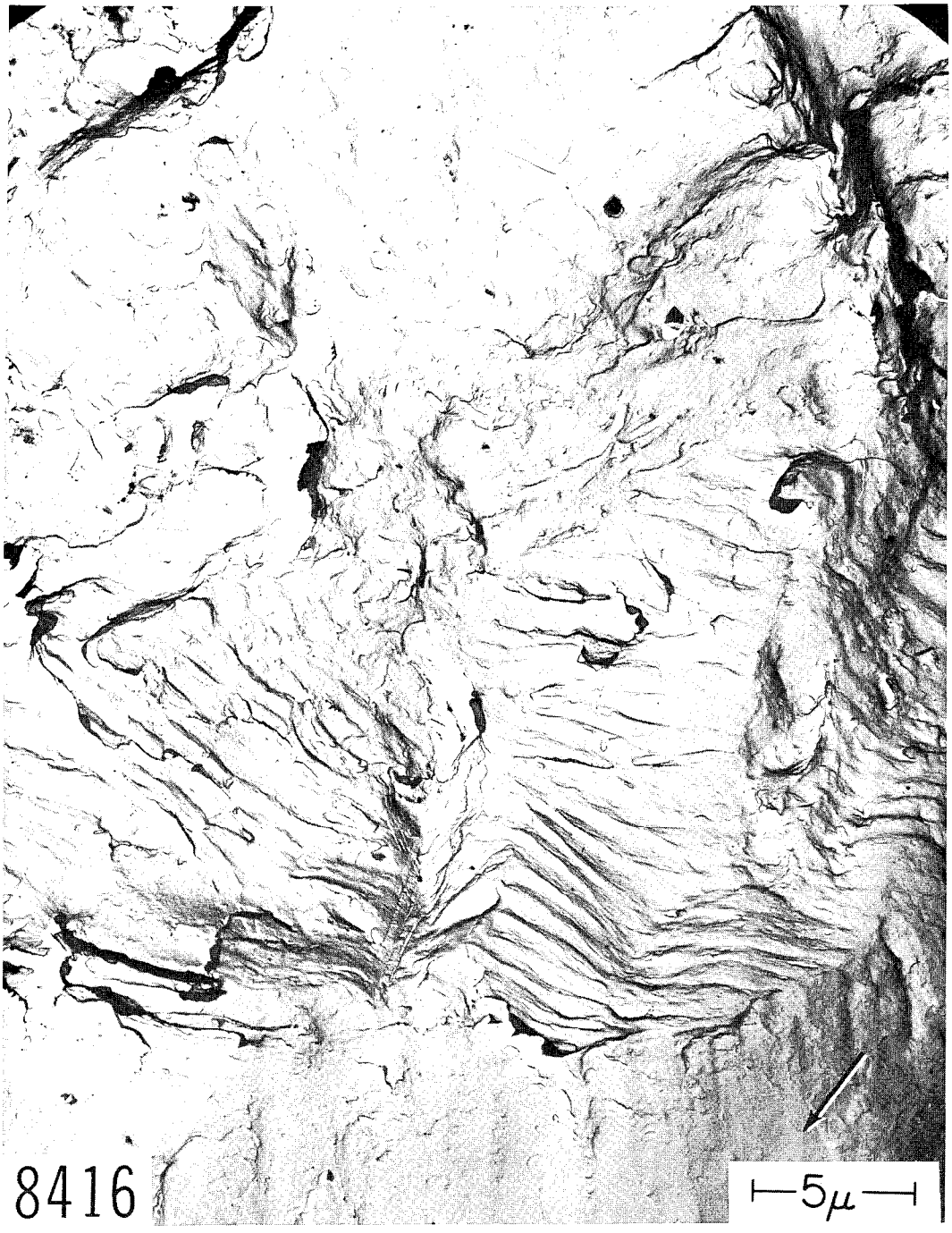

Fig. 61 - Fatigue markings in Ti-6Al-4V. Cellulose acetate-carbon replication technique. Palladium shadowed. 6000X.

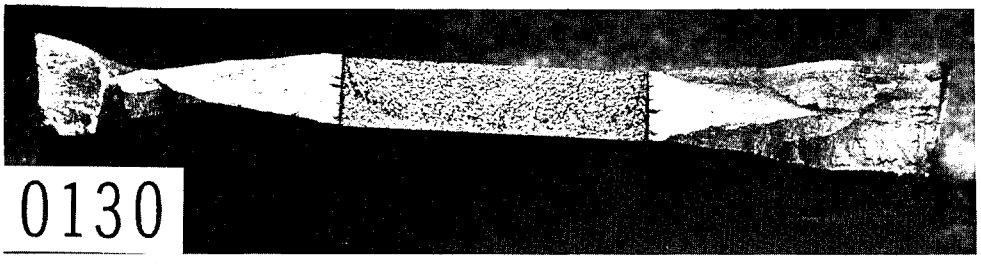

Fig. 62 - Center-cracked crack toughness specimen of Ti-6Al-4V, with an RW crack. 4X.

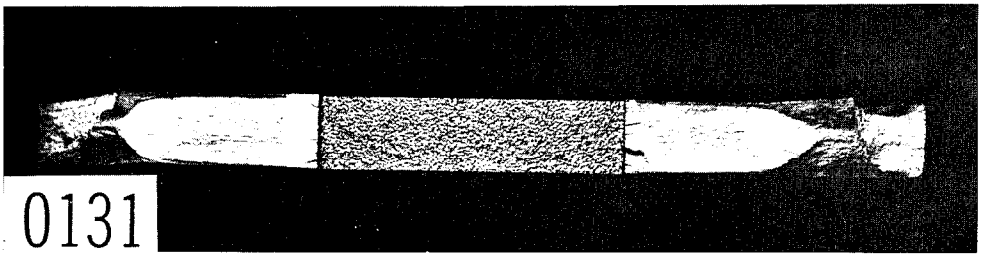

Fig. 63 - Center-cracked crack toughness specimen of Ti-6Al-4V, with a WR crack. 4X.

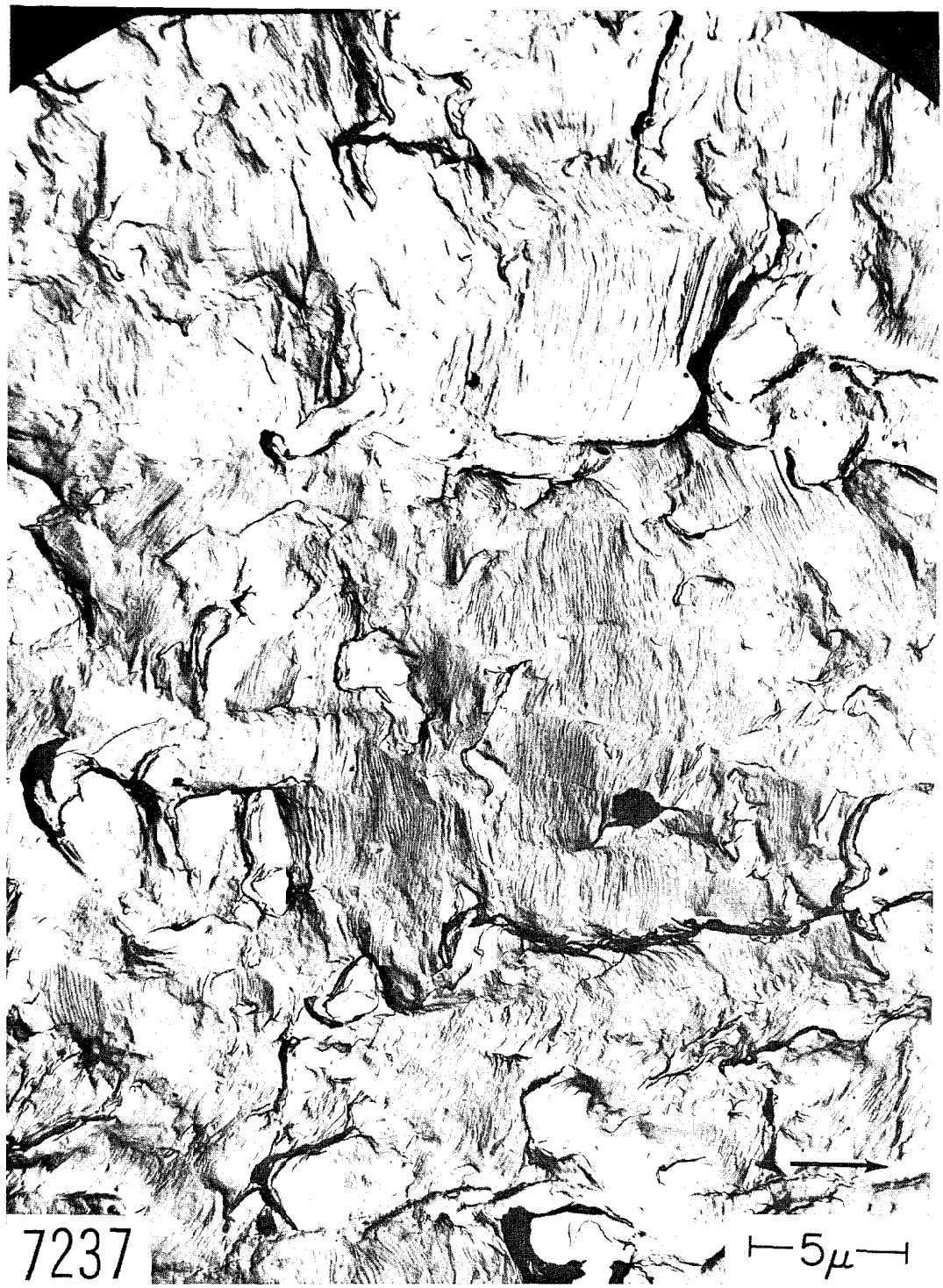

Fig. 64 - Fatigue markings in the RW crack shown in the specimen in Fig. 62. Cellulose acetate-carbon replication technique. Palladium shadowed. 6000X.

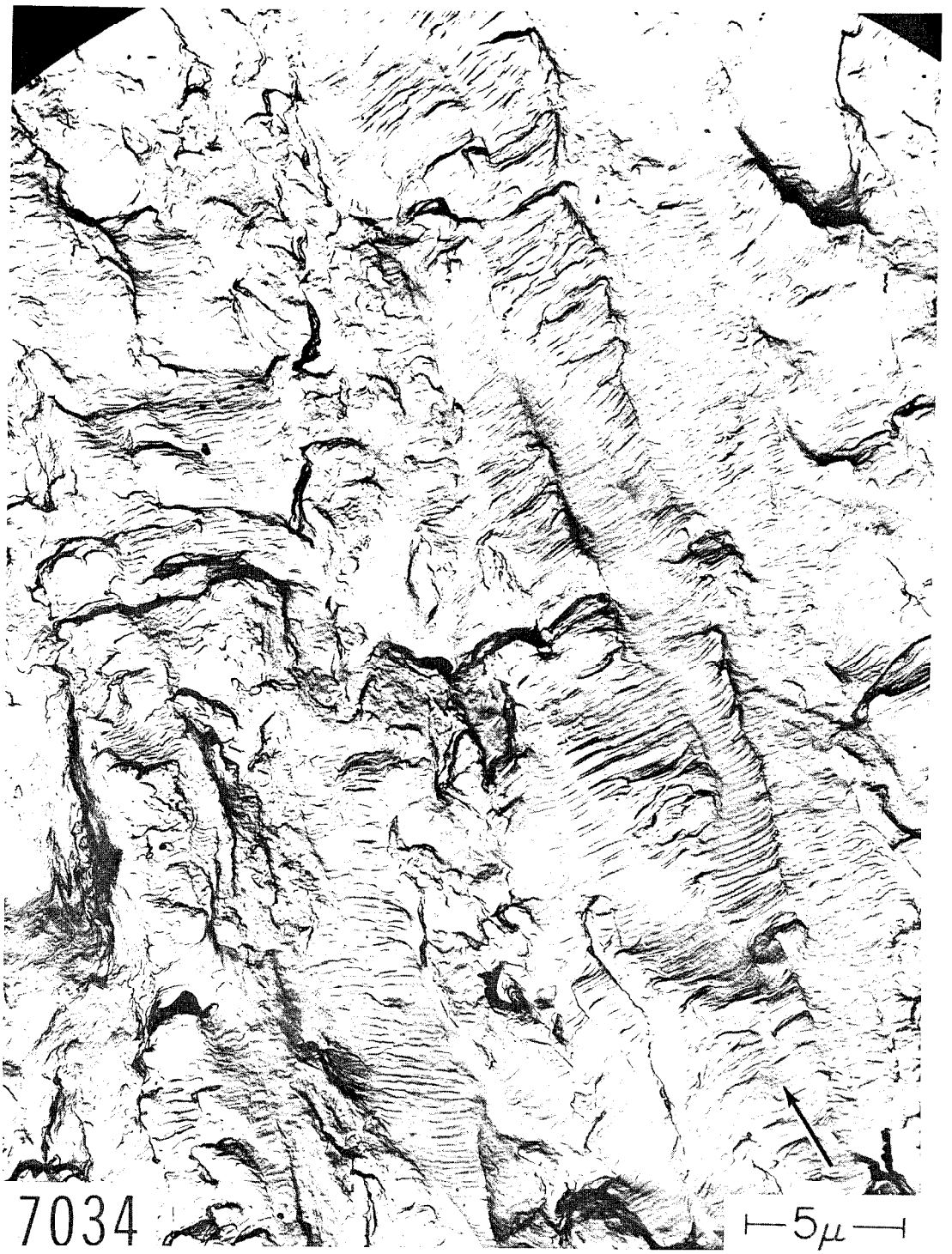

Fig. 65 - Fatigue markings in the WR crack shown in the specimen in Fig. 63.
Cellulose acetate-carbon replica. Palladium shadowed. 6000X.

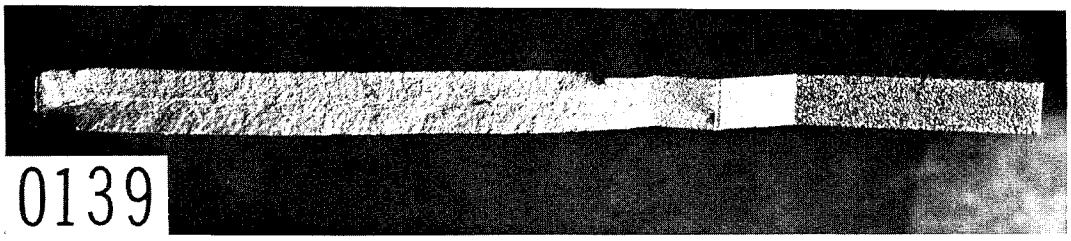

Fig. 66. Edge notched and fatigued crack toughness specimen of Ti-8Al-1Mo-1V. 6X.

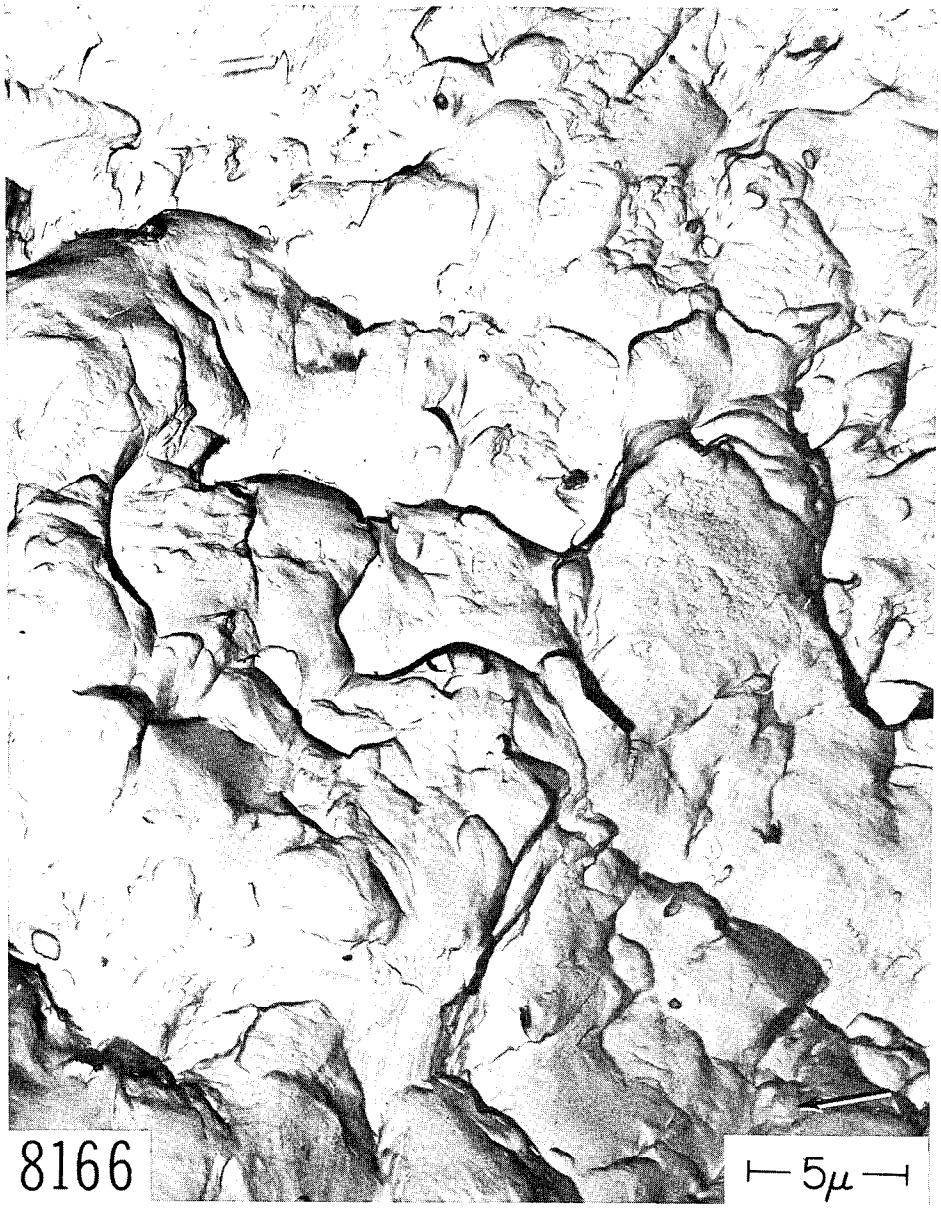

Fig. 67 - Monotonic plane-strain fracture surface in Ti-8Al-1Mo-1V specimen shown in Fig. 66. Cellulose acetate-carbon replication technique. Palladium shadowed. 6000X.

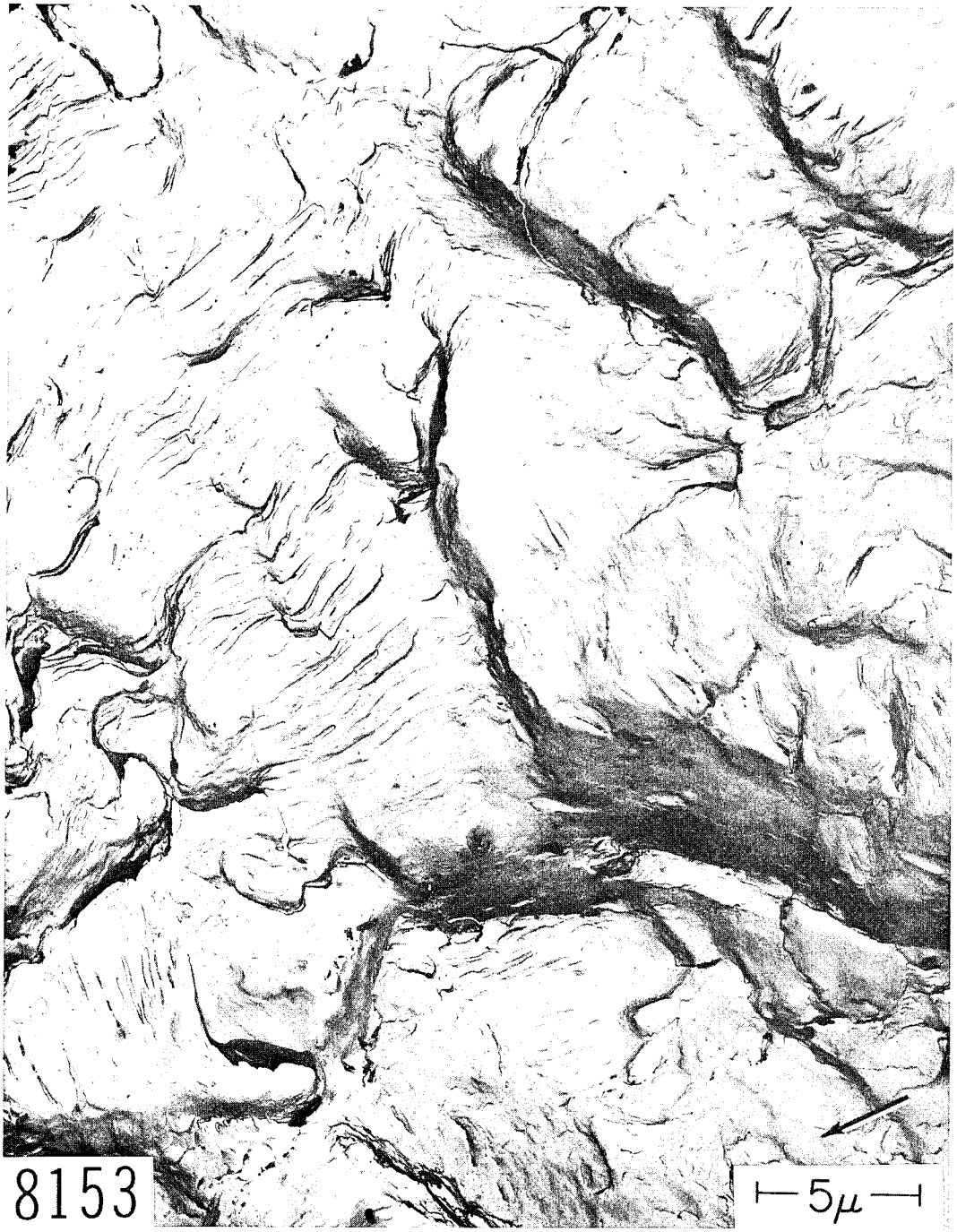

Fig. 68 - Characteristic fatigue markings in Ti-8Al-1Mo-1V specimen shown in Fig. 66. Cellulose acetate-carbon replication technique. Palladium shadowed. 6000X.

Fig. 69 - Characteristic fatigue markings in Ti-8Al-1Mo-1V specimen shown in Fig. 66. Cellulose acetate-carbon replication technique. Palladium shadowed. 6000X.

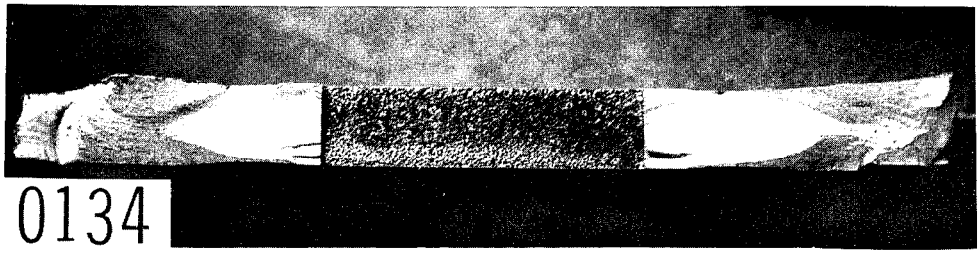

Fig. 70 - WR fatigue crack and monotonic fracture in a center-cracked crack toughness specimen of Ti-4Al-3Mo-1V. 6X.

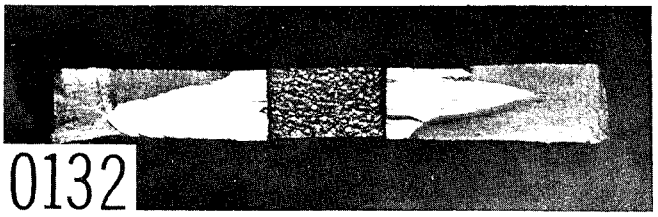

Fig. 71 - RW fatigue crack and monotonic fracture in a center-cracked crack toughness of specimen Ti-4Al-3Mo-1V. 6X.

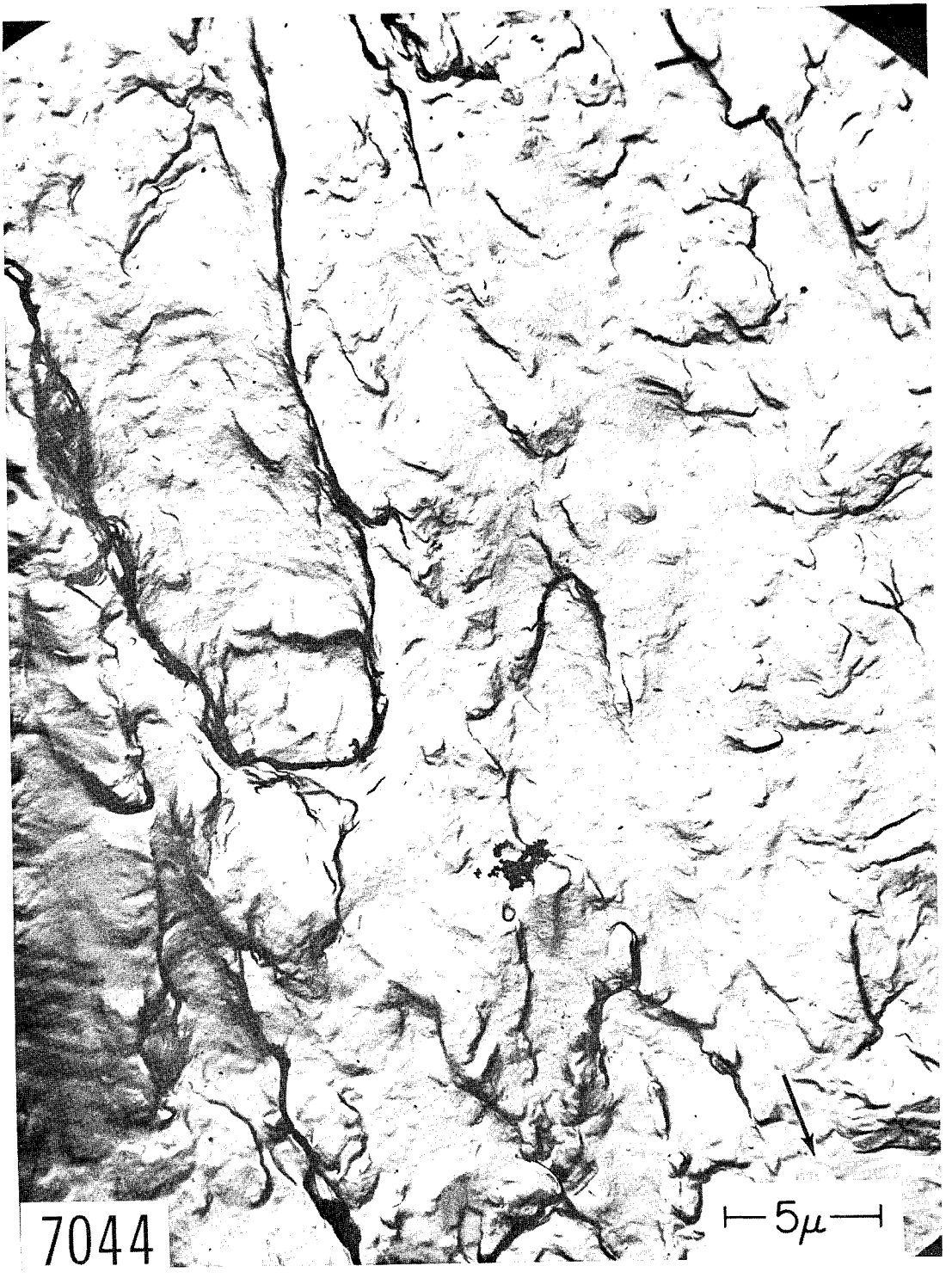

Fig. 72 - WR fatigue markings in Ti-4Al-3Mo-1V. From the specimen shown in Fig. 70. Cellulose acetate-carbon replication technique. Palladium shadowed. 6000X.

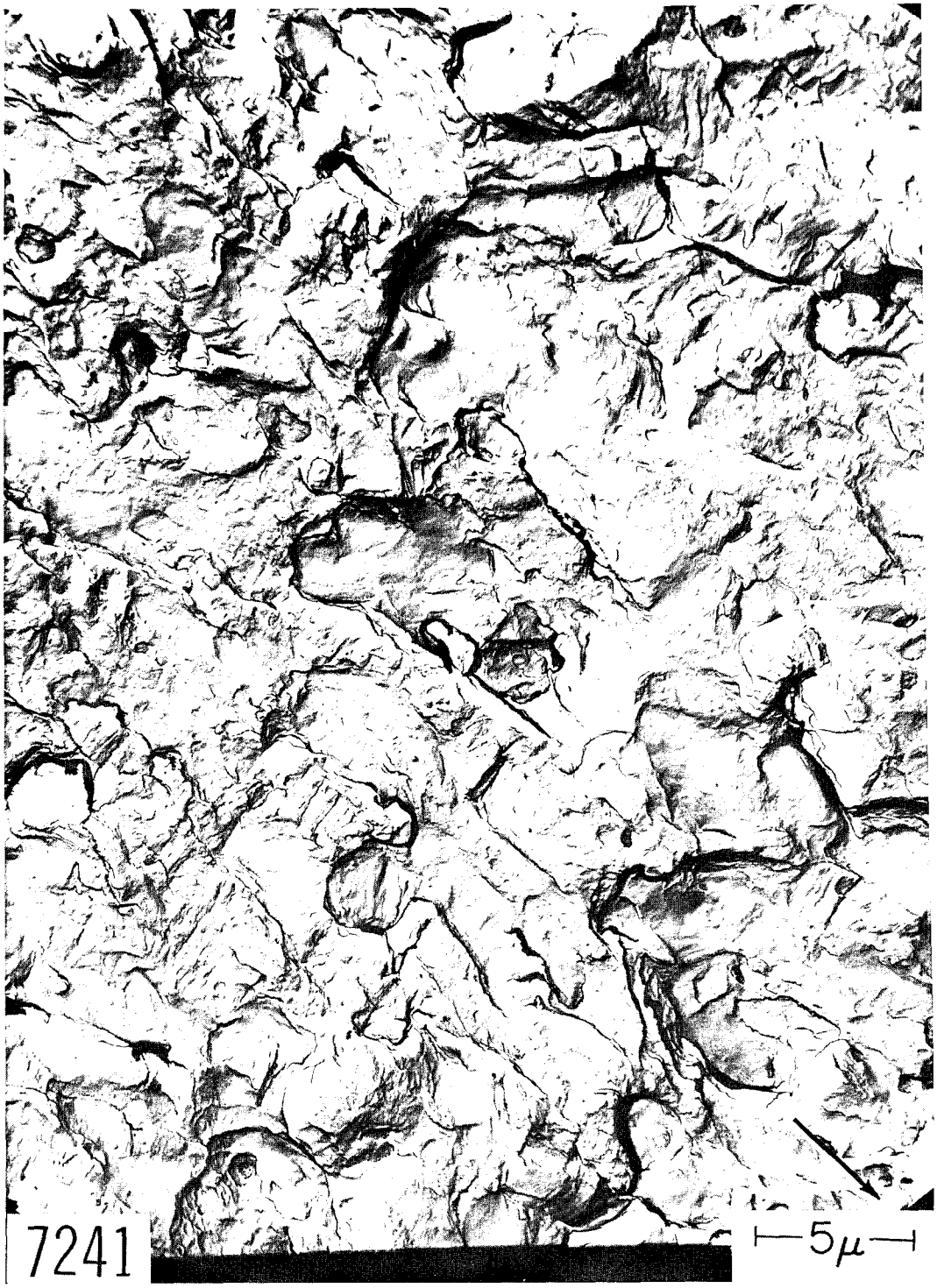

Fig. 73 - RW fatigue markings in Ti-4Al-3Mo-1V. From the specimen shown in Fig. 71. Cellulose acetate-carbon replication technique. Palladium shadowed. 6000X.

Fig. 74 - RW fatigue markings in Ti-4Al-3Mo-1V. From the specimen shown in Fig. 71. Cellulose acetate-carbon replication technique. Palladium shadowed. 6000X.

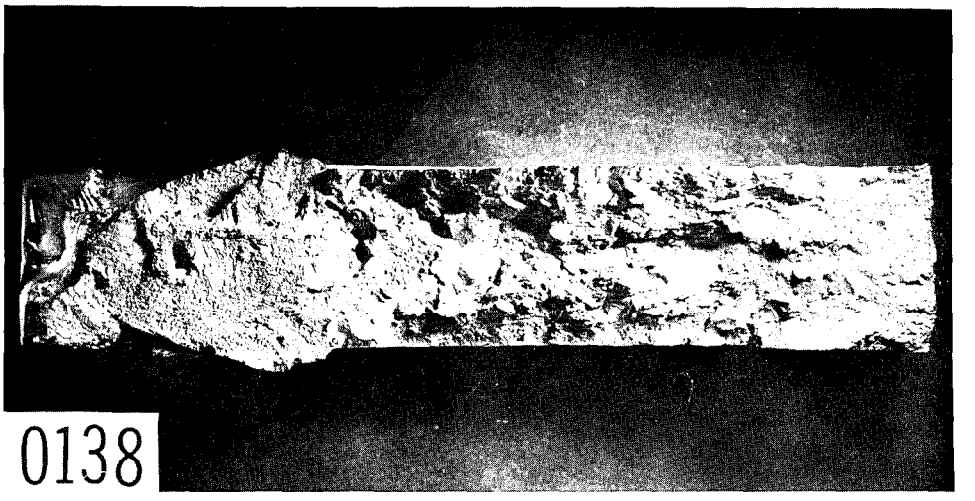

Fig. 75 - Drop weight tear specimen of as-cast Ti-5Al-3Sn-2Mo-2V alloy. 1-1/2X.

(R_C 42). The greatest difference in appearance is between the WR fracture surface in the specimen aged at 1150°F and the RW fracture surface in the specimen aged at 925°F. The RW fracture surface of the specimen aged at 925°F had more equiaxed features. The striation groups of the RW fracture surface in the specimen aged at 1150°F are only slightly more equiaxed than those in the WR fracture surface in the other specimen aged at the same temperature. The absence of well-marked striations seems typical of the alpha-beta alloys so far examined. The equiaxed features of the RW fracture in fatigue strongly resemble the dimples produced by fast fracture in the same (RW) mode.

e. Ti-5Al-3Sn-2Mo-2V As Cast

Figure 75 shows the fracture surface of a drop weight tear test specimen* of an as-cast piece of Ti-5Al-3Sn-2Mo-2V alloy. The intergranular nature of the part of the fracture is apparent. Figure 76 shows dimples on one facet of one of the grain surfaces. Figures 77-80 show dimples and other features seen on transgranular portions of the fracture. Figure 80 shows long shallow trough-like dimples associated with angular constituent particles (arrows).

f. Ti-2-1/2Al-16V

Two center-cracked sheet specimens of Ti-2-1/2Al-16V, both 1 in. wide, 0.062 in. thick, and aged for four hours at 900°F (R_C 41), are shown in Figs. 81 and 82. The fatigue crack in the specimen shown in Fig. 81 was propagated in the RW direction and the crack in Fig. 82 was propagated in the WR direction. Figures 83 and 84 are high magnification fractographs of the RW fatigue crack and Figs. 85 and 86 are fractographs of the WR fatigue crack. The difference between the two modes in this material is quite pronounced – the RW mode exhibits extremely equiaxed features, with few striations. It is not at all certain what the striation-like markings on the WR fracture surface are.

g. Ti-13V-11Cr-4Al

Figure 87 shows a center-cracked sheet specimen of Ti-13V-11Cr-4Al, 1-1/2 in. wide and 0.067 in. thick. The fatigue cracks were introduced by loading the specimen in tension-tension fatigue between loads of 600 pounds and 1200 pounds for 23,000 cycles at

*For a description of this specimen see Reference No. 5.

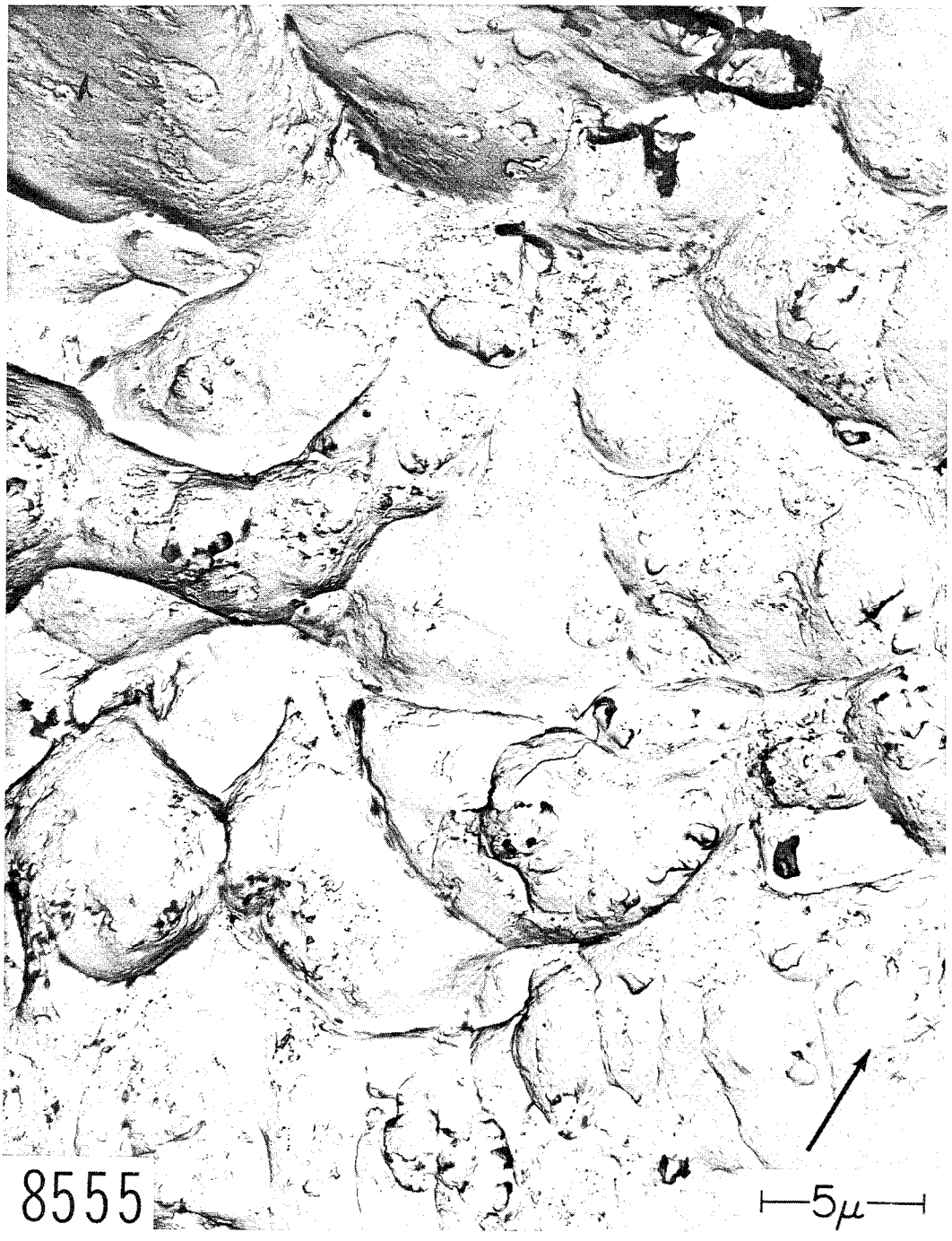

Fig. 76 - Dimples on a grain facet of the specimen shown in Fig. 75. Cellulose acetate-carbon replication technique. Palladium shadowed. 6000X.

Fig. 77 - Transgranular monotonic impact fracture surface of as cast Ti-5Al-3Sn-2Mo-2V specimen shown in Fig. 75. Cellulose acetate-carbon replication technique. Palladium shadowed. 6000X.

Fig. 78 - Transgranular monotonic impact fracture surface of as cast Ti-5Al-3Sn-2Mo-2V specimen shown in Fig. 75. Cellulose acetate-carbon replication technique. Palladium shadowed. 6000X.

Fig. 79 - Transgranular monotonic impact fracture surface of as cast Ti-5Al-3Sn-2Mo-2V specimen shown in Fig. 75. Cellulose acetate-carbon replication technique. Palladium shadowed. 6000X.

Fig. 80 - Transgranular monotonic impact fracture surface of as cast Ti-5Al-3Sn-2Mo-2V specimen shown in Fig. 75. Cellulose acetate-carbon replication technique. Palladium shadowed. 6000X.

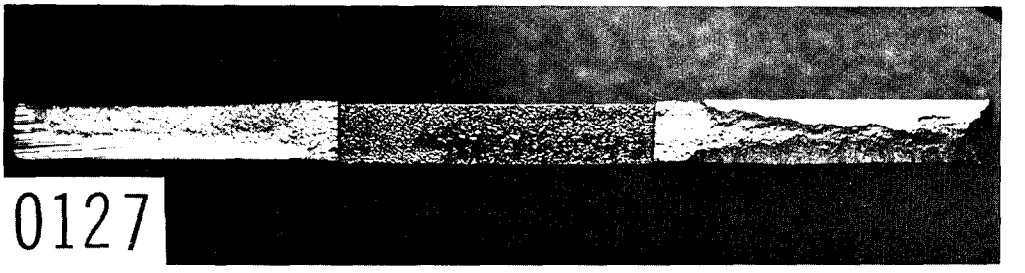

Fig. 81 - RW fracture surface in aTi-2-1/2Al-16V alloy center-cracked crack toughness specimen. 5X.

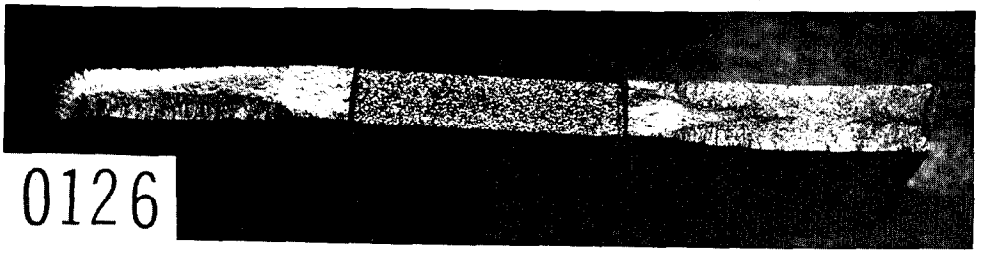

Fig. 82 - WR fracture surface in a Ti-2-1/2Al-16V alloy center-cracked crack toughness specimen. 5X.

Fig. 83 - Fatigue markings in the RW crack shown in Fig. 81. Cellulose acetate-carbon replication technique. Palladium shadowed. 2200X.

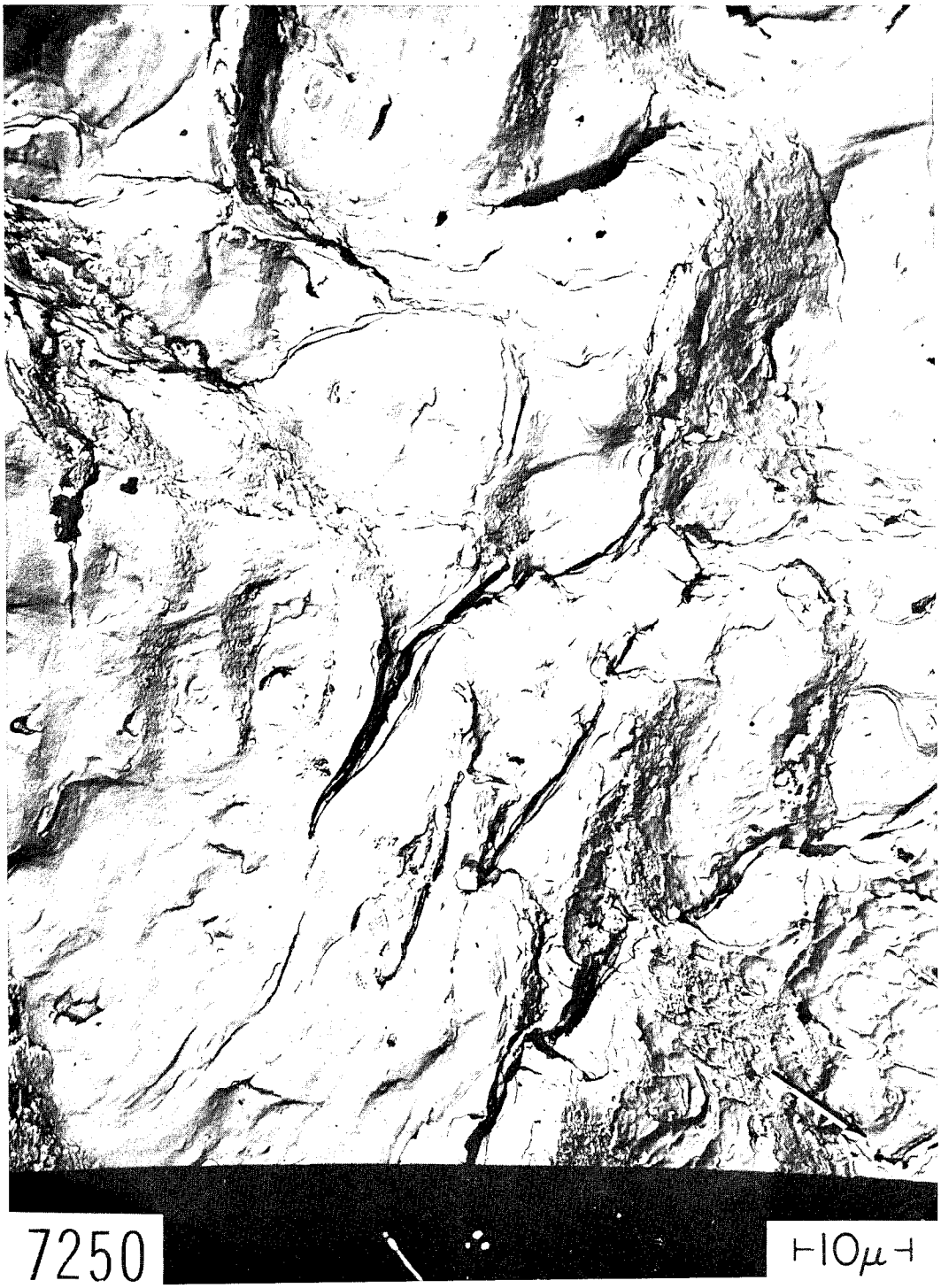

Fig. 84 - Fatigue markings in the RW crack shown in Fig. 81. Cellulose acetate-carbon replication technique. Palladium shadowed. 2200X.

Fig. 85 - Fatigue markings in the WR crack shown in Fig. 82. Cellulose acetate-carbon replication technique. Palladium shadowed. 2500X.

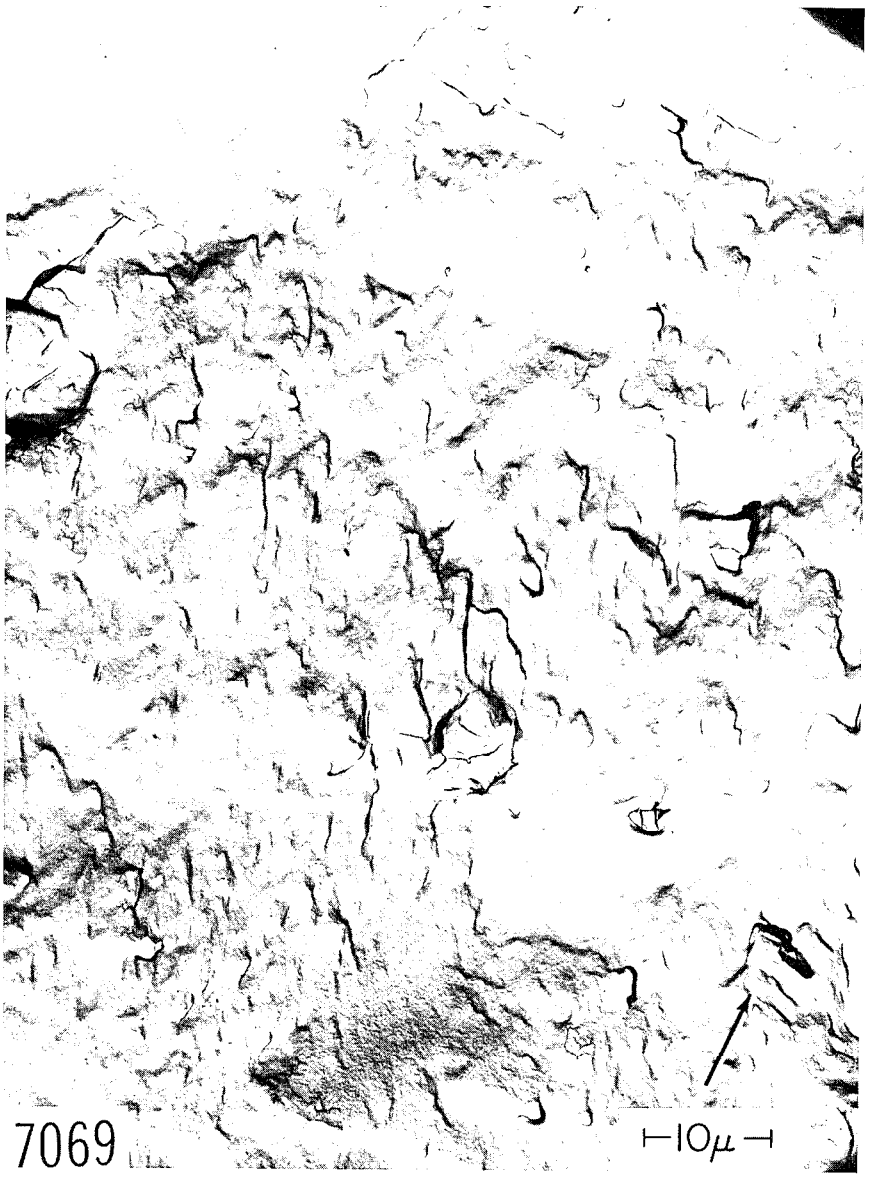

Fig. 86 - Fatigue markings in the WR crack shown in Fig. 82. Cellulose acetate-carbon replication technique. Palladium shadowed. 2500X.

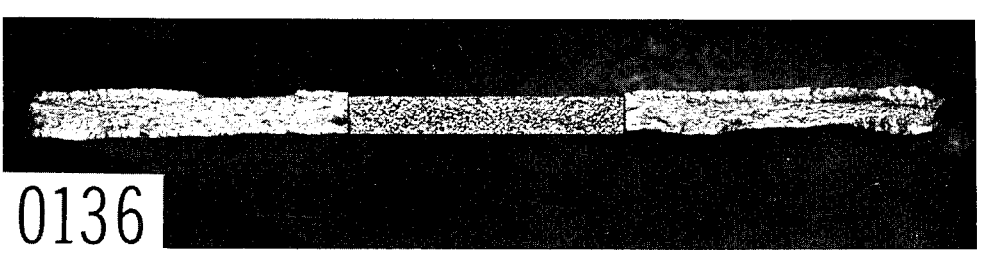

Fig. 87 - Center-cracked specimen of Ti-13V-11Cr-4Al Alloy. 2X.

room temperature. The specimen was aged for 100 hours at 850° F. Figure 88 shows the characteristic appearance of fatigue surfaces in this specimen, while Fig. 89 is an enlargement of a small region in Fig. 88. The fatigue striations are visible at 9000X as very fine lines, often crossing other parallel lines which are probably related to the crystallographic orientation of the grains through which the crack passed. The low magnification picture clearly shows a number of individual grains, and one can see that the distinctive surface markings do not seem to cross the grain boundaries. The solution treated specimens show the same fatigue fracture features.

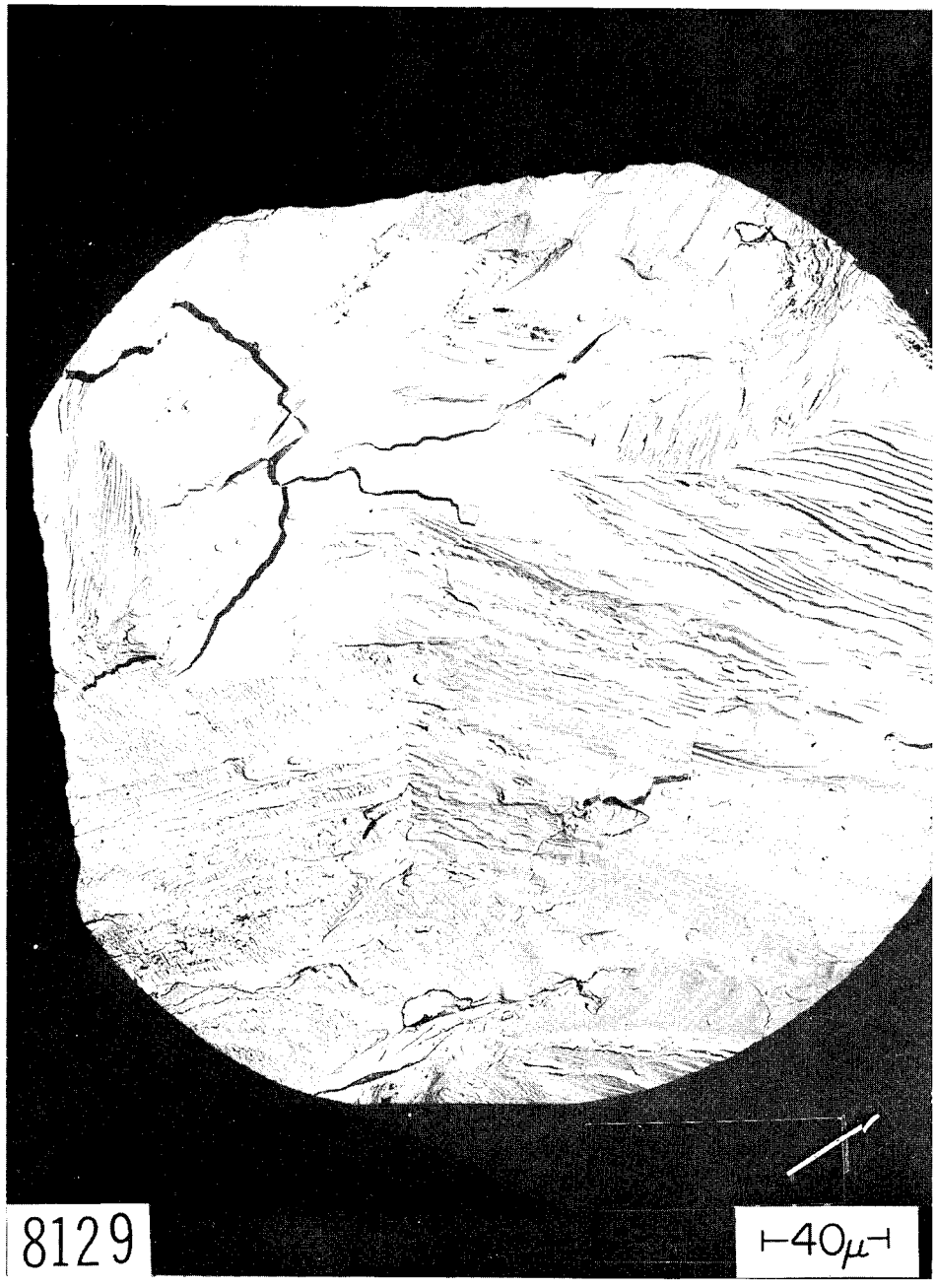

Fig. 88 - Fatigue markings in crack shown in Fig. 87. Cellulose acetate-carbon replication technique. Palladium shadowed. 630X.

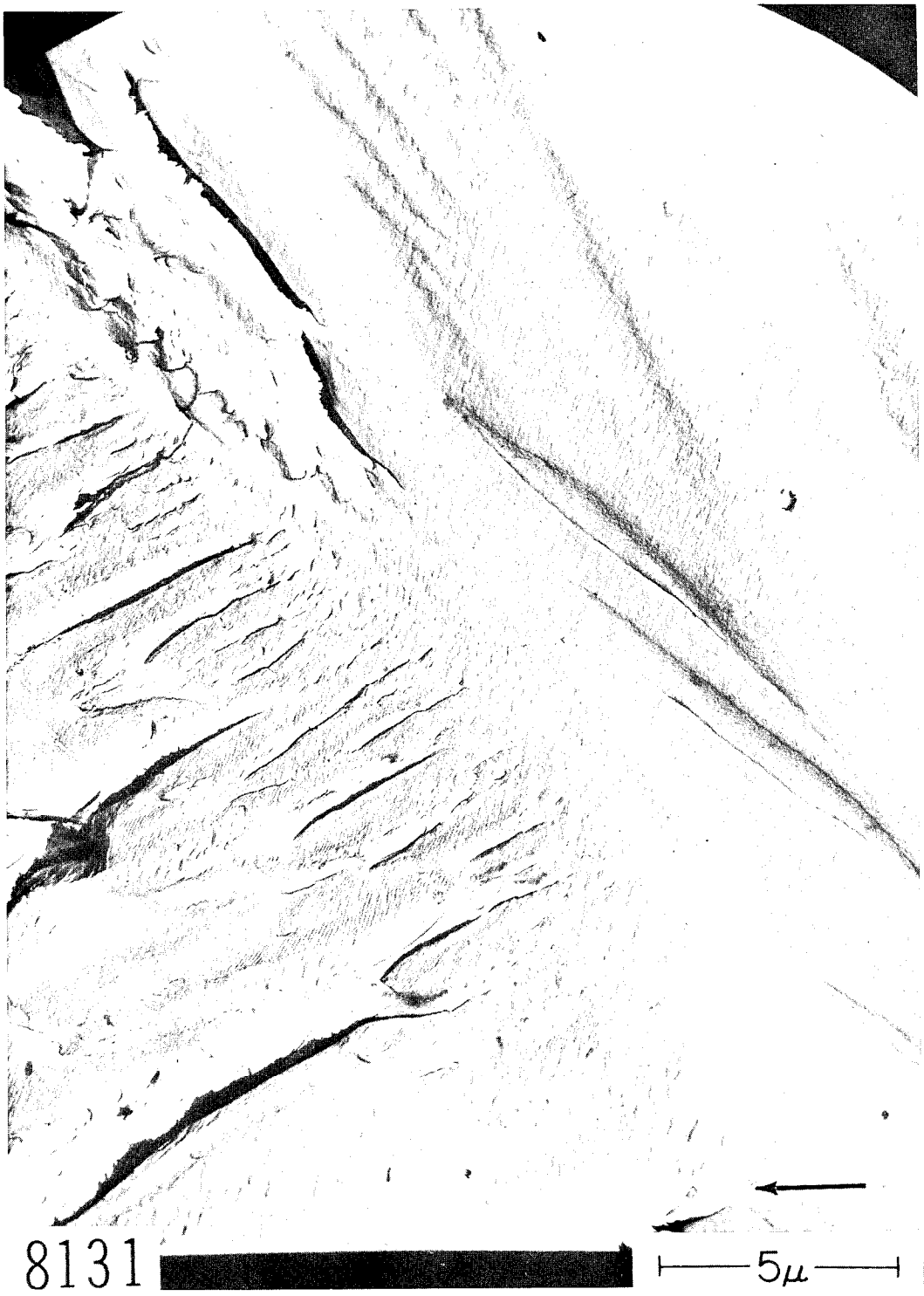

Fig. 89 - Higher magnification view of a portion of Fig. 88. 9000X.

4. CHARACTERIZATION OF STEEL FRACTURE SURFACES

Four steels of current interest were examined. Fatigue and overload fracture surfaces in three HY 80 compositions were characterized. Maraging steel TIG weld metal fatigue, overload, and hydrogen embrittlement fracture surfaces were characterized.

a. HY 80 Steel

Figure 90 shows the macroscopic appearance of the Lehigh-type fatigue specimen. The central fatigue fracture was grown by a repeated bending load, and then the specimen was fractured in tension. Figures 91 and 92 show the characteristic appearance of the fatigue striations in this specimen. Figures 93 and 94 respectively show equiaxed and tear dimples in the square portion of the fracture surface.

b. HY 110 Steel

This higher strength modification with the HY 80 composition was obtained by adjusting the tempering temperature (6). The Lehigh-type fatigue specimen is shown at low magnification in Fig. 95. It was fatigued and then broken at room temperature. Characteristic fatigue markings are shown in Figs. 96 and 97, and dimples that are characteristic of the overload fracture are shown in Figs. 98 and 99.

c. HY 150 Steel

This further modification of yield strength with the HY 80 steel composition was also obtained by adjusting the tempering temperature. Figure 100 shows the Lehigh-type fatigue specimen, Figs. 101 and 102 show the characteristic fatigue markings, and Figs. 103-105 show the characteristic appearance of the dimples.

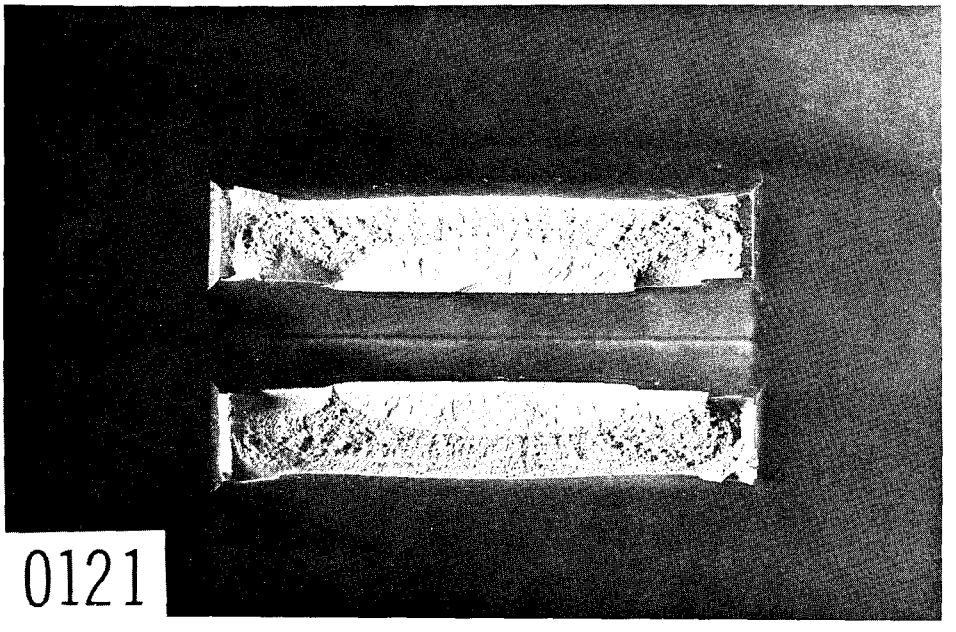

Fig. 90 - Lehigh fatigue specimen fracture surface in HY 80 steel. 1X.

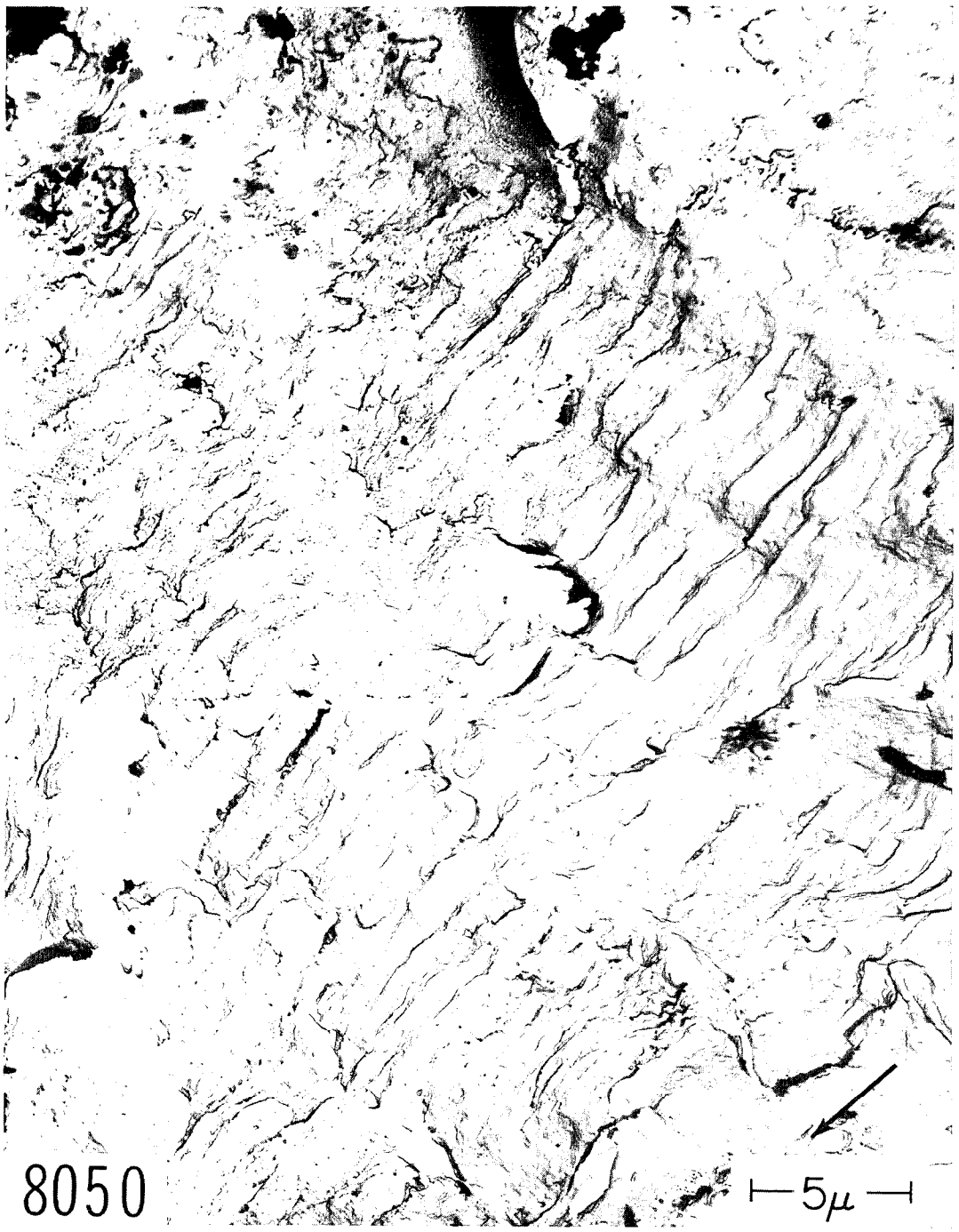

Fig. 91 - Fatigue striations in the fatigue crack shown in the HY 80 specimen in Fig. 90. Cellulose acetate-carbon replication technique. Palladium shadowed. 6000X.

Fig. 92 - Fatigue striations in the fatigue crack shown in the HY 80 specimen in Fig. 90. Cellulose acetate-carbon replication technique. Palladium shadowed. 6000X.

Fig. 93 - Equiaxed dimples in the square monotonic fracture portion of the HY 80 specimen shown in Fig. 90. Cellulose acetate-carbon replication technique. Palladium shadowed. 6000X.

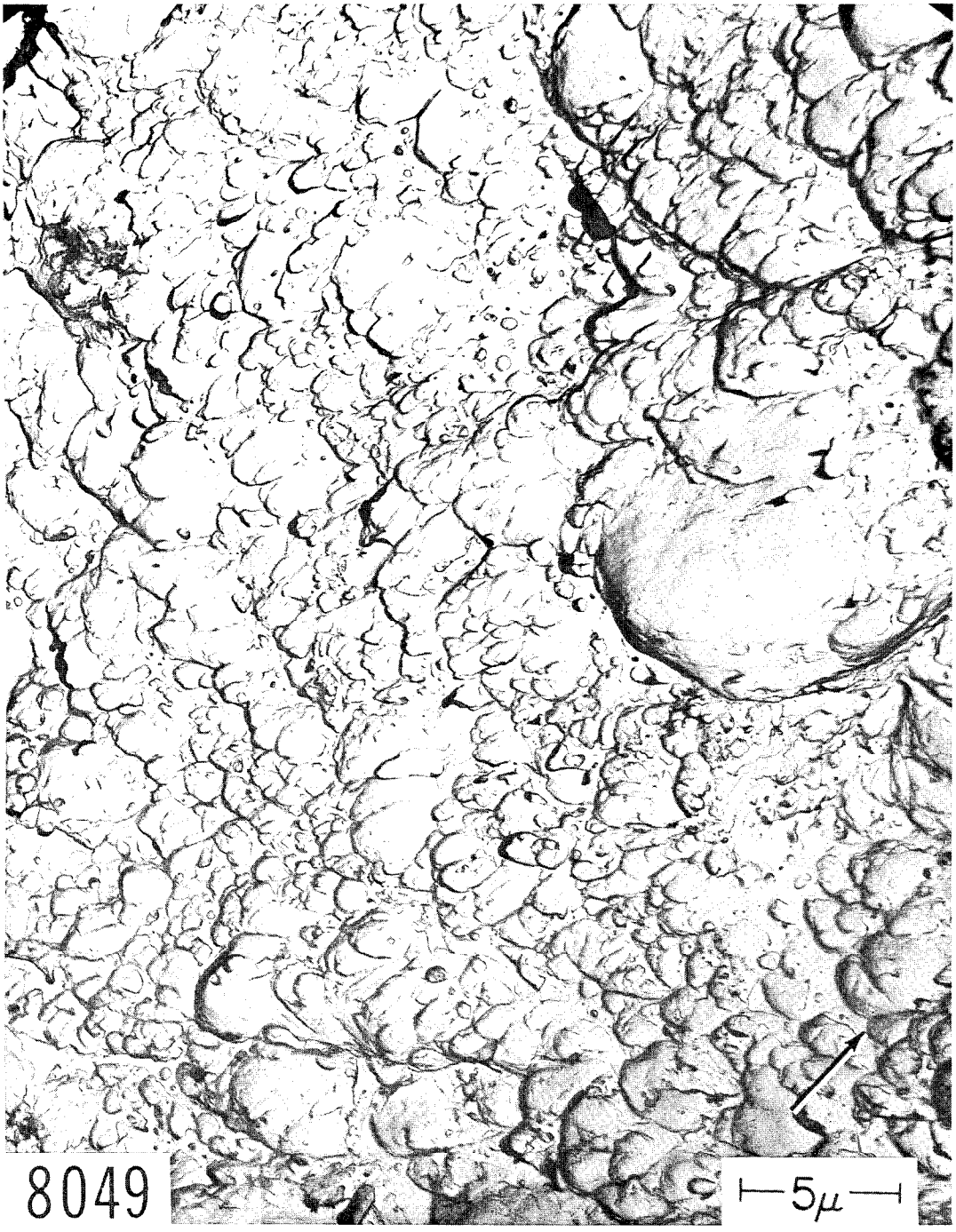

Fig. 94 - Tear dimples in the square monotonic fracture portion of the HY 80 specimen shown in Fig. 90. Cellulose acetate-carbon replication technique. Palladium shadowed. 6000X.

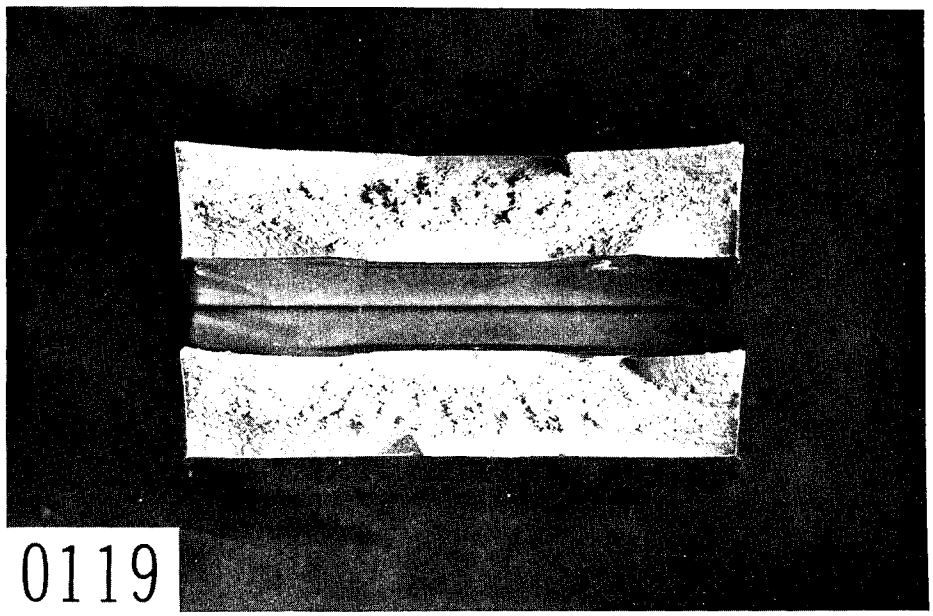

Fig. 95 - Lehigh fatigue specimen of HY 110 steel. 1-1/2X.

Fig. 96 - Fatigue markings in HY 110 steel. Cellulose acetate-carbon replication technique. Palladium shadowed. 3000X.

Fig. 97 - Fatigue markings in HY 110 steel. Cellulose acetate-carbon replication technique. Palladium shadowed. 4500X.

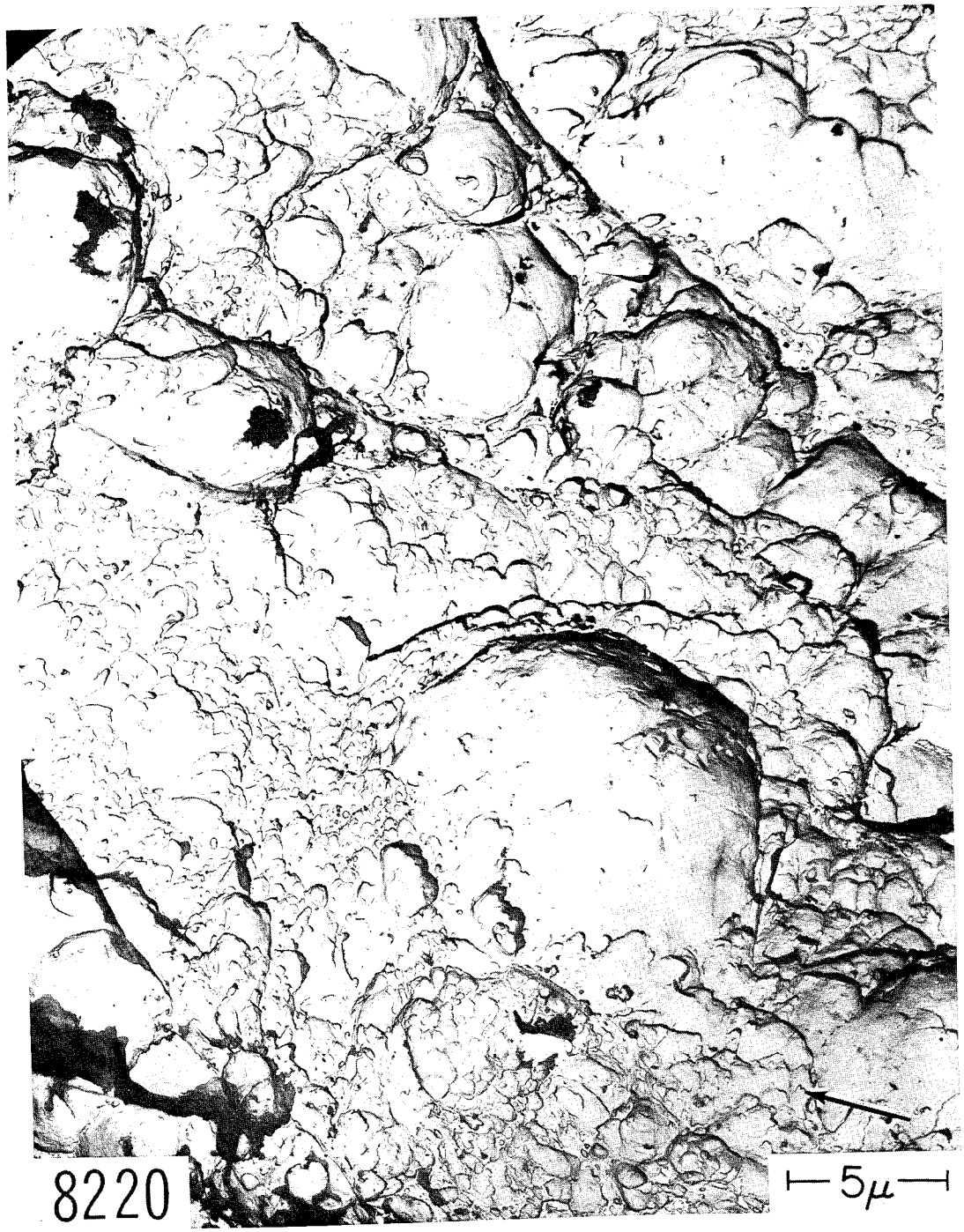

Fig. 98 - Dimples in monotonic fracture surface of HY 110 steel. Cellulose acetate-carbon replica technique. Palladium shadowed. 6000X.

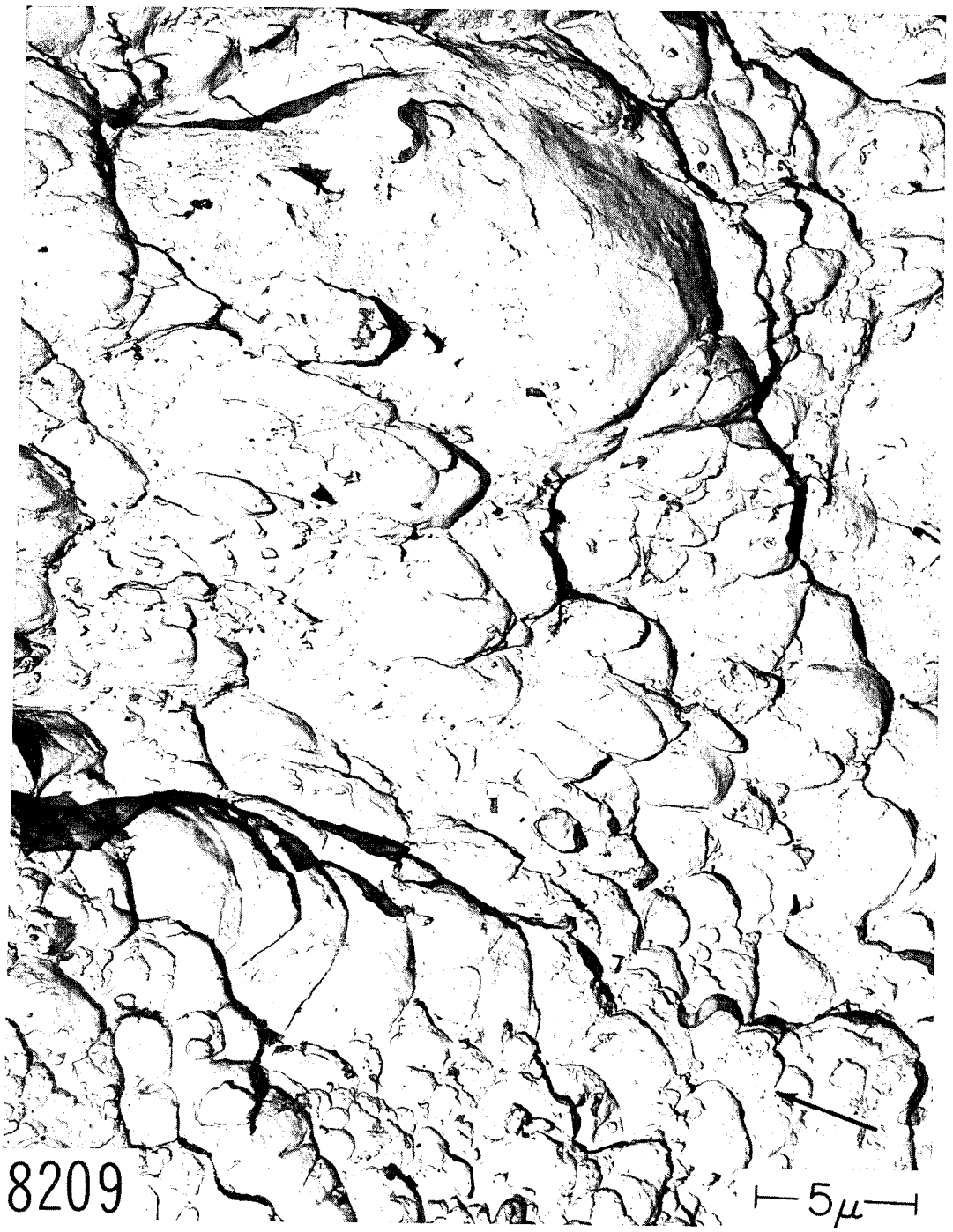

Fig. 99 - Dimples in monotonic fracture surface of HY 110 steel. Cellulose acetate-carbon replica technique. Palladium shadowed. 6000X.

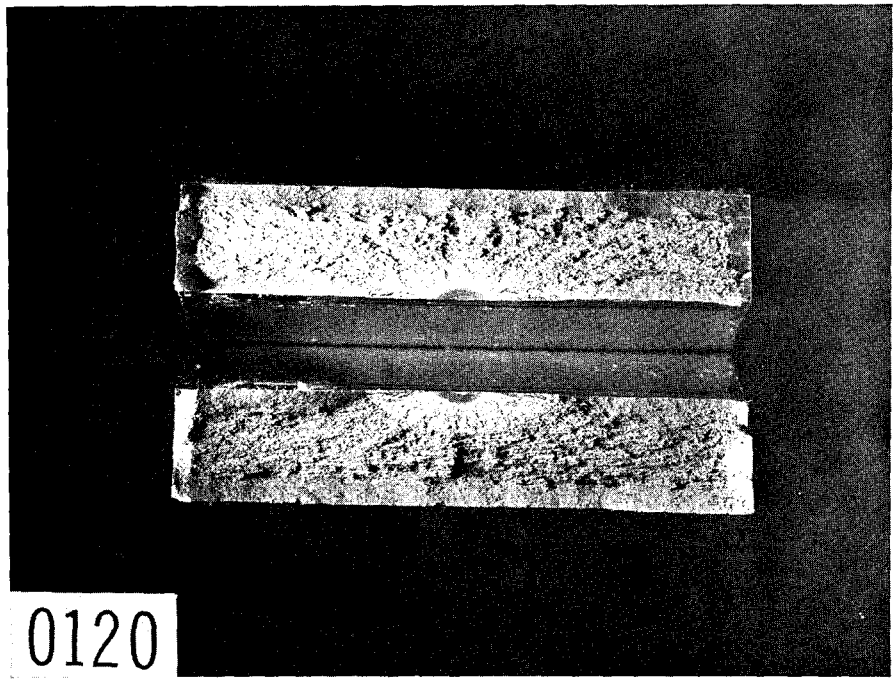

Fig. 100 - Lehigh fatigue specimen of HY 150 steel.1-1/2X.

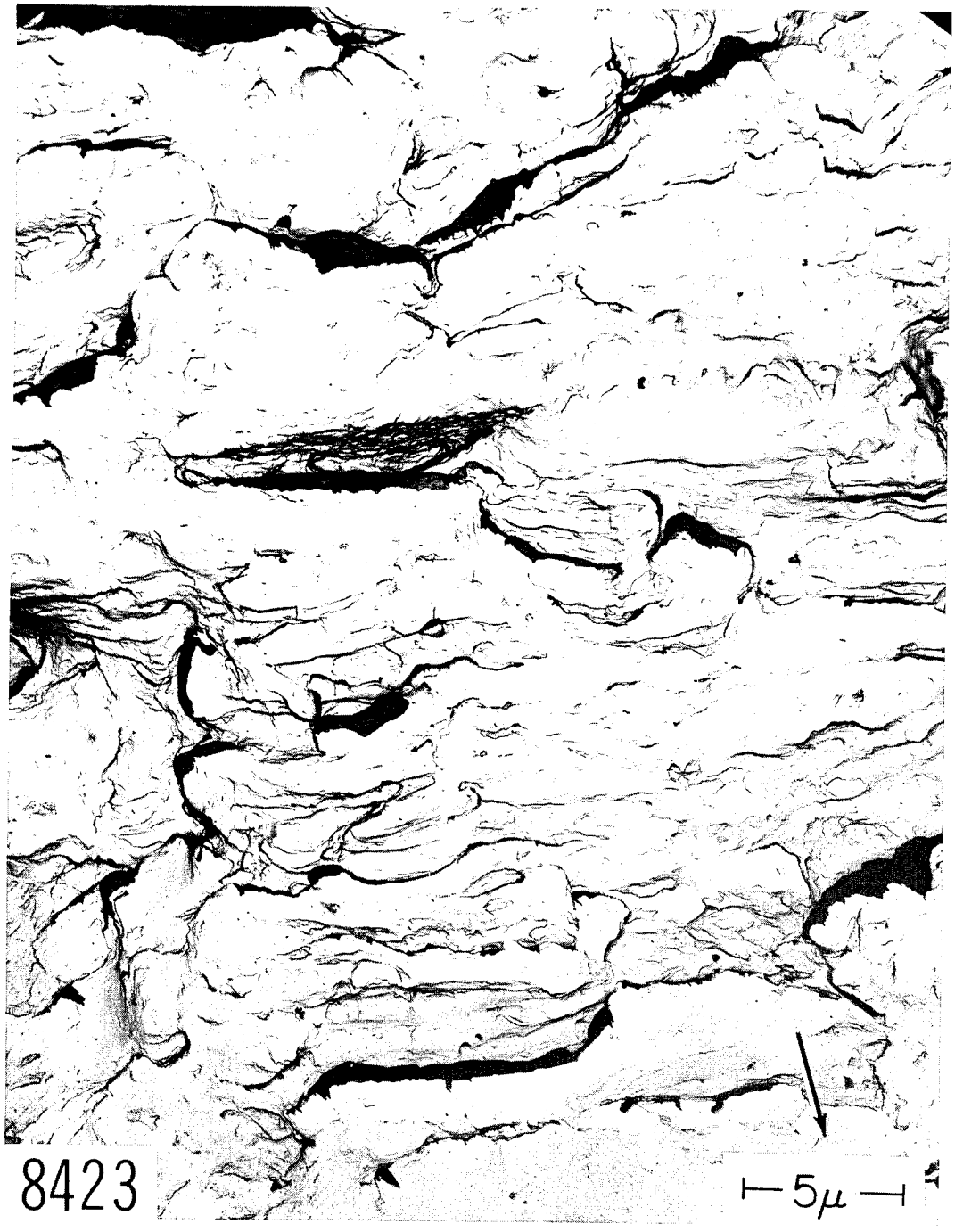

Fig. 101 - Characteristic fatigue markings in HY 150 steel. Cellulose acetate-carbon replication technique. Palladium shadowed. 6000X.

Fig. 102 - Characteristic fatigue markings in HY 150 steel. Cellulose acetate-carbon replication technique. Palladium shadowed. 12,000X.

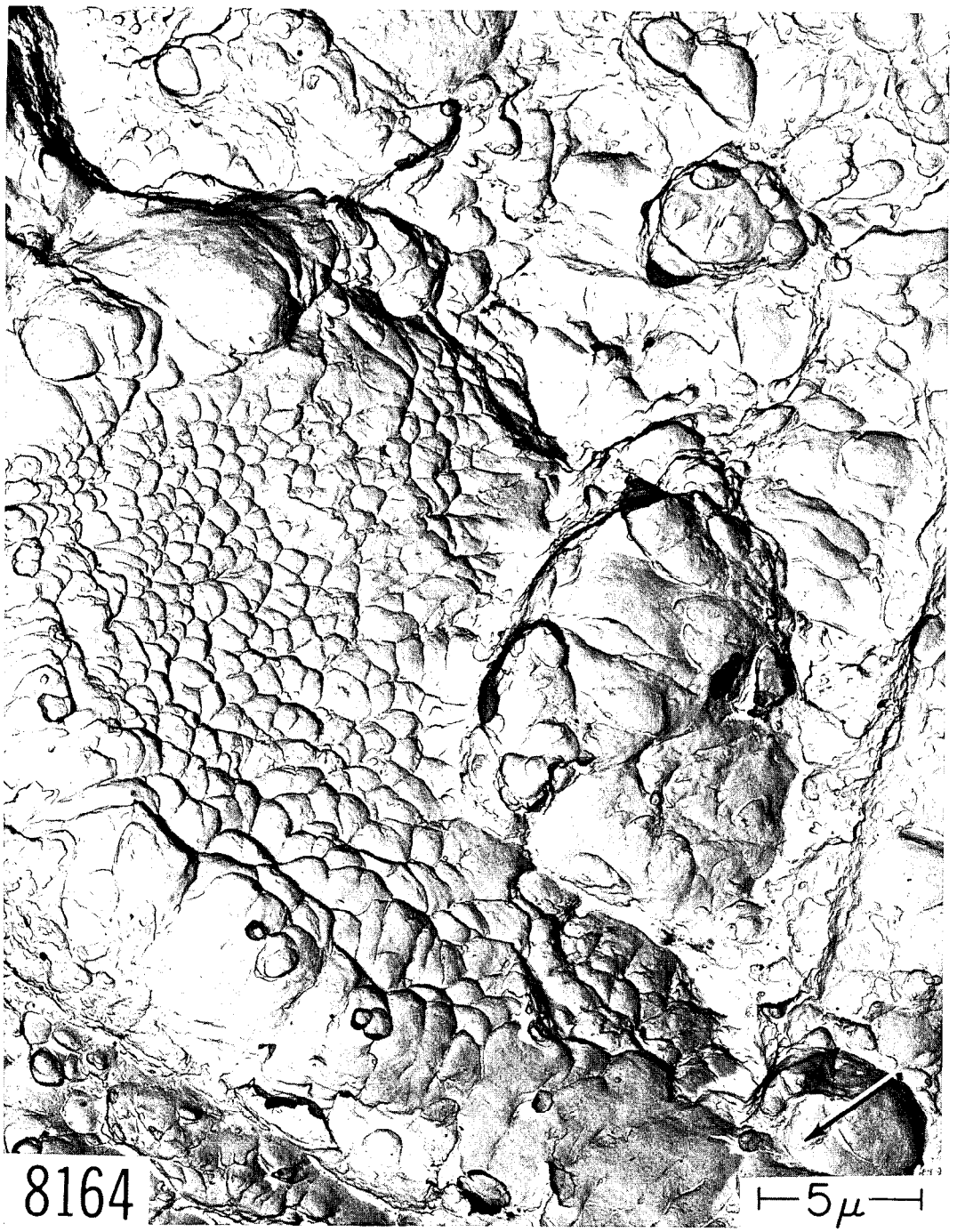

Fig. 103 - Dimples in monotonic fracture surface of HY 150 steel. Cellulose acetate-carbon replication technique. Palladium shadowed. 6000X.

Fig. 104 - Dimples in monotonic fracture surface of HY 150 steel. Cellulose acetate-carbon replication technique. Palladium shadowed. 6000X.

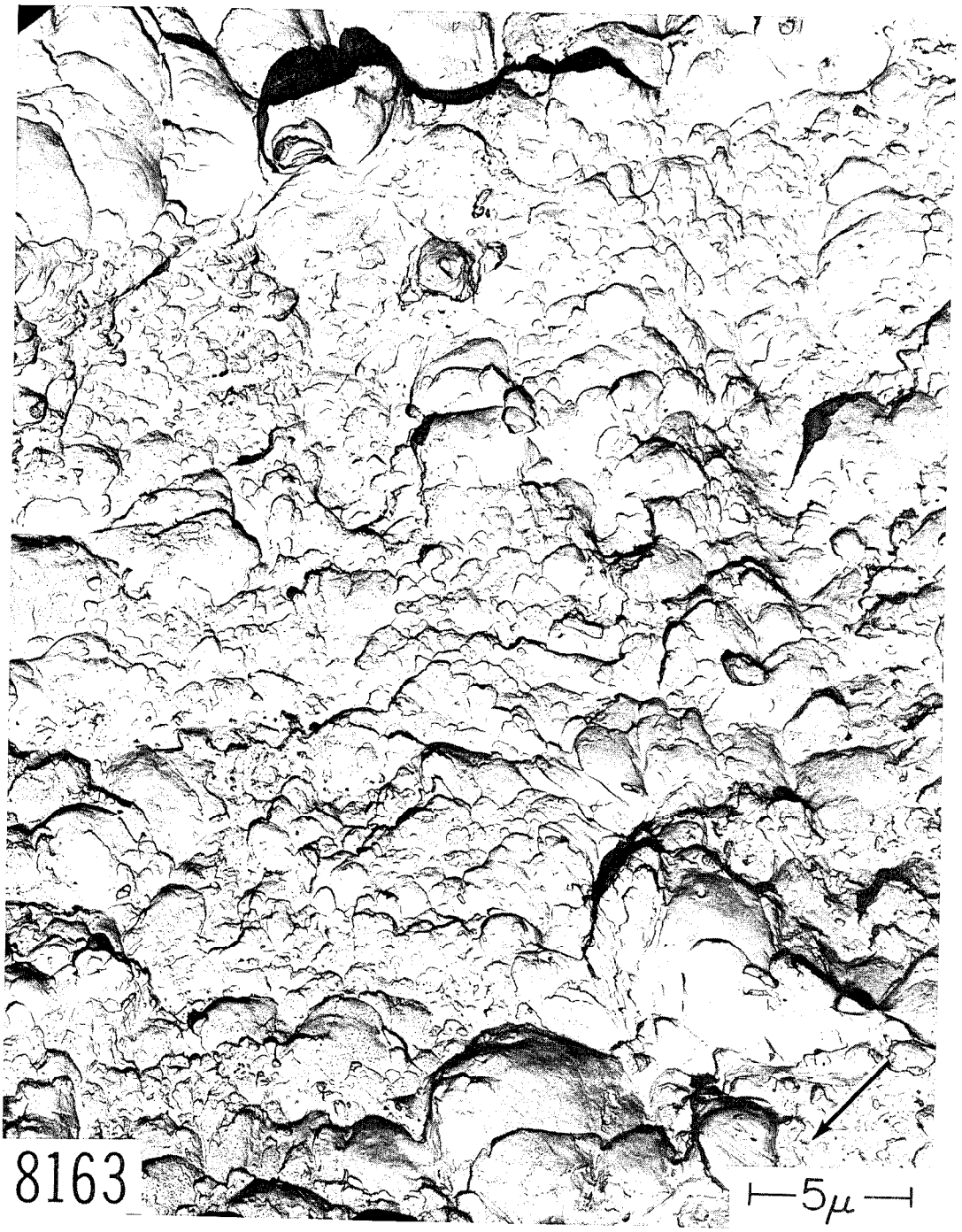

Fig. 105 - Dimples in monotonic fracture surface of HY 150 steel. Cellulose acetate-carbon replication technique. Palladium shadowed. 6000X.

d. Maraging Steel Weld Metal

Fracture through maraging steel weld metal is of potential interest and therefore fatigue, overload, and hydrogen embrittlement fracture surfaces in this material have been examined. The material selected was of the 250 KSI yield strength variety of 18% nickel maraging steel. Plates 3/4 in. thick were TIG welded together and 3/4 in. square cross-section specimens were cut with their 7 in. lengths perpendicular to the length of the weld. The welds were ground flush and then surface notched and fatigue-cracked so that the plane of the crack passed through the length and center of the weld metal. The specimens were broken by bending (7) after aging at 915° F for four hours. Figures 106 and 107 show the macroscopic fracture surface of one of the specimens. Figure 106 shows the effect of layers of weak microstructural heterogeneities on the fracture path in one of the specimens. The specimens were broken by three-point bending, and a large number of such specimen split, or delaminated, as seen in Fig. 106. Figure 107 is a higher magnification optical fractograph showing a network of high reflectivity regions, one portion of which is bounded by arrows. Figures 108 and 109 show the sources of the relatively high and low reflectivity respectively. The network is shiny because it is composed of numerous flat platelets of some unidentified constituents, and the regions of low reflectivity are composed of dimples. High magnification fractographs of the specimen shown in Fig. 110 are shown in Figs. 111-115. Figures 111-113 show characteristic fatigue markings in this specimen. The specimens were precracked by fatigue at room temperature. Figures 114 and 115 show the typical appearance of the dimpled rupture surfaces found in maraging steels of this strength level.

To date there have been only two conditions in maraging steel that have produced quasi cleavage. One was a 160,000 psi yield strength experimental heat where specimens were broken at low temperatures. The other condition was slow crack propagation ("static fatigue") through hydrogen embrittled weld metal and base metal in specimens like those described in the previous paragraph. Figures 116 and 117 show quasi-cleavage in hydrogen embrittled weld metal. Figure 116 shows a mixture of dimples and quasi-cleavage with the characteristic steps, river patterns, and tear ridges seen in quasi-cleavage.

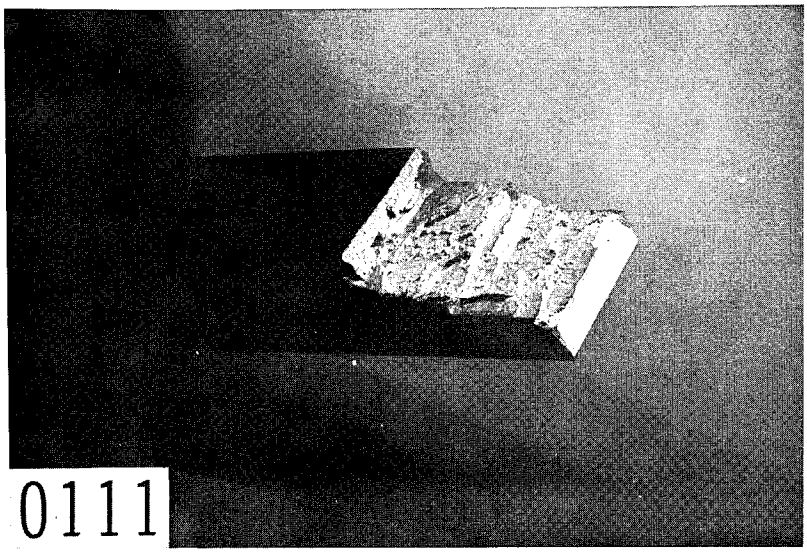

Fig. 106 - Slow bend fracture toughness specimen of 250 KSI yield strength maraging steel which split, or delaminated, when tested at room temperature. 2X.

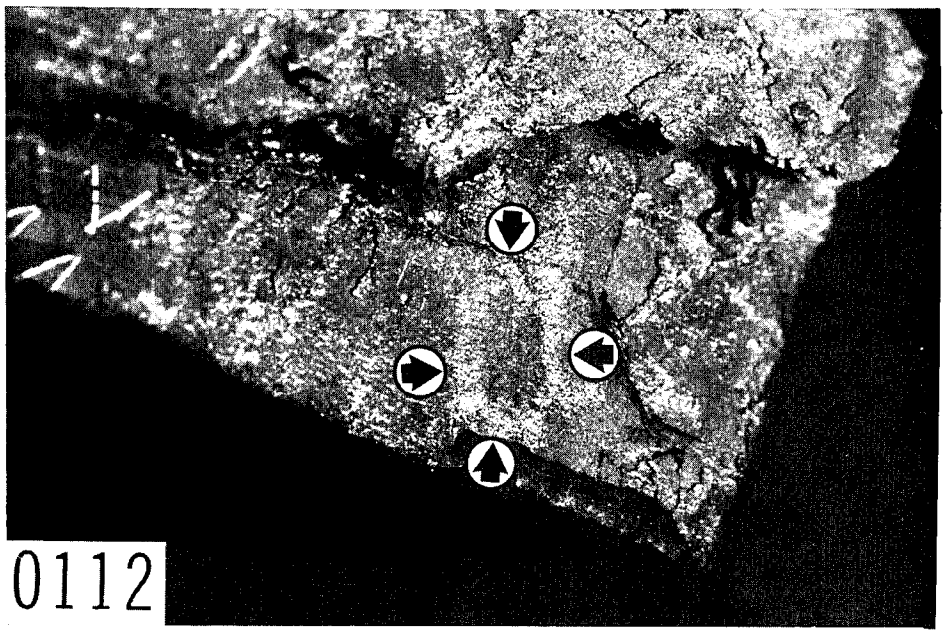

Fig. 107 - Network of regions of high reflectivity seen on the delaminated surfaces in maraging steel. 16X.

Fig. 108 - Thin flat particles that caused the delamination of the specimen shown in Fig. 106. The particles were broken and separated by rolling. Cellulose acetate-carbon replication technique. Palladium shadowed. 6000X.

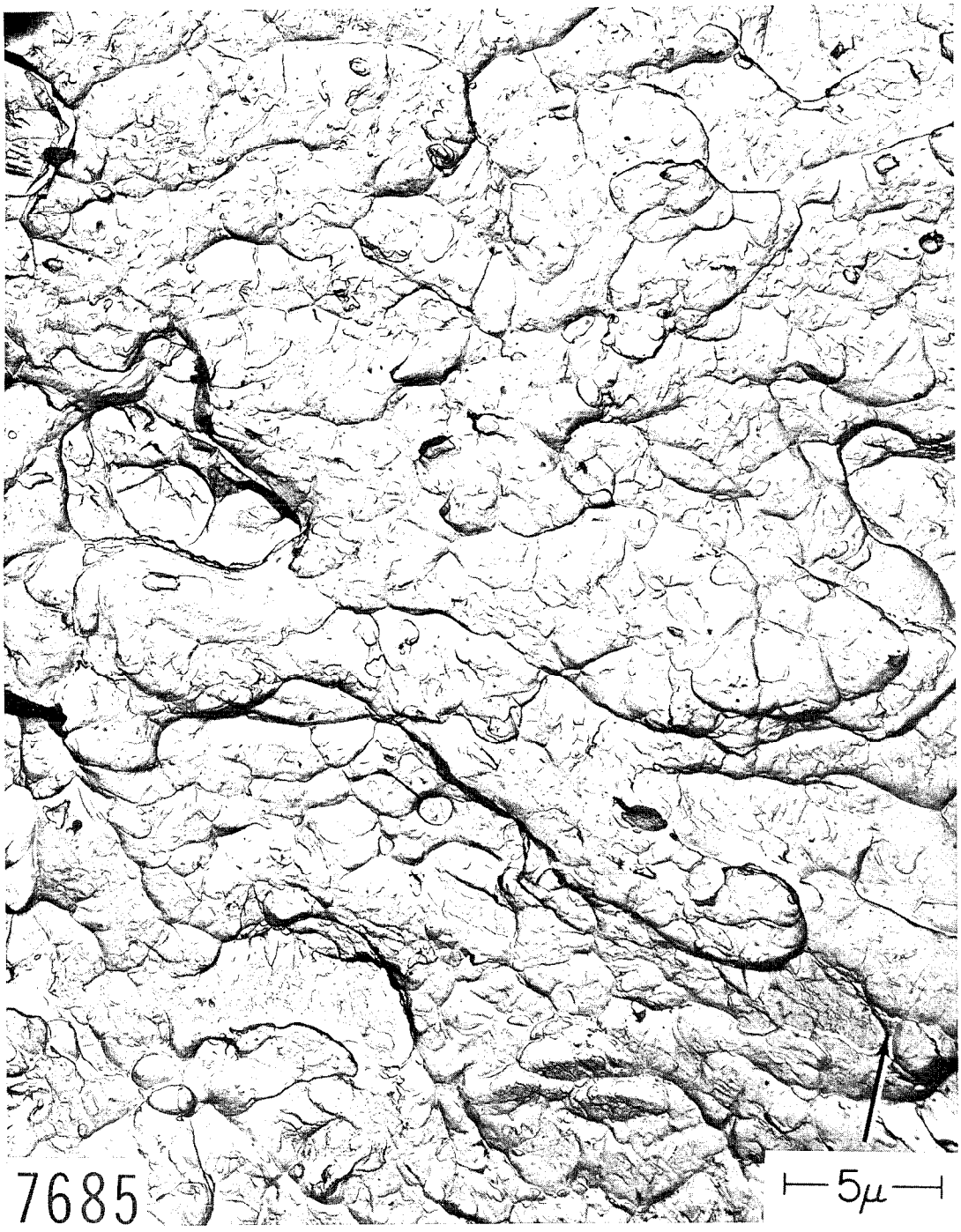

Fig. 109 - Dimples that were found between the zones of high reflectivity in Fig. 106. Cellulose acetate-carbon replication technique. Palladium shadowed. 6000X.

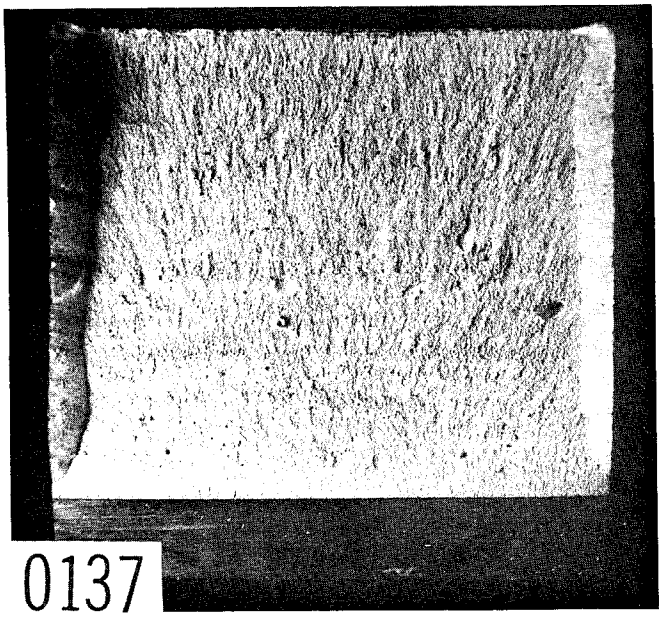

Fig. 110 - Slow bend fracture toughness specimen of 250 KSI yield strength maraging steel weld metal

Fig. 111 - Fatigue markings in 250 KSI yield strength maraging steel weld metal. Cellulose acetate-carbon replication technique. Palladium shadowed. 6000X.

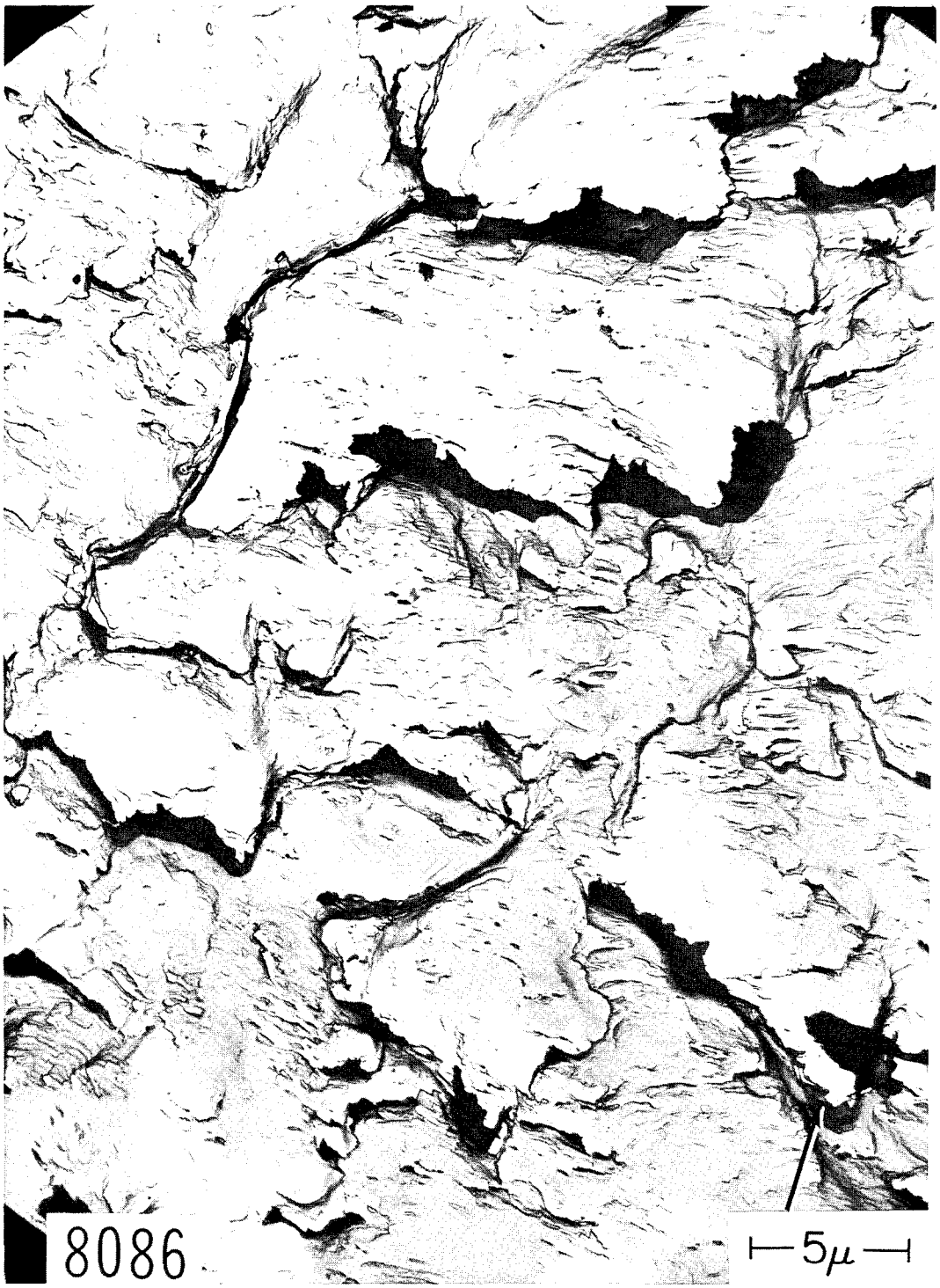

Fig. 112 - Fatigue markings in 250 KSI yield strength maraging steel weld metal. Cellulose acetate-carbon replication technique. Palladium shadowed. 6000X.

Fig. 113 - Fatigue markings in 250 KSI yield strength maraging steel weld metal. Cellulose acetate-carbon replication technique. Palladium shadowed. 6000X.

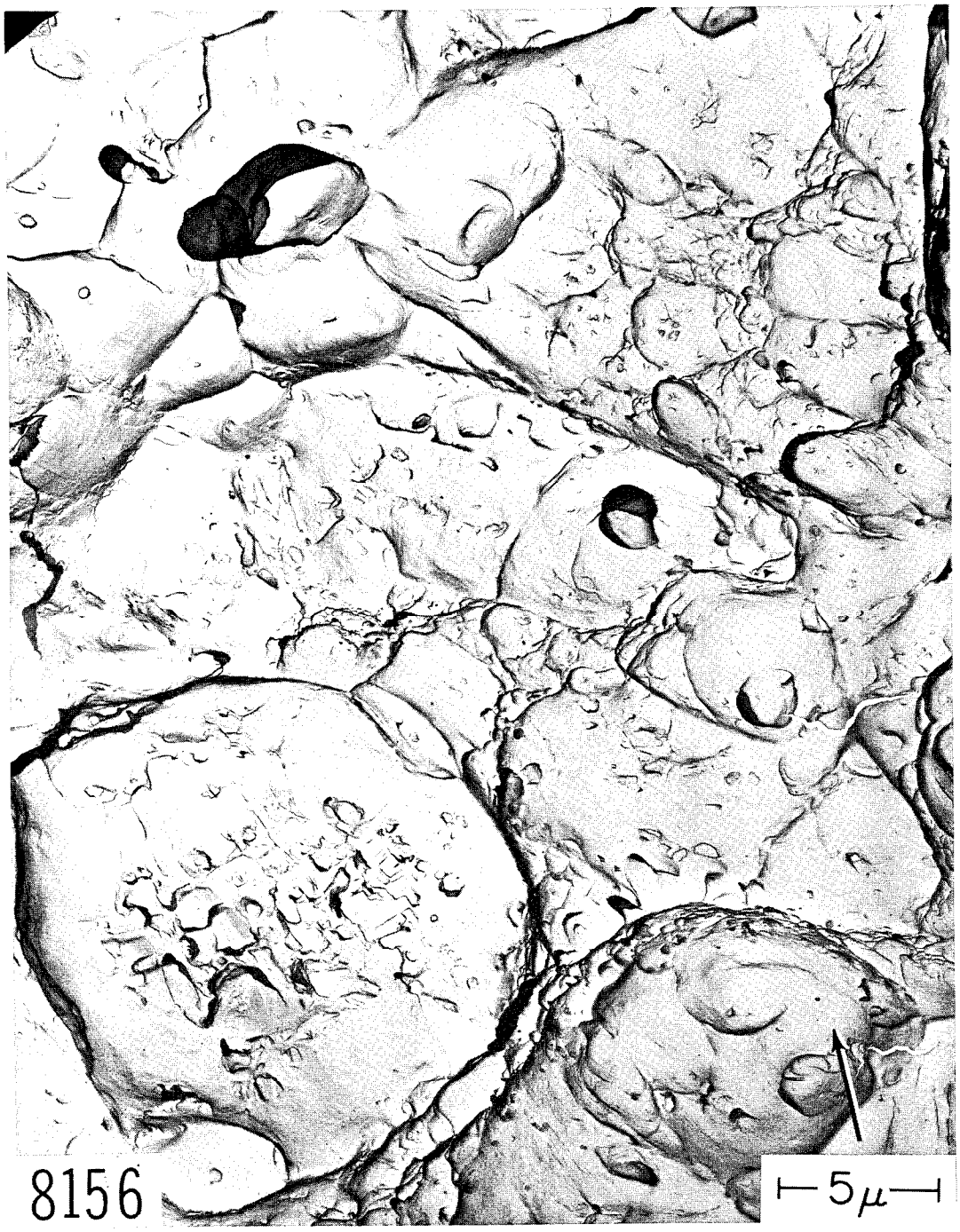

Fig. 114 - Dimples on the overload fracture surface in maraging steel weld metal. Cellulose acetate-carbon replication technique. Palladium shadowed. 6000X.

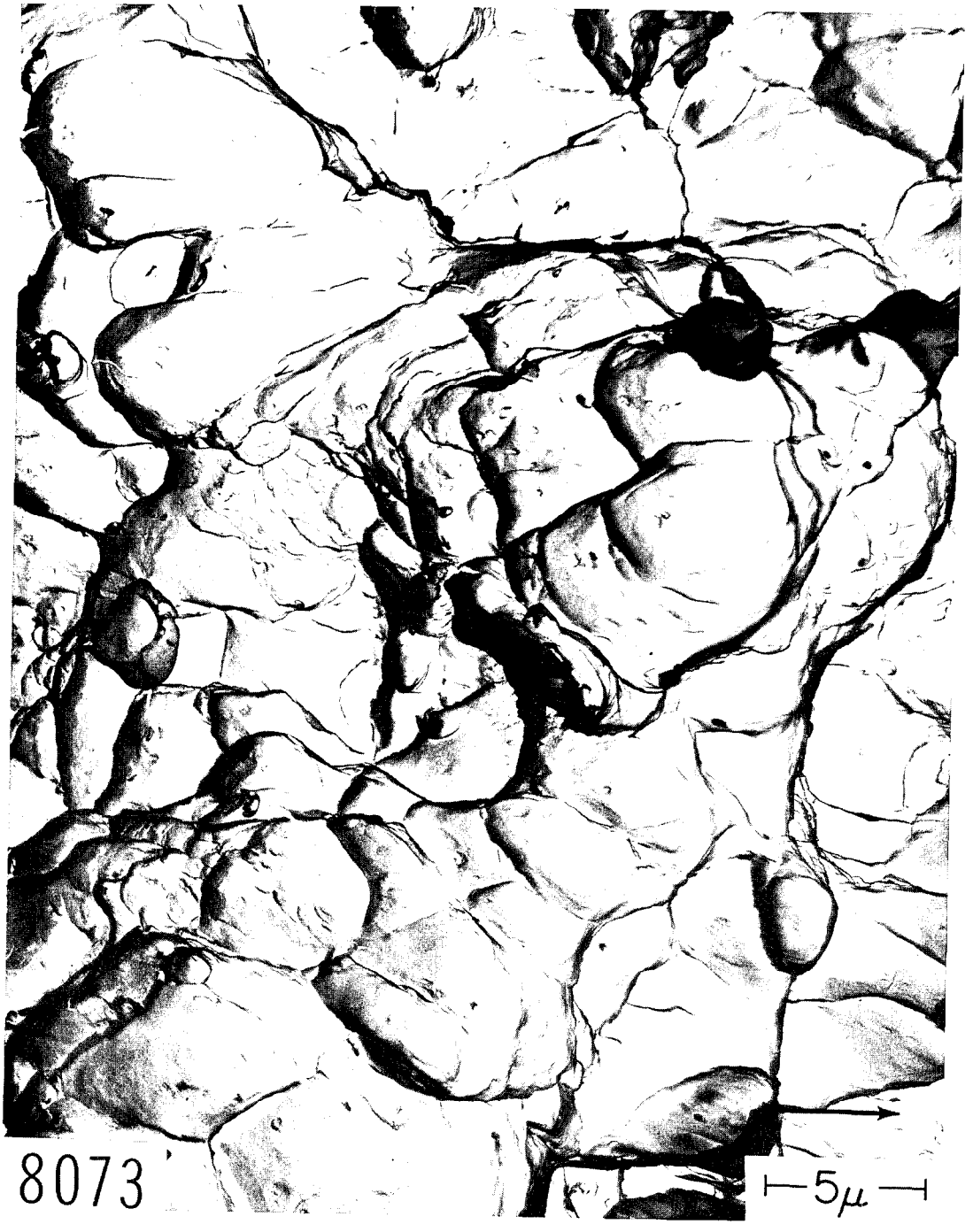

Fig. 115 - Dimples on the overload fracture surface in maraging steel weld metal. Cellulose acetate-carbon replication technique. Palladium shadowed. 6000X.

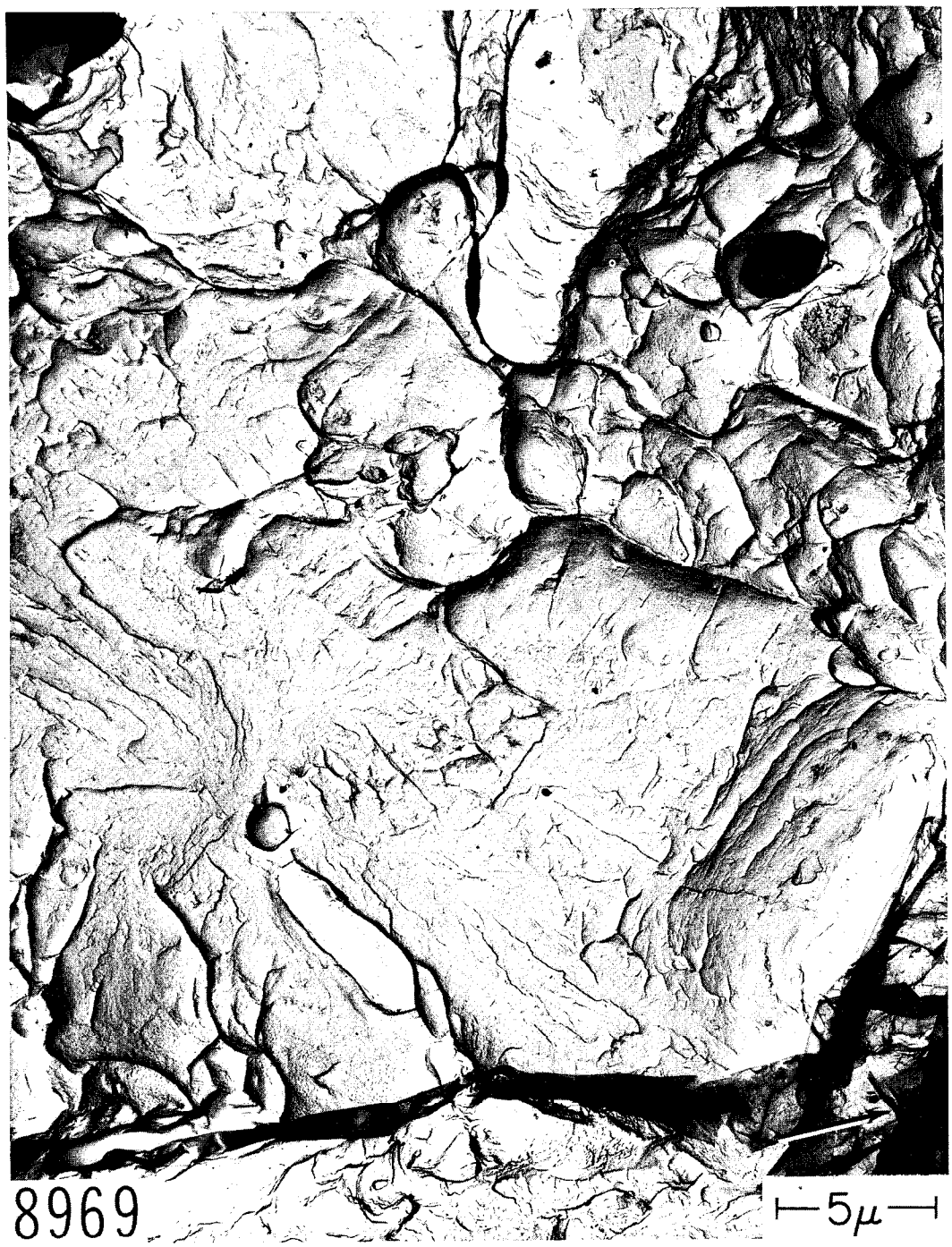

Fig. 116 - Quasi-cleavage in 250 KSI yield strength maraging steel weld metal, embrittled by hydrogen and broken under sustained load at room temperature. Cellulose acetate-carbon replication technique. Palladium shadowed. 6000X.

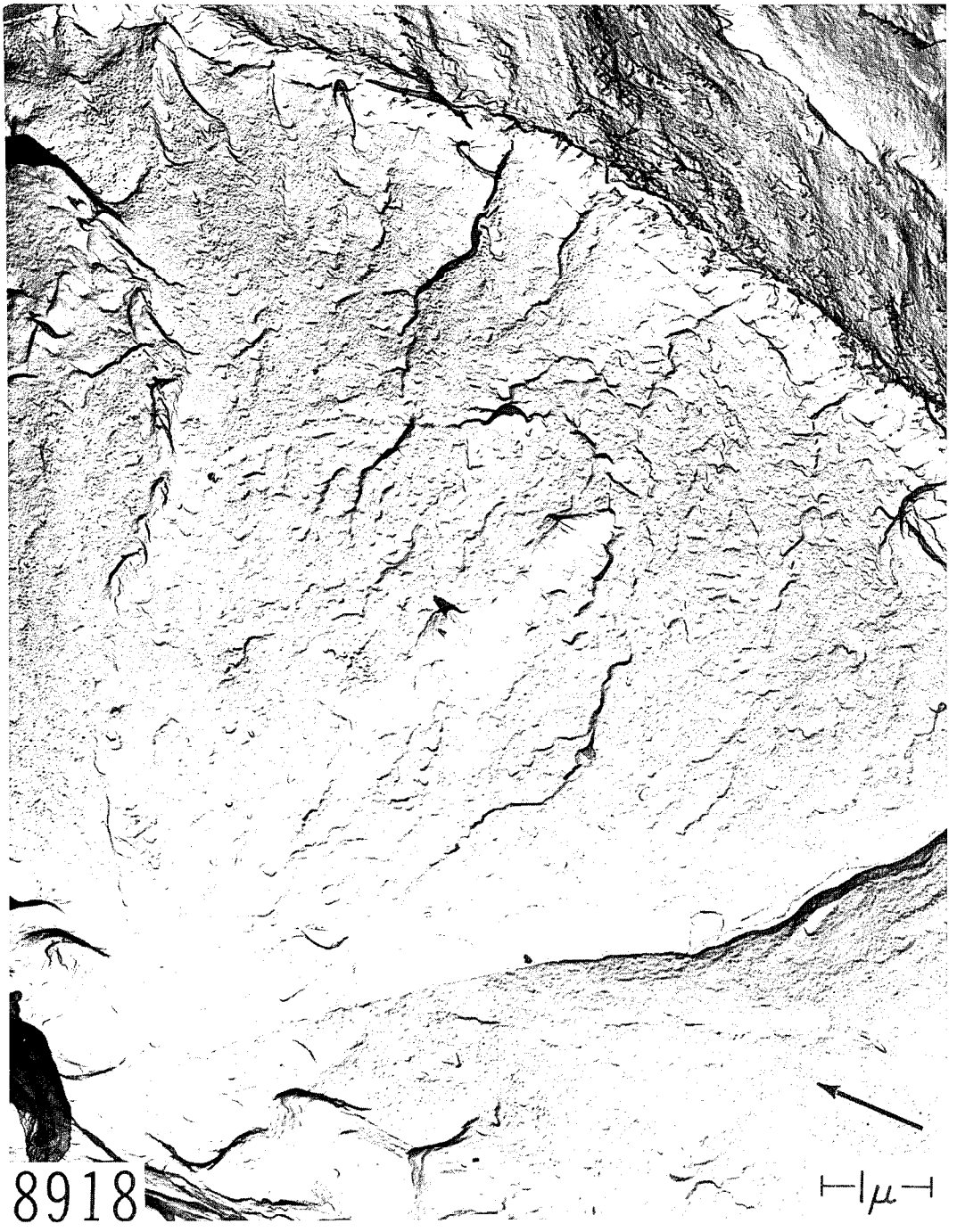

Fig. 117 - Quasi-cleavage in 250 KSI yield strength maraging steel weld metal, embrittled by hydrogen and broken under sustained load at room temperature. Cellulose acetate-carbon replication technique. Palladium shadowed. 21,000X.

5. MONOTONIC FRACTURE SURFACE MARKINGS THAT MAY BE MISTAKEN FOR FATIGUE MARKINGS

Wallner's lines (8), scraping artifacts (2), and other parallel fracture surface markings arising from factors other than repeated loading are likely to be mistaken for fatigue markings by the novice. Figure 118 shows serpentine glide (4) (i.e., unidentified slip markings forming a plaited pattern) formed when the interfaces between silicate fibers and matrix in wrought iron were plastically deformed in fracture at room temperature. The markings near the top of Fig. 118 in particular might be erroneously identified with fatigue loading conditions.

Fig. 118 - Serpentine glide in wrought iron ferrite matrix. Cellulose acetate-carbon replication technique. Palladium shadowed. 6000X.

Figures 119 and 120 show markings observed in spot-weld metal in a 7075 aluminum alloy. The markings at the top and bottom of Fig. 119 bear a resemblance to fatigue markings but were formed from the cast structure of localized eutectic alloy that was formed when the spot weld solidified. Figure 120 is another example of the same structure. Here the parallel markings are in the middle of the fractograph with their lengths extending diagonally from lower left to upper right.

6. FRACTURE PROPAGATION DIRECTION DIAGNOSIS BY EXAMINATION OF DIMPLE ORIENTATION

Efforts to establish a failure analysis tool to aid in determining the fracture propagation direction by observing the orientation of shear rupture dimples in full shear (or slant) fractures have been totally unsuccessful. The basis for expecting that there might be a dependence of dimple orientation upon propagation direction is the fact that full shear fractures must result from some combination of shear rupture and tearing, with the tearing component giving a corresponding directional sense to the dimples (9).

Aluminum alloy 6061 T6 specimens, 0.063 in. thick, were designed and tested to accentuate the tearing component in full shear, and replicas from these fracture surfaces were critically examined. The effect of the tearing component was not pronounced enough to make dimple orientation dependence evident.

7. OTHER PROGRAM RESPONSIBILITIES

Four failure analyses were performed on fractured critical aircraft components. The results were reported in the form of memorandum reports. The results of an additional failure analysis were given verbally to a representative of Edwards Air Force Base.

Guidance has been given to Douglas Aircraft Company during the preparation of their failure analysis handbook. Special fractographs have been prepared for Douglas for inclusion in the handbook and sent to them.

8. SUGGESTIONS FOR FUTURE WORK

Time duration available for future failure analyses with the aid of electron fractography should be expanded to permit the persons doing the analyses to conduct pertinent controlled experiments in the laboratory to prepare standard fracture surfaces. These surfaces, when compared or contrasted with the fracture surfaces of the service items, would permit the highest confidence in the analyses.

ACKNOWLEDGMENT

The author thanks the members of the Strength of Metals Branch and Welding Branch of the Metallurgy Division, and the members of the Ballistics Branch of the Mechanics Division for providing fractured specimens for examination and records for inclusion in this report.

Mr. J.E. Flint performed the painstaking characterizations of most of the fractographs.

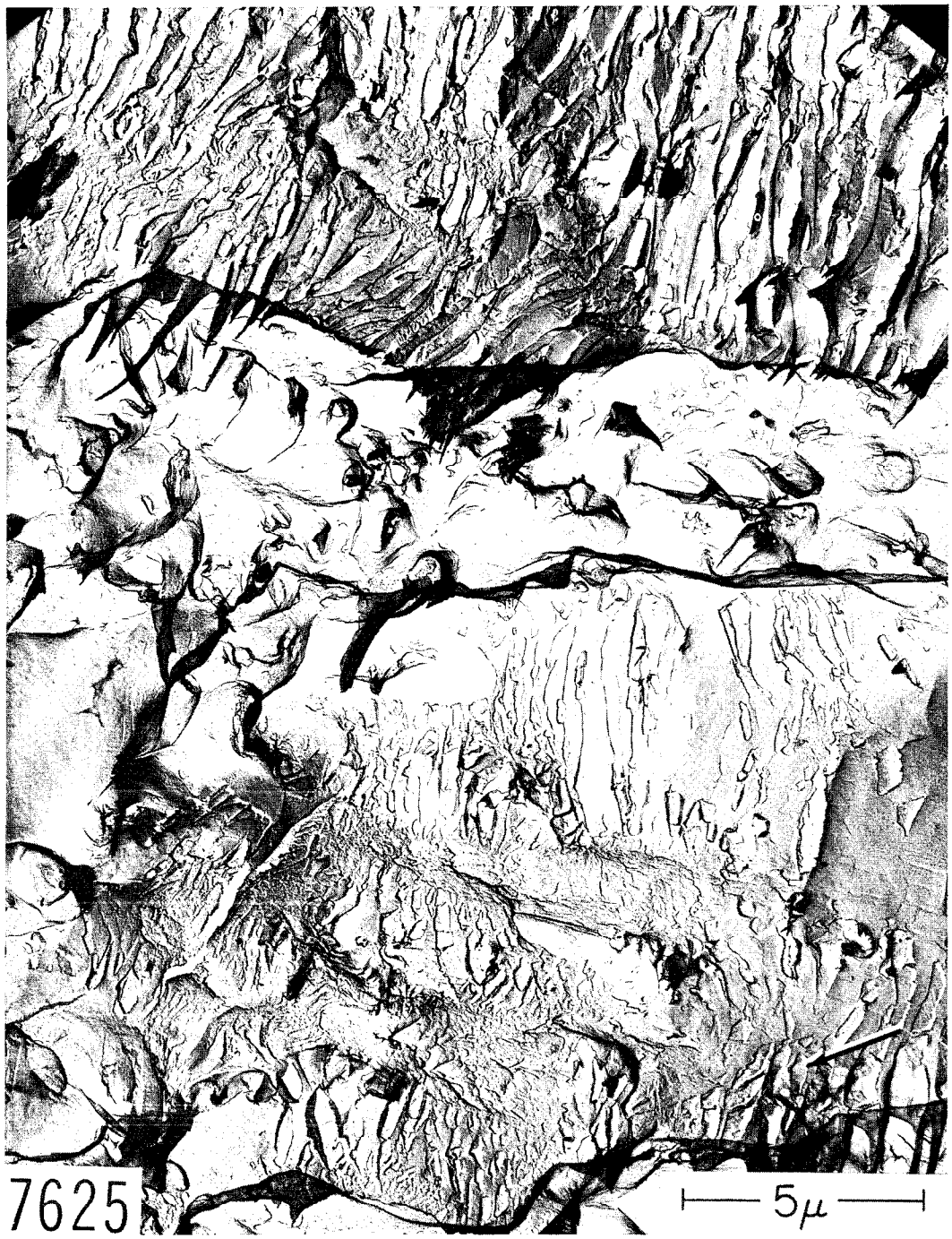

Fig. 119 - Monotonic fracture through eutectic structure in 7075 aluminum alloy. Cellulose acetate-carbon replication technique. Palladium shadowed. 9000X.

Fig. 120 - Monotonic fracture through eutectic structure in 7075 aluminum alloy. Cellulose acetate-carbon replication technique. Palladium shadowed. 9000X.

REFERENCES

1. "The Slow Growth and Rapid Propagation of Cracks." Second Report of a Special ASTM Committee. Materials Research and Standards, Vol. 1, No. 5, May 1951

2. Dahlberg, E.P., and Beachem, C.D., "Fractography, Part XV. Some Artifacts Possible with the Two-Stage Plastic Carbon Replication Technique," NRL Memorandum Report 1457, Sept. 1963

3. Goode, R.J., et al., "Metallurgical Characteristics of High Strength Structural Materials (Fifth Quarterly Report)," NRL Report 6196, Sept. 1964

4. Beachem, C.D., and Meyn, D.A., "Illustrated Glossary of Fractographic Terms. Section 2. Glide Plane Decohesion, Serpentine Glide, Ripples, Stretching, and Microvoid Coalescence," NRL Memorandum Report 1547, June 1964

5. Pellini, W.S., and Puzak, P.P., "Factors that Determine the Applicability of High Strength Quenched and Tempered Steels to Submarine Hull Construction," NRL Report 5892, Dec. 1962

6. Puzak, P.P., Lloyd, K.B., Lange, E.A., Goode, R.J., and Huber, R.W., "Metallurgical Characteristics of High Strength Structural Materials," NRL Memorandum Report 1461, Sept. 1963

7. Kies, J.A., Smith, H.L., Romine, H.E., and Bernstein, H., "Fracture Testing of Weldments," ASTM Symposium on Fracture Toughness Testing and Its Applications, Chicago, Ill., June 23-24, 1964

8. Beachem, C.D., and Pelloux, R.M.N., "Electron Fractography – A Tool for the Study of Micro-Mechanisms of Fracturing Processes," ASTM Symposium on Fracture Toughness Testing and Its Applications, Chicago, Ill., June 23-24, 1964

9. Beachem, C.D., "An Electron Fractographic Study of the Influence of Plastic Strain Conditions upon Ductile Rupture Processes in Metals," ASM, Transactions Quarterly, Vol. 56, Sept. 1963

(PAGE 120 BLANK)

DOCUMENT CONTROL DATA - R&D

(Security classification of title, body of abstract and indexing annotation must be entered when the overall report is classified)

1. ORIGINATING ACTIVITY *(Corporate author)*

U.S. Naval Research Laboratory
Washington, D.C. 20390

2a. REPORT SECURITY CLASSIFICATION

Unclassified

2b. GROUP

3. REPORT TITLE

ELECTRON MICROSCOPE FRACTURE EXAMINATION TO CHARACTERIZE AND IDENTIFY MODES OF FRACTURE

4. DESCRIPTIVE NOTES *(Type of report and inclusive dates)*

This is a final report on the problem

5. AUTHOR(S) *(Last name, first name, initial)*

Beachem, C.D.

6. REPORT DATE	7a. TOTAL NO. OF PAGES	7b. NO. OF REFS
September 28, 1965	124	9

8a. CONTRACT OR GRANT NO.

NRL Problem M01-08

b. PROJECT NO.

MIPR AS-4-132 Project 7381

c.

d.

9a. ORIGINATOR'S REPORT NUMBER(S)

NRL Report 6293

9b. OTHER REPORT NO(S) *(Any other numbers that may be assigned this report)*

AFML-TR-64-408

10. AVAILABILITY/LIMITATION NOTICES

Distribution of this document is unlimited

11. SUPPLEMENTARY NOTES

12. SPONSORING MILITARY ACTIVITY

Air Force

13. ABSTRACT

The fine-scale fracture topographies of both monotonic and fatigue fracture surfaces of several steels and aluminum and titanium alloys have been characterized. Some effects of orientation of specimen upon the fatigue crack surface appearance in 2024 T851 were found. Quasi-cleavage in hydrogen embrittled, 250,000 psi yield strength, maraging steel was discovered. Four overload fracture modes, including a previously unreported mode, were found in a 7075 T6 aluminum alloy by precision matching techniques. A number of failure analyses were made.

DD FORM 1 JAN 64 1473

14. KEY WORDS	LINK A		LINK B		LINK C	
	ROLE	WT	ROLE	WT	ROLE	WT
Fracture (Mechanics) Failure (Mechanics) Fractography Aluminum alloys Titanium Alloys Steel						

INSTRUCTIONS

1. ORIGINATING ACTIVITY: Enter the name and address of the contractor, subcontractor, grantee, Department of Defense activity or other organization *(corporate author)* issuing the report.

2*a*. REPORT SECURITY CLASSIFICATION: Enter the overall security classification of the report. Indicate whether "Restricted Data" is included. Marking is to be in accordance with appropriate security regulations.

2*b*. GROUP: Automatic downgrading is specified in DoD Directive 5200.10 and Armed Forces Industrial Manual. Enter the group number. Also, when applicable, show that optional markings have been used for Group 3 and Group 4 as authorized.

3. REPORT TITLE: Enter the complete report title in all capital letters. Titles in all cases should be unclassified. If a meaningful title cannot be selected without classification, show title classification in all capitals in parenthesis immediately following the title.

4. DESCRIPTIVE NOTES: If appropriate, enter the type of report, e.g., interim, progress, summary, annual, or final. Give the inclusive dates when a specific reporting period is covered.

5. AUTHOR(S): Enter the name(s) of author(s) as shown on or in the report. Enter last name, first name, middle initial. If military, show rank and branch of service. The name of the principal author is an absolute minimum requirement.

6. REPORT DATE: Enter the date of the report as day, month, year; or month, year. If more than one date appears on the report, use date of publication.

7*a*. TOTAL NUMBER OF PAGES: The total page count should follow normal pagination procedures, i.e., enter the number of pages containing information.

7*b*. NUMBER OF REFERENCES: Enter the total number of references cited in the report.

8*a*. CONTRACT OR GRANT NUMBER: If appropriate, enter the applicable number of the contract or grant under which the report was written.

8*b*, 8*c*, & 8*d*. PROJECT NUMBER: Enter the appropriate military department identification, such as project number, subproject number, system numbers, task number, etc.

9*a*. ORIGINATOR'S REPORT NUMBER(S): Enter the official report number by which the document will be identified and controlled by the originating activity. This number must be unique to this report.

9*b*. OTHER REPORT NUMBER(S): If the report has been assigned any other report numbers *(either by the originator or by the sponsor)*, also enter this number(s).

10. AVAILABILITY/LIMITATION NOTICES: Enter any limitations on further dissemination of the report, other than those imposed by security classification, using standard statements such as:

(1) "Qualified requesters may obtain copies of this report from DDC."

(2) "Foreign announcement and dissemination of this report by DDC is not authorized."

(3) "U. S. Government agencies may obtain copies of this report directly from DDC. Other qualified DDC users shall request through

_____."

(4) "U. S. military agencies may obtain copies of this report directly from DDC. Other qualified users shall request through

_____."

(5) "All distribution of this report is controlled. Qualified DDC users shall request through

_____."

If the report has been furnished to the Office of Technical Services, Department of Commerce, for sale to the public, indicate this fact and enter the price, if known.

11. SUPPLEMENTARY NOTES: Use for additional explanatory notes.

12. SPONSORING MILITARY ACTIVITY: Enter the name of the departmental project office or laboratory sponsoring *(paying for)* the research and development. Include address.

13. ABSTRACT: Enter an abstract giving a brief and factual summary of the document indicative of the report, even though it may also appear elsewhere in the body of the technical report. If additional space is required, a continuation sheet shall be attached.

It is highly desirable that the abstract of classified reports be unclassified. Each paragraph of the abstract shall end with an indication of the military security classification of the information in the paragraph, represented as *(TS), (S), (C), or (U)*.

There is no limitation on the length of the abstract. However, the suggested length is from 150 to 225 words.

14. KEY WORDS: Key words are technically meaningful terms or short phrases that characterize a report and may be used as index entries for cataloging the report. Key words must be selected so that no security classification is required. Identifiers, such as equipment model designation, trade name, military project code name, geographic location, may be used as key words but will be followed by an indication of technical context. The assignment of links, roles, and weights is optional.